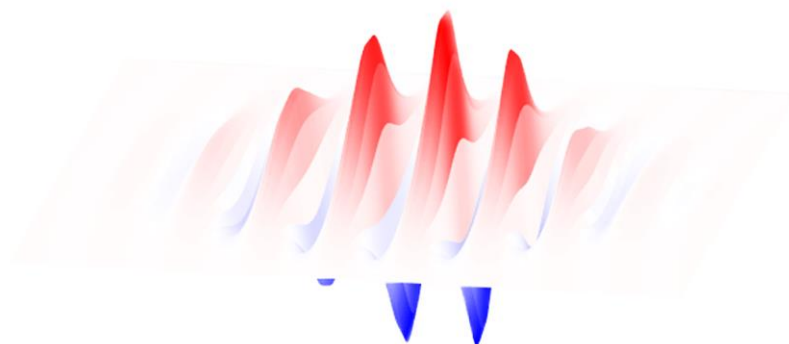


 УНИВЕРСИТЕТ ИТМО

**M.V. Melnik, I.O. Vorontsova, E.A. Ponomareva,
M.O. Zhukova, A.N. Tsyarkin, S.A. Kozlov**

**MATHEMATICAL METHODS IN
FEMTOSECOND OPTICS**



**Санкт-Петербург
2020**

МИНИСТЕРСТВО НАУКИ И ВЫСШЕГО ОБРАЗОВАНИЯ РОССИЙСКОЙ
ФЕДЕРАЦИИ

УНИВЕРСИТЕТ ИТМО

**М.В. Мельник, И.О. Воронцова, Е.А.,
Пономарева, М.О. Жукова, А.Н. Цыпкин,
С.А. Козлов**

**MATHEMATICAL METHODS IN
FEMTOSECOND OPTICS**

УЧЕБНО-МЕТОДИЧЕСКОЕ ПОСОБИЕ

РЕКОМЕНДОВАНО К ИСПОЛЬЗОВАНИЮ В УНИВЕРСИТЕТЕ ИТМО
по направлению подготовки 12.04.03 Фотоника и оптоинформатика
в качестве учебно-методического пособия для реализации основных
профессиональных образовательных программ высшего образования
магистратуры,

 УНИВЕРСИТЕТ ИТМО

Санкт-Петербург
2020

Мельник М.В., Воронцова И.О., Пономарева Е.А., Жукова М.О., Цыпкин А.Н., Козлов С.А., *Mathematical methods in femtosecond optics* – СПб: Университет ИТМО, 2020. – 68 с.

Рецензент(ы):

Петров Николай Владимирович, доктор физико-математических наук, доцент, доцент (квалификационная категория "ординарный доцент") факультета фотоники и оптоинформатики, Университета ИТМО.

В данном методическом пособии рассматриваются основные математические методы и техники, используемые в современных научных исследованиях в области фемтосекундной и нелинейной оптики. Приведено описание математических подходов для изучения динамики фемтосекундных импульсов при их распространении в различных средах на основе полевого, спектрального подходов, а также на основе огибающих поля. Рассмотрены аналитические модели для оценки нелинейного, дисперсионного и дифракционного вкладов в отдельности в динамику фемтосекундных импульсов. Продемонстрированы основные методы численного моделирования, позволяющие описывать изученные аналитические модели. На основе представленных математических моделей описаны основные явления, возникающие при взаимодействии высокоинтенсивных фемтосекундных импульсов с веществом. Продемонстрированы аналитические модели для таких явлений как: генерация спектрального суперконтинуума, самофокусировка, генерация терагерцового излучения из плазмы. Приведены аналитические выражения для оценки нелинейности различных сред как в ИК, так и в ТГц диапазоне частот.

 УНИВЕРСИТЕТ ИТМО

Университет ИТМО – ведущий вуз России в области информационных и фотонных технологий, один из немногих российских вузов, получивших в 2009 году статус национального исследовательского университета. С 2013 года Университет ИТМО – участник программы повышения конкурентоспособности российских университетов среди ведущих мировых научно-образовательных центров, известной как проект «5 в 100». Цель Университета ИТМО – становление исследовательского университета мирового уровня, предпринимательского по типу, ориентированного на интернационализацию всех направлений деятельности.

© Университет ИТМО, 2020

© Мельник М.В., Воронцова И.О., Пономарева Е.А., Жукова М.О., Цыпкин А.Н., Козлов С.А., 2020

Table of contents

I. Analytical models of femtosecond pulses dynamics in optical media	4
I.1. Principles for construction of femtosecond pulses dynamic equations	4
I.2. Nonlinear dynamics of plane waves field equations	6
I.3. Nonlinear dynamics of paraxial waves field equations	9
I.4. Femtosecond pulses field dynamics equations based on the envelope approach.....	12
I.5. Linear equations of the spectral dynamics of non-paraxial waves	14
I.6. Nonlinear equations of the spectrum dynamics of non-paraxial waves	19
I.7. Spectral approach for femtosecond pulse reduction to the field equations of pulse dynamics	23
I.8. Femtosecond pulses self-action in waveguides	24
I.8.1. Femtosecond pulses dispersion broadening	25
I.8.2. Femtosecond pulses temporal spectrum ultrabroadening.....	27
I.9. Self-focusing of femtosecond pulses in bulk media.....	28
II. Effect of laser-ionized liquid nonlinear characteristics on the optical-to-terahertz conversion efficiency.....	35
III. Nonlinear refractive index in the THz frequency range in semiconductor crystals and liquids.....	40
III.1. Theoretical approach for assessing vibrational low-inertial nonlinearity of crystals within the THz frequency range.....	40
III.2. Calculation of the coefficient of nonlinear refractive index considering the vibrational nonlinearity of electro-optical crystals in the THz frequency range.....	44
III.3. Application and modification of the theoretical approach to assess the vibrational nonlinearity of liquid water in the THz frequency range	45
III.4. Z-scan technique for measuring third-order nonlinearities.....	48
III.5. Theory of Z-scan technique	49
III.6. Experimental verification of the water nonlinear refractive index estimation in the THz frequency range by z-scan technique	54
References.....	59

I. Analytical models of femtosecond pulses dynamics in optical media

Laser technology has gone a long way of improvements since the first laser was developed over 60 years ago. Not only did the size of laser setups themselves change significantly, from full-table sized systems to those of a fingertip size, but also the time scaling, from microseconds to femtosecond ($1 \text{ fs} = 10^{-15} \text{ s}$) [1,2] and even attosecond ($1 \text{ as} = 10^{-18} \text{ s}$) [3] values currently common.

Switch to femtosecond mode allowed an important increase of radiation intensity, without any medium destruction [4]. This gave rise to a study of new nonlinear phenomena, impossible to observe using pulses of longer duration. One example of such an effect is ultrabroadening of the radiation spectrum (supercontinuum generation), when the width of the latter becomes commensurate with its central frequency [5]. The phenomenon can be observed in most transparent materials when working in femtosecond mode and is usually accompanied by other nonlinear effects, e.g., self-action and self-focusing [6–13].

Another common phenomenon observed in femtosecond range, apart from the supercontinuum generation, is generation of light pulses characterized by few field oscillations [14–16]. The term “extremely short”, used to denote such pulses, does not refer to their duration but to the number of cycles involved. For example, such pulses can be obtained in picosecond range, when the spectrum occupies the far IR spectral range [17,18], while their duration would reach attosecond values for UV spectrum [3,16,19,20]. Regarding visible and near IR ranges, pulses of 20-30 fs obtained by commercially available lasers (e.g. the Ti:Sapphire) include ca. 10 electromagnetic field oscillations.

For an analytical description of nonlinear optical processes, the technique of a slowly varying envelope is used, supposing the radiation is quasi-monochromatic. However, there are additional limitations to be imposed to correctly describe extremely short pulses, which makes the mathematical model very cumbersome [1,21]. Both the modification of the method and a search of another theoretical model have been amply described [7,16,21–25]. Among them there is the field approach, featuring the pulse field rather than its envelope. The course suggested below considers the application of the latter approach for a mathematic description of nonlinear processes and phenomena resulting from the interaction between high-intensity femtosecond pulses and transparent dielectric media.

I.1. Principles for construction of femtosecond pulses dynamic equations

In this section the basics of the equations construction for transversely homogeneous plane waves are described in accordance with the field approach. The corresponding assumption is valid to describe the behavior of femtosecond pulses propagating through waveguides. In this case, it is possible to neglect the longitudinal field component for the power values below critical [10]. Taking it into consideration, Maxwell’s equation can be reduced to the form corresponding to that for non-magnetic dielectric media [26]:

$$\frac{\partial^2 E}{\partial z^2} - \frac{1}{c^2} \frac{\partial^2 E}{\partial t^2} = \frac{4\pi}{c^2} \frac{\partial^2 P_L}{\partial t^2} + \frac{4\pi}{c^2} \frac{\partial^2 P_{NL}}{\partial t^2}, \quad (\text{I.1.1})$$

where \mathbf{E} stands for the electric field of the light wave, \mathbf{P}_L for the linear (relative to the field) polarization response of the medium, \mathbf{P}_{NL} for the nonlinear polarization response, z for the spatial coordinate along which the radiation propagates, t for time, c for the light velocity in vacuum.

The dispersion of both linear and nonlinear parts of the polarization response is the crucial parameter to precisely describe the propagation of femtosecond pulses in transparent optical media. The reason to it lies in the fact that the spectrum of such short pulses can be very wide due to the self-action processes. Let us now refer to the way the equation (I.1.1) can be modified to describe accurately the propagation of the pulse having a wide spectrum in the media without nonlinearity ($\mathbf{P}_{NL} = 0$). The dependence of the isotropic optical media linear refractive index n on the light frequency ω , which lies in the media transparency window, can be described by the following equation to arbitrary precision [27]:

$$n^2(\omega) = N_0^2 + 2cN_0a\omega^2 + 2cN_0a_1\omega^4 + \dots - 2cN_0b\omega^{-2} - 2cN_0b_1\omega^{-4} \dots, \quad (\text{I.1.2})$$

where $N_0, a, a_1, \dots, b, b_1, \dots$ are the empirical constants of the medium dispersion. The wave equation can be expressed as follows [28] for the dispersion relation (I.1.2):

$$\frac{\partial^2 \mathbf{E}}{\partial z^2} - \frac{N_0^2}{c^2} \frac{\partial^2 \mathbf{E}}{\partial t^2} = -\frac{2N_0}{c} a \frac{\partial^4 \mathbf{E}}{\partial t^4} + \frac{2N_0}{c} a_1 \frac{\partial^6 \mathbf{E}}{\partial t^6} - \dots + \frac{2N_0}{c} b \mathbf{E} - \frac{2N_0}{c} b_1 \int_{-\infty}^t dt' \int_{-\infty}^{t'} \mathbf{E} dt'' + \dots. \quad (\text{I.1.3})$$

The validity of the statement can be proved by partial solution of the equation (I.1.3) for the monochromatic radiation of the form:

$$\mathbf{E} = \frac{1}{2} \varepsilon_\omega e^{i(kz - \omega t)} + c. c., \quad (\text{I.1.4})$$

where ε_ω is the amplitude of spectral components of radiation, $k(\omega)$ is the wavenumber. Thus, if the refractive index $n(\omega) = \frac{c}{\omega} k(\omega)$ dependence on the frequency has the form of (I.1.2), the relation (I.1.4) is the solution of the equation (I.1.3).

The equation (I.1.3) describes pulse propagation both forward and backward along the z -axis. To concentrate on the pulse dynamics analysis in one direction only, the switch to new variables is convenient $\tau = t - \frac{N_0}{c} z, z' = z$. The relation (I.1.3) is then reduced to:

$$\frac{\partial^2 \mathbf{E}}{\partial z'^2} - \frac{2N_0}{c} \frac{\partial^2 \mathbf{E}}{\partial z' \partial \tau} = -\frac{2N_0}{c} a \frac{\partial^4 \mathbf{E}}{\partial \tau^4} + \frac{2N_0}{c} a_1 \frac{\partial^6 \mathbf{E}}{\partial \tau^6} - \dots + \frac{2N_0}{c} b \mathbf{E} - \frac{2N_0}{c} b_1 \int_{-\infty}^{\tau} d\tau' \int_{-\infty}^{\tau'} \mathbf{E} d\tau'' + \dots. \quad (\text{I.1.5})$$

Slowly varying envelope approximation [26] frequently used for acoustic waves (i.e. assuming the pulse profile changes less than central wavelength value) allows to neglect term $\frac{\partial^2 \mathbf{E}}{\partial z'^2}$ in (I.1.5). Consequently, one can easily integrate the equation (I.1.5) over the time variable τ to simplify it to the form:

$$\frac{\partial^2 \mathbf{E}}{\partial z'} - a \frac{\partial^3 \mathbf{E}}{\partial \tau^3} + a_1 \frac{\partial^5 \mathbf{E}}{\partial \tau^5} - \dots + b \int_{-\infty}^{\tau} \mathbf{E} d\tau' - b_1 \int_{-\infty}^{\tau} d\tau' \int_{-\infty}^{\tau'} \mathbf{E} d\tau'' + \dots = 0. \quad (\text{I.1.6})$$

Contracted (to the first order derivative of z') version of the wave equation (I.1.6) corresponds to the following dispersion relation:

$$n(\omega) = N_0 + ca\omega^2 + ca_1\omega^4 + \dots - cb\omega^{-2} - cb_1\omega^{-4} - \dots. \quad (\text{I.1.7})$$

This shows that the slowly varying envelope approximation leads to the substitution of $n^2 - N_0^2$ in the expression (I.1.2) for $2N_0(n - N_0)$. Expression (I.1.7) allows to describe with high precision the refractive index dispersion of optical materials in the transparency window [27]. This justifies using slowly varying envelope approximation not only for acoustics but for optics as well (if the medium is transparent). It is important that expression (I.1.6) helps to describe the dynamics of both a plane transversely uniform wave and a non-uniform mode in a waveguide [29]. For example, when capillary waveguide is filled with gas with a normal group dispersion, the combination of the dispersion and waveguide contribution allows to observe the anomalous group velocity dispersion (GVD) as well [29,30].

A comparative analysis of the equations (I.1.1) and (I.1.3), can easily bring about the form of a generalized equation (I.1.3) for the case of a nonlinear medium:

$$\frac{\partial^2 E}{\partial z} - \frac{N_0^2}{c^2} \frac{\partial^2 E}{\partial t^2} = \frac{2N_0}{c} a \frac{\partial^4 E}{\partial t^4} + \frac{2N_0}{c} a_1 \frac{\partial^6 E}{\partial t^6} - \dots + \frac{2N_0}{c} bE - \frac{2N_0}{c} b_1 \int_{-\infty}^t dt' \int_{-\infty}^{t'} E dt'' + \dots + \frac{4\pi}{c^2} \frac{\partial^2 P_{NL}}{\partial t^2}. \quad (\text{I.1.8})$$

A physical interpretation of slowly varying approximation is known to imply that light propagates in one direction only. In this regard, the nonlinearity of polarization response does not suggest there is also a backward wave, and equation (I.1.8) can be written in the following truncated form:

$$\frac{\partial^2 E}{\partial z'} - a \frac{\partial^3 E}{\partial \tau^3} + a_1 \frac{\partial^5 E}{\partial \tau^5} - \dots + b \int_{-\infty}^{\tau} E d\tau' - b_1 \int_{-\infty}^{\tau} d\tau' \int_{-\infty}^{\tau'} E d\tau'' + \dots + \frac{2\pi}{cN_0} \frac{\partial P_{NL}}{\partial \tau} = 0. \quad (\text{I.1.9})$$

Thus, an analysis of the wave equation (I.1.9) in combination with material equations for the nonlinear polarization response P_{NL} makes it possible to estimate the dependences of femtosecond pulses propagation on the initial energy, polarization, and their spectral and temporal characteristics. However, it is necessary to refer to the features of nonlinear material equations construction and their requirements before proceeding with the aforementioned problem analysis.

I.2. Nonlinear dynamics of plane waves field equations

The mathematical model describing field dynamics of femtosecond pulses propagating in transparent optical media (I.1.9) is quite general. There are ways to considerably simplify it for most practical cases. For example, provided the mode of radiation propagation is linear, the first, the second and the fourth terms of equation (I.1.9) are sufficient to describe the field dynamics to a high precision. When dealing with such a widespread material as fused silica, the dependence (I.1.7) reduced to the form containing the first, the second and the fourth terms only corresponds to the data obtained experimentally up to the third decimal for the spectral range from 460 to 1800 nm [31]. The given range comprises the larger part of the normal GVD region (limited by two-photon resonance in the UV range) and the entire anomalous GVD region lying within the medium transparency window. Due to the electronic nonlinearity of non-resonant origin in the spectral range mentioned, the dispersion of nonlinear refractive index coefficient of electronic nature can be neglected. Moreover, owing to the

short duration of the femtosecond radiation, one can eliminate the nonlinearity electron–phonon mechanism as well [32,33].

The inferences mentioned justify the simplification of the expression (I.1.9) for the case when linearly polarized radiation is propagating in the dielectric medium of a wide transparency window. The simplified expression has the form of [32]:

$$\frac{\partial E}{\partial z} - a \frac{\partial^3 E}{\partial \tau^3} + b \int_{-\infty}^{\tau} E d\tau' + gE^2 \frac{\partial E}{\partial \tau} = 0, \quad (\text{I.2.1})$$

where $g = \frac{\gamma_e}{\omega_{e1}^2 \omega_{e2}^2}$.

The expression (I.2.1) is sufficient to describe the nonlinear dynamics of ultrashort pulses even though they are of wide spectrum and imply few oscillations. In view of the above, the expression can be considered as that on a par with the cubic Schrödinger equation [1,21], widely employed for ultrashort quasi-monochromatic pulse dynamics description. Thus, all assumptions and approximations considered, the equation still addresses all the physical parameters needed to describe the dynamics (linear dispersion and inertialess nonlinearity) of ultrashort pulses propagating in dielectric media to a high precision.

Much attention (e.g. [1,21]) has been focused on various modifications of the Schrödinger equation aimed at the description of ultrashort pulse dynamics giving an accurate consideration of the cases of their different polarizations, spectral compositions, and other input parameters of both radiation and propagation media. The equation (I.2.1) can also be modified according to the same principles.

If the light is polarized not linearly, the equation (I.2.1) transforms to [34,35]:

$$\frac{\partial \mathbf{E}}{\partial z} - a \frac{\partial^3 \mathbf{E}}{\partial \tau^3} + b \int_{-\infty}^{\tau} \mathbf{E} d\tau' + g(\mathbf{E}, \mathbf{E}) \frac{\partial \mathbf{E}}{\partial \tau} + h\mathbf{E} \times \left(\mathbf{E} \times \frac{\partial \mathbf{E}}{\partial \tau} \right) = 0, \quad (\text{I.2.2})$$

where h , akin g , denotes inertialess nonlinearity of the medium polarization response. A vector equation, similar to the one above, was derived in [36,37] for the two-level medium assumption, which suggests $b = 0, g < 0$.

The equation (I.1.9) can also be modified to address the inertial electron–vibrational nonlinearity contribution to the ultrashort pulse dynamics. Thus, it takes the form of [28,38]:

$$\begin{cases} \frac{\partial E}{\partial z} - a \frac{\partial^3 E}{\partial \tau^3} + b \int_{-\infty}^{\tau} E d\tau' + gE^2 \frac{\partial E}{\partial \tau} + \frac{\partial}{\partial \tau} (R_v E) = 0 \\ \frac{\partial^2 R_v}{\partial t^2} + \frac{2}{T_v} \frac{\partial R_v}{\partial t} + \omega_v^2 R_v = \gamma_v E^2 \end{cases} \quad (\text{I.2.3})$$

It is obvious that apart from the terms describing linear dispersion and inertialess nonlinearity, the expression (I.2.3) also contains Raman scattering and two-photon absorption, which makes it different from the expression (I.2.1). The authors in [39,40] suggest a similar mathematical model allowing to describe ultrashort pulse self-action in Raman-active media. The model considers more profoundly the contribution to nonlinearity occurring due to the change in the population of vibrational states, however, ignoring the linear medium dispersion.

However, the nonlinear medium inertia of electronic nature cannot be neglected in some situations. One example here is the case of the radiation spectrum lying in the high-frequency range, which

results in a two-photon electronic resonant nonlinearity [41]. Thus, the expression (I.2.1) is to be changed to the following form [28,29]:

$$\left\{ \begin{array}{l} \frac{\partial E}{\partial z} - a \frac{\partial^3 E}{\partial \tau^3} + b \int_{-\infty}^{\tau} E d\tau' + g' E^2 \frac{\partial E}{\partial \tau} + \frac{\partial}{\partial \tau} (R_e E) = 0 \\ \frac{\partial^2 R_e}{\partial t^2} + \frac{2}{T_{e2}} \frac{\partial R_e}{\partial t} + \omega_{e2}^2 R_e = \gamma_e E^2 \end{array} \right. , \quad (\text{I.2.4})$$

where g' characterizes the inertialess contribution of excited electronic states mismatching the two-photon resonance condition. The expression (I.2.4) may be employed to describe the contribution to pulse self-action from the dispersion of non-resonant electronic nonlinearity when its spectral components are far from the two-photon resonances. The authors in [42] were the first to analyze the way the refractive index nonresonant nonlinearity dispersion of electronic nature influences the dynamics of femtosecond pulses featuring ultrawide spectrum, utilizing a mathematical model (I.1.9). When ultrashort pulses propagate in a dielectric medium with wide bandgap and activator centers, in the case of one-photon resonance the expression (I.2.1) takes the following form:

$$\left\{ \begin{array}{l} \frac{\partial E}{\partial z} - a \frac{\partial^3 E}{\partial \tau^3} + b \int_{-\infty}^{\tau} E d\tau' + g E^2 \frac{\partial E}{\partial \tau} + \frac{2\pi}{cN_0} \frac{\partial P_c}{\partial \tau} = 0 \\ \frac{\partial^2 P_c}{\partial \tau^2} + \frac{2}{T_2} \frac{\partial P_c}{\partial \tau} + \omega_0^2 P_c = \alpha U E \\ \frac{\partial U}{\partial \tau} + \frac{U - U^0}{T_1} = \beta \frac{\partial P_c}{\partial \tau} E \end{array} \right. , \quad (\text{I.2.5})$$

where N_0 , a , b and g are the parameters of linear dispersion and inertialess nonlinearity of the dielectric matrix, and P_c is the term added to the polarization response nonlinearity caused by the presence of impurities in dielectric medium, ω_0 , T_1 , T_2 , α and β characterize the activator centers contributing to the latter process.

Linear absorption can be considered by rewriting the expression (I.2.1) as follows [28,29]:

$$\frac{\partial E}{\partial z} + \Gamma_0 E - a \frac{\partial^3 E}{\partial \tau^3} + b \int_{-\infty}^{\tau} E d\tau' + g E^2 \frac{\partial E}{\partial \tau} - \Gamma_1 \frac{\partial^2 E}{\partial \tau^2} - \Gamma_2 \int_{-\infty}^{\tau} d\tau' \int_{-\infty}^{\tau'} E d\tau'' = 0. \quad (\text{I.2.6})$$

The refractive index then becomes complex $n' = n + i\kappa$, whereas the absorption coefficient dispersion takes the form of:

$$\kappa(\omega) = c \left(\frac{\Gamma_0}{\omega} + \Gamma_1 \omega + \frac{\Gamma_2}{\omega^3} \right). \quad (\text{I.2.7})$$

This section has developed the ideas describing the derivation of a field dynamics equation for ultrashort pulses featuring wide spectrum propagating in various optical media under the assumption of plane transversely homogeneous waves. The next step is to consider a more sophisticated case of paraxial wave packets with weak transverse inhomogeneity.

I.3. Nonlinear dynamics of paraxial waves field equations

The expression describing the radiation electric field dynamics in the case of arbitrary spatial field distribution when radiation propagates in dielectric nonmagnetic media, similar to that from Section I.2, can be written as [26]:

$$\nabla \times \nabla \times \mathbf{E} + \frac{1}{c^2} \frac{\partial^2 \mathbf{D}}{\partial t^2} = 0, \quad (\text{I.3.1})$$

where \mathbf{E} stands for the electric field applied, \mathbf{D} characterizes the electric induction, t stands for time, and c is the speed of light in vacuum. Equation (I.3.1) can be easily transformed to equation (I.1.1) assuming waves are plane.

If the light field is time-limited, the expression (I.3.1) immediately becomes consistent with Maxwell's equation:

$$\nabla \mathbf{D} = 0. \quad (\text{I.3.2})$$

The first step is to consider the case of nonresonant interaction between light and dielectric media, their spectrum lying in the transparency window. If the medium is homogeneous and isotropic, its response to the incident radiation can be expressed in the form of [43]:

$$\mathbf{D} = \varepsilon \mathbf{E} + \mathbf{D}_{in} + \mathbf{D}_{nl}, \quad (\text{I.3.3})$$

The first term of (I.3.3) is responsible for the electric induction inertialess linear part, the second one deals with its inertial linear part, whereas the third one describes the nonlinear part of the medium response. The constant ε in the expression (I.3.3) may be addressed as the medium dielectric permittivity at the radiation central frequency.

Thus, considering the expression (I.3.3), the equation (I.3.2) is transformed to:

$$\nabla \mathbf{E} = -\frac{1}{\varepsilon} \nabla (\mathbf{D}_{in} + \mathbf{D}_{nl}). \quad (\text{I.3.4})$$

Considering the expression (I.3.4) and employing the vector relation $\nabla \times \nabla \times = \nabla (\nabla \cdot) - \Delta$, the equation (I.3.1) can be rewritten as [44,45]:

$$\Delta \mathbf{E} - \frac{\varepsilon}{c^2} \frac{\partial^2 \mathbf{E}}{\partial t^2} - \frac{1}{c^2} \frac{\partial^2 \mathbf{D}_{in}}{\partial t^2} - \frac{1}{c^2} \frac{\partial^2 \mathbf{D}_{nl}}{\partial t^2} + \frac{1}{\varepsilon} \nabla (\nabla \mathbf{D}_{in}) - \frac{1}{\varepsilon} \nabla (\nabla \mathbf{D}_{nl}). \quad (\text{I.3.5})$$

The terms in (I.3.3) are related as:

$$\varepsilon \mathbf{E} \gg \mathbf{D}_{in}, \mathbf{D}_{nl}. \quad (\text{I.3.6})$$

Therefore, the expression above determines the possibility to represent the nonresonant light and matter interaction. As follows from the expression (I.3.6), the first two first are only sufficient to describe the field dynamics in the expression (I.3.5). The other terms represent the effects of dispersion, self-action, and are close in value.

This section is devoted to the analysis of light beams dynamics having no transverse inhomogeneities and featuring transverse sizes much greater than the radiation central wavelength and small longitudinal field component. It seems to be evident that if the conditions are met, the two final terms of (I.3.5) are much lower than the third and the fourth ones, let alone the first two. For example, for a pulse propagating at an arbitrary point inside a medium, accompanied by electric induction oscillations, the following expression is true:

$$\frac{1}{c^2} \frac{\partial^2 \mathbf{D}_{in,nl}}{\partial t^2} \sim \frac{\mathbf{D}_{in,nl}^m}{(cT_m/4)^2}, \quad (\text{I.3.7})$$

where $\mathbf{D}_{in,nl}^m$ stands for the maximum values of $\mathbf{D}_{in,nl}$, and T_m describes the average oscillation period. Alongside that, the following expression is valid for the vectors $\nabla(\nabla \mathbf{D}_{in,nl})$, components in the Cartesian coordinate system:

$$\nabla(\nabla \mathbf{D}_{in,nl})_j \sim \frac{\partial^2 (\mathbf{D}_{in,nl})_i}{\partial j \partial i}, \frac{\partial^2 (\mathbf{D}_{in,nl})_z}{\partial j \partial z}, \quad (\text{I.3.8})$$

where z is propagation direction; x, y are transverse coordinates; $i = x, y; j = x, y, z$. For a light beam considered as short, the following expression is always true:

$$\frac{\partial^2 (\mathbf{D}_{in,nl})_i}{\partial j \partial i}, \frac{\partial^2 (\mathbf{D}_{in,nl})_z}{\partial j \partial z} \ll \frac{(\mathbf{D}_{in,nl})_i}{(\lambda_c/4)^2}, \quad (\text{I.3.9})$$

when $\lambda_c = cT_m$, the relation (I.3.5) can be transformed to the form below:

$$\Delta \mathbf{E} - \frac{\varepsilon}{c^2} \frac{\partial^2 \mathbf{E}}{\partial t^2} - \frac{1}{c^2} \frac{\partial^2 \mathbf{D}_{in}}{\partial t^2} - \frac{1}{c^2} \frac{\partial^2 \mathbf{D}_{nl}}{\partial t^2} = 0. \quad (\text{I.3.10})$$

It is sufficient though not necessary for the transverse size of the beam to be much greater than the central wavelength λ_c value in order to (I.3.5) to switch (I.3.10). For example, the two last terms in (I.3.5) are eliminated for two-dimensional linearly polarized TE-wave. Self-action of such pulses containing few field oscillations with the transverse sizes being significantly greater than λ_c was studied in [45], commensurate with λ_c in [46], and for the non-paraxial monochromatic radiation in [47].

The dependence of the dielectric permittivity ε_l linear part on the radiation frequency ω , the form of the polinom, as well as the refractive index n_l linear part, is described by the expression derived according to (I.1.2):

$$\varepsilon_l(\omega) = n_l^2(\omega) = N_0^2 + 2cN_0a\omega^2 - 2cN_0\frac{b}{\omega^2}, \quad (\text{I.3.11})$$

This expression is consistent with Zelmeyer's formula, as mentioned in section I.1, assuming all the spectral components of the pulse are much higher than the lattice oscillation frequencies and much lower than the electronic subsystem oscillation frequencies. The empirical constants N_0, a and b from the expression (I.3.11) allows to describe the dispersion of the nonresonant part of the medium transparency window and takes account of the waveguide dispersion contribution with high accuracy if accurately chosen [29,30].

The transparent isotropic medium nonresonant nonlinear response of electronic nature occurring when exposed to the field of ultrashort pulses, the spectrum of which lies in the medium transparency window, can be roughly described as [28,41]:

$$\mathbf{D}_{nl} = \varepsilon_{nl}(\mathbf{E} \cdot \mathbf{E})\mathbf{E}. \quad (\text{I.3.12})$$

ε_{nl} represents the nonlinear dielectric permittivity coefficient for the linearly polarized radiation and is related to the nonlinear refractive index coefficient n_2 in the following way:

$$n_2 = \frac{3\varepsilon_{nl}}{4N_0}. \quad (\text{I.3.13})$$

The electronic-vibrational medium nonlinearity is not considered in this section. [48] shows that its contribution brings a negligibly small change in the result when the ultrawide spectrum pulses propagate in silica fibers. If the nonlinearity mentioned is not overlooked, the expression (I.2.3) can be

employed. A more sophisticated treatment of the way the nonlinearity of the electronic-vibrational nature influences self-action of ultrashort pulses is provided in section I.8. Besides, plasma nonlinearity is disregarded here as well [16]. Importantly, the latter does change the dynamics of the pulse tail quite significantly [49], resulting in filamentation [50,51], temporal pulse compression [52], and optical breakdown [53], when dealing with high-intensity femtosecond pulses.

To characterize the nonlinear spatio-temporal dynamics of the radiation field for the paraxial case, the expression (I.3.10) featuring the electric induction linear part corresponding to the dispersion description (I.3.11), and the induction nonlinear part (I.3.12) takes the following form:

$$\Delta \mathbf{E} - \frac{N_0^2}{c^2} \frac{\partial^2 \mathbf{E}}{\partial t^2} + \frac{2N_0}{c} a \frac{\partial^4 \mathbf{E}}{\partial t^4} - \frac{2N_0}{c} b \mathbf{E} - \frac{\varepsilon_{nl}}{c^2} \frac{\partial^2 (\mathbf{E} \cdot \mathbf{E}) \mathbf{E}}{\partial t^2} = 0. \quad (\text{I.3.14})$$

When solving the linearized equation (I.3.14) regarding monochromatic waves, it can be noted that the equation of field dynamics (I.3.14) considers the medium linear dispersion according to (I.3.11):

$$\mathbf{E} = \frac{1}{2} \mathbf{e} \varepsilon_\omega e^{i(kz - \omega t)} + c. c., \quad (\text{I.3.15})$$

where ε_ω describes the spectral radiation component amplitude, the radiation being linearly polarized along the \mathbf{e} vector (I.3.15), $k(\omega)$ is the wavenumber. If the refractive index linear part dispersion can be written as $n_l(\omega) = \frac{c}{\omega} k(\omega)$ (as in (I.3.11)), the expression (I.3.15) represents the solution to the equation (I.3.14).

Employing the slowly varying envelope approximation and considering radiation propagating in one direction (as described in I.1), expression (I.3.14) can be reconstructed to the form:

$$\frac{\partial \mathbf{E}}{\partial z} + \frac{N_0}{c} \frac{\partial \mathbf{E}}{\partial t} - a \frac{\partial^3 \mathbf{E}}{\partial t^3} + b \int_{-\infty}^t \mathbf{E} dt' + g \left[(\mathbf{E} \cdot \mathbf{E}) \frac{\partial \mathbf{E}}{\partial t} + \frac{2}{3} \mathbf{E} \times \left(\mathbf{E} \times \frac{\partial \mathbf{E}}{\partial t} \right) \right] = \frac{c}{2N_0} \Delta_\perp \int_{-\infty}^t \mathbf{E} dt'. \quad (\text{I.3.16})$$

Here $g = \frac{3\varepsilon_{nl}}{2cN_0}$, z stands for the propagation direction, Δ_\perp denotes the transverse Laplacian. It can be shown that the simplified equation (I.3.16) conforms with the full refractive index dispersion of the medium expressed below when (I.3.15) is substituted into it:

$$n(\omega) = N_0 + \Delta n_l(\omega) + \Delta n_{nl}(\omega), \quad (\text{I.3.17})$$

where by the expression (I.1.7)

$$\Delta n_l(\omega) = ca\omega^2 - c \frac{b}{\omega^2}, \quad (\text{I.3.18})$$

$$\Delta n_{nl}(\omega) = \frac{1}{2} n_2 |\varepsilon_\omega|^2. \quad (\text{I.3.19})$$

For the dispersion expressed as (I.3.17), the initial assumption of resonancelessness (I.3.6) can be rewritten as:

$$N_0 \gg \Delta n_l(\omega), \Delta n_{nl}(\omega). \quad (\text{I.3.20})$$

The expression (I.3.20) is in agreement with the experimental data obtained for self-focusing ultrashort pulses in transparent media, intensity reaching the values up to 10^{14} W/cm². Thus, utilizing

Ti:sapphire laser as a source of radiation and fused silica as a medium, Δn_{nl} equals $\Delta n_{nl} = 0.1N_0$ for the intensity value $I = 5 \cdot 10^{14} \text{ W/cm}^2$

Assuming the slowly varying envelope approximation the dispersion dependence for (I.3.16) is simplified to the form:

$$n(\omega) = \sqrt{N_0^2 + 2N_0\Delta n_l(\omega)} \approx N_0 + \Delta n_l(\omega). \quad (\text{I.3.21})$$

The validity of the expression immediately follows from (I.3.20):

As mentioned above, the expression (I.3.16) describes the electric field dynamics featuring arbitrary polarization. It can be simplified in the following way considering linearly polarized radiation:

$$\frac{\partial E}{\partial z} + \frac{N_0}{c} \frac{\partial E}{\partial t} - a \frac{\partial^3 E}{\partial t^3} + b \int_{-\infty}^t E dt' + gE^2 \frac{\partial E}{\partial t} = \frac{c}{2N_0} \Delta_{\perp} \int_{-\infty}^t E dt'. \quad (\text{I.3.22})$$

Assuming $a = b = g = 0$ in (I.3.22), the resulting equation will describe the radiation diffraction in vacuum, as shown in [54]. [32] was the first to suggest the expression (I.3.22), considering the effects of diffraction, dispersion and nonlinearity, which was obtained through simplification of the wave equation and material equations characterizing polarization of electronic and vibrational nature. The expression (I.3.16) was first mentioned in [34,55].

To simplify numerical simulation for rapid estimations of the peculiarities of ultrashort pulse propagation employing the expression (I.3.22), the latter is to be normalized. It is also necessary switch to the moving coordinate system $\tau = t - \frac{N_0}{c}z$, and introduce new variables: $\tilde{E} = \frac{E}{E_0}$,

$\tilde{z} = a\omega_0^3 z$, $\tilde{y} = \frac{y}{\Delta r}$, $\tilde{x} = \frac{x}{\Delta r}$, $\tilde{t} = \omega_0 t$, where E_0 denotes the maximal incident pulse field amplitude, ω_0 is the field central frequency, and Δr its transverse coordinate. After substitutions, the expression (I.3.22) transforms to [44,45]:

$$\frac{\partial E}{\partial z} - \frac{\partial^3 E}{\partial \tau^3} + B \int_{-\infty}^{\tau} E d\tau' + GE^2 \frac{\partial E}{\partial \tau} = D \Delta_{\perp} \int_{-\infty}^{\tau} E d\tau'. \quad (\text{I.3.23})$$

The sign \sim is omitted in the expression (I.3.23). $B = 3 \left(\frac{\omega_{cr}}{\omega_0} \right)^4$, $\omega_{cr} = \left(\frac{b}{3a} \right)^{-4}$ denotes the radiation frequency, which corresponds to the medium GVD equal to zero. $G = 4 \frac{\Delta n_{nl}}{\Delta n_l}$, $\Delta n_{nl} = \frac{1}{2} n_2 E_0^2$ is the additional nonlinear term of the medium full refractive index, which is caused by the external field of the amplitude E_0 . $\Delta n_l = a c \omega_0^2$ is a linear dispersion term, and $D = \frac{c}{2N_0 \omega_0^2 \Delta r^2 \Delta n_l}$. The values of B, G and D variables depend on the media characteristics and the incident radiation parameters. The fact that one of them is stronger than the others describes the effect dominating during the propagation: normal (or anomalous) GVD, self-action or diffraction.

I.4. Femtosecond pulses field dynamics equations based on the envelope approach

Importantly, the expression (I.3.22) is more general compared to the widely used envelope dynamics approach to ultrashort pulse analysis [1,21], and, therefore, contains it as a particular case. One example is the equation modification for few-cycle pulse description [16,22]. The following substitution are applied to (I.3.22) to switch from field to envelope approach:

$$E(\mathbf{r}, t) = \frac{1}{2} \varepsilon(\mathbf{r}, t) e^{i(k_0 z - \omega_0 t)} + c. c. \quad (\text{I.4.1})$$

Here ω_0 denotes arbitrary frequency, $k_0 = \frac{\omega_0 n(\omega_0)}{c}$, where $n(\omega)$ is given by the expression (I.3.17), $\varepsilon(\mathbf{r}, t)$ is a new variable. The expression (I.3.22) takes the following form after the substitution:

$$\frac{\partial \varepsilon}{\partial z} + \frac{1}{v} \frac{\partial \varepsilon}{\partial t} + i \frac{\beta_2}{2} \frac{\partial^2 \varepsilon}{\partial t^2} - \frac{\beta_3}{6} \frac{\partial^3 \varepsilon}{\partial t^3} - \sum_{n=4}^{\infty} \beta_n \frac{i^{n+1}}{n!} \frac{\partial^n \varepsilon}{\partial t^n} - i \gamma_1 |\varepsilon|^2 \varepsilon + \gamma_2 \frac{\partial}{\partial t} (|\varepsilon|^2 \varepsilon) - \left(i \gamma_1 \varepsilon^3 - \gamma_2 \varepsilon^2 \frac{\partial \varepsilon}{\partial t} \right) \exp[2i(k_0 z - \omega_0 t)] = \frac{i}{2k_0} \Delta_{\perp} \left[\frac{\omega_0}{i} \int_{-\infty}^t \varepsilon(\mathbf{r}, t') \exp(i\omega_0(t - t')) dt' \right], \quad (\text{I.4.2})$$

where

$$V = \left(\frac{\partial k}{\partial \omega} \right)_{\omega_0}^{-1}, \beta_n = \left(\frac{\partial^n k(\omega)}{\partial \omega^n} \right)_{\omega_0}, k = \frac{N_0}{c} \omega + a \omega^3 - \frac{b}{\omega}, \gamma_1 = \frac{g \omega_0}{4}, \gamma_2 = \frac{g}{4}.$$

To analyze the dynamics of a quasi-monochromatic pulse in nonlinear media it is reasonable to assume that ω_0 features the carrier frequency in the expression (I.4.2) and $\varepsilon(\mathbf{r}, t)$, on the other hand, describes the pulse envelope. Supposing the third and the fourth terms from the expression (I.4.2) are sufficient to precisely describe the medium dispersion, while the last one, featuring the harmonics generation, is neglected, the diffraction term is transformed to the form of [44,45]:

$$\frac{i}{2k_0} \Delta_{\perp} \left[\frac{\omega_0}{i} \int_{-\infty}^t \varepsilon(\mathbf{r}, t') \exp(i\omega_0(t - t')) dt' \right] = \frac{i}{2k_0} \Delta_{\perp} \left[\varepsilon(\mathbf{r}, t) - \frac{i}{\omega_0} \frac{\partial \varepsilon(\mathbf{r}, t)}{\partial t} + \left(\frac{i}{\omega_0} \right)^2 \frac{\partial^2 \varepsilon(\mathbf{r}, t)}{\partial t^2} - \dots \right], \quad (\text{I.4.3})$$

The latter expression can be obtained by means of partial integration of the first term of the right part in expression (I.4.2). Then the known nonlinear equation of ultrashort pulse dynamics can be obtained [1,21]:

$$\frac{\partial \varepsilon}{\partial z} + \frac{1}{v} \frac{\partial \varepsilon}{\partial t} + i \frac{\beta_2}{2} \frac{\partial^2 \varepsilon}{\partial t^2} - \frac{\beta_3}{6} \frac{\partial^3 \varepsilon}{\partial t^3} - i \gamma_1 |\varepsilon|^2 \varepsilon + \gamma_2 \frac{\partial}{\partial t} (|\varepsilon|^2 \varepsilon) = \frac{i}{2k_0} \Delta_{\perp} \varepsilon. \quad (\text{I.4.4})$$

For an accurate description of the $k(\omega)$ dependence in a wide spectral range, intrinsic to few-cycle pulses, the number of dispersion orders accounted in the equation (I.4.2) can be increased preserving the integrator responsible for diffraction. However, this term can be represented in a different form, for example, as in [22]:

$$\frac{\omega_0}{i} \int_{-\infty}^t \varepsilon(\mathbf{r}, z, t') \exp(i\omega_0(t - t')) dt' = \left[1 + \frac{i}{\omega_0} \frac{\partial}{\partial t} \right]^{-1} \varepsilon(\mathbf{r}, z, t). \quad (\text{I.4.5})$$

The expression (I.4.5) validity can be easily checked by the operator $\left[1 + \frac{i}{\omega_0} \frac{\partial}{\partial t} \right]$ applied to the left and right parts of the equation.

The last term of the left part in the equation (I.4.2) is neglected when working with envelopes. This results from the fact that the approach does not account for the “fast” field oscillation dynamics. Therefore, despite the complete equivalence of the linearized equations (I.3.22) and (I.4.2) regarding nonlinearity, the latter does not consider generation of high harmonics and interaction between them and the input radiation (if no extra equations are introduced to the system), unlike the former. Moreover, advantages the envelope approach has over the work with a set of separate oscillations

almost disappear when applied to few-cycle pulses. This is explained by the fact that such pulses contain only a little more than one period of oscillation. The envelope thus loses its physical meaning, which also results in the expression (I.4.2) overcomplicated in comparison with (I.4.4) and field equation (I.3.22).

Consequently, the equation (I.3.22) transforms to the cubic nonlinear Schrödinger equation for the pulse envelope modified to take into account high orders of dispersion in the extreme case of quasi-monochromatic pulses. Thus, the equation (I.3.22) is more general than the fundamental equation of ultrashort pulse nonlinear optics. Similarly, it can be shown that expressions (I.2.2) and (I.2.3) can be converted to the Schrödinger equation in the extreme case mentioned, which is shown in [34] and [56].

As follows from the analysis above, light pulse dynamics is usually considered in the perspective of slowly varying envelope approximation. Regarding the linear propagation mode with no diffraction effect, using such equations has no advantages over the envelope approach. However, the field equation potentials for an accurate description of the diffraction contribution for the case of single-direction pulse propagation and nonlinear processes of the femtosecond pulse wide spectrum components generation and cross-modulation makes them a convenient tool for analyzing such pulses. The next section addresses the spectral approach to the propagation dynamics description of pulses featuring wide spectra (both spatial and temporal). This approach allows to accurately describe femtosecond pulse dynamics even when slowly varying envelope approximation is inapplicable. However, there are ways to modify the spectral approach to meet this assumption. One important difference of the spectral approach from field equations is a significant simplification of the non-paraxial diffraction description. Its advantages are meaningful even in the field of linear optics.

I.5. Linear equations of the spectral dynamics of non-paraxial waves

First, diffraction of monochromatic radiation (i.e. pulses featuring narrow temporal, but wide spatial spectra) is to be analyzed. For simplicity, a dielectric, nonmagnetic, isotropic and homogeneous medium is considered. For such case, the fundamental equations of classical optics, e.g. Maxwell equations, take the form [26]:

$$\begin{cases} \nabla \times \mathbf{E} = -i \frac{\omega}{c} \mathbf{H} \\ \nabla \times \mathbf{H} = i \frac{\omega}{c} \varepsilon \mathbf{E} \end{cases}, \quad (\text{I.5.1 a, b})$$

where E and H denote the amplitudes of the full electric $\mathbf{E}' = \frac{1}{2} \mathbf{E} e^{i\omega t} + c.c.$ and magnetic $\mathbf{H}' = \frac{1}{2} \mathbf{H} e^{i\omega t} + c.c.$ fields correspondingly, ω is the frequency of radiation, ε is dielectric permittivity of the medium at this frequency, c is the light velocity in vacuum. The two terms left, describing the solenoidity of vectors \mathbf{E} and \mathbf{H} (i.e. that their divergence is equal to 0), are easily derived from (I.5.1a) and thus are omitted. For convenience in operation, only the dynamics of the electric field is considered. For this purpose, the operator $\nabla \times$ should be applied to both left and right parts of the equation (I.5.1a). Then, substituting $\nabla \times \mathbf{H}$ with the right part of the equation (I.5.1b) right part and considering the electric field is solenoid, a simplified Helmholtz equation for \mathbf{E} can be obtained [26]:

$$\Delta \mathbf{E} + k^2 \mathbf{E} = 0, \quad (\text{I.5.2})$$

where $k = \frac{\omega}{c} \sqrt{\epsilon}$ is the wavenumber. Due to the equation (I.5.2) linearity and k scalarity, the field dynamics can be analysed for each of the Cartesian components separately solving the scalar Helmholtz equation with different boundary conditions considered for each of them.

Supposing that $E \rightarrow 0$ and $\frac{\partial E}{\partial x}, \frac{\partial E}{\partial y} \rightarrow 0$ at $x, y \rightarrow \pm\infty$, i.e. the radiation propagates along z axis, the spatial spectrum can be written as:

$$g(k_x, k_y, z) = \int_{-\infty}^{\infty} \int_{-\infty}^{\infty} E(x, y, z) e^{-i(k_x x + k_y y)} dx dy, \quad (\text{I.5.3})$$

with k_x, k_y referring to spatial frequencies. Using (I.5.3), Helmholtz equation can be rewritten to obtain [57]:

$$\frac{d^2 g}{dz^2} + (k^2 - k_x^2 - k_y^2) g = 0. \quad (\text{I.5.4})$$

The equation (I.5.4) is a second order ordinary differential equation with the solution of the following form:

$$g(k_x, k_y, z) = c_1(k_x, k_y) e^{-i\sqrt{k^2 - k_x^2 - k_y^2} z} + c_2(k_x, k_y) e^{+i\sqrt{k^2 - k_x^2 - k_y^2} z}, \quad (\text{I.5.5})$$

where arbitrary constants c_1 and c_2 are defined according to the boundary conditions.

The solution (I.5.5) has two terms, the first one describing the wave diffraction along the propagation direction, and the second one referring to the backward diffraction. As follows from the (I.5.5), the equation (I.5.4) can be simplified to the form below considering the diffraction along the propagation direction only (i.e. $c_2 = 0$):

$$\frac{dg}{dz} + \sqrt{k^2 - k_x^2 - k_y^2} \cdot g = 0. \quad (\text{I.5.6})$$

For a wide input pulse (i.e. at $z = 0$) changing smoothly in transverse coordinate, its spectrum is narrow. In this case, the following equation is valid for all the components of the spectrum:

$$\{k_x^2, k_y^2\} \ll k^2, \quad (\text{I.5.7})$$

and thus, the expression (I.5.6) can be reconstructed to [58]:

$$\frac{dg}{dz} + i \left[k - \frac{k_x^2 + k_y^2}{2k} - \frac{(k_x^2 + k_y^2)^2}{8k^3} - \dots \right] g = 0. \quad (\text{I.5.8})$$

The expressions obtained for the case of unidirectional propagation (I.5.6) and (I.5.8) represents the known non-paraxial and paraxial diffraction equations correspondingly. Performing their Fourier transform

$$EE(x, y, z) = \frac{1}{4\pi^2} \int_{-\infty}^{\infty} \int_{-\infty}^{\infty} g(k_x, k_y, z) e^{+i(k_x x + k_y y)} dk_x dk_y, \quad (\text{I.5.9})$$

one can get their field equivalents.

For example, accounting for the expressions (I.5.8) and (I.5.9), the paraxial field evolution equation is [58]:

$$\frac{\partial E}{\partial z} + ikE + \frac{i}{2k} \frac{\partial^2 E}{\partial x^2} + \frac{i}{2k} \frac{\partial^2 E}{\partial y^2} - \frac{i}{8k^3} \frac{\partial^4 E}{\partial x^4} - \frac{i}{4k^3} \frac{\partial^4 E}{\partial x^2 \partial y^2} - \frac{i}{8k^3} \frac{\partial^4 E}{\partial y^4} + \dots = 0. \quad (\text{I.5.10})$$

Introducing the following substitution

$$E = \varepsilon e^{-ikz} \quad (\text{I.5.11})$$

and considering the expression (I.5.10) terms with the transverse coordinate derivatives lower than the second order, the equation can be reconstructed to a parabolic one:

$$-2ik \frac{\partial \varepsilon}{\partial z} + \frac{\partial^2 \varepsilon}{\partial x^2} + \frac{\partial^2 \varepsilon}{\partial y^2} = 0. \quad (\text{I.5.12})$$

Equation (I.5.12) represents the Fresnel diffraction widely known and used in linear optics. The equation (I.5.12) can be derived from the Helmholtz equation under the approximation of slowly varying amplitude with substitution of (I.5.11) [26]:

$$k \left| \frac{\partial \varepsilon}{\partial z} \right| \gg \left| \frac{\partial^2 \varepsilon}{\partial z^2} \right|. \quad (\text{I.5.13})$$

Thus, slowly varying amplitude approximation (I.5.13) is similar to paraxial approximation in linear optics.

Regarding non-paraxial diffraction, the expression (I.5.6) has a field equivalent [59]:

$$\frac{\partial E}{\partial z} + \frac{1}{4\pi^2} \int_{-\infty}^{\infty} \int_{-\infty}^{\infty} E(x', y', z) S(x - x', y - y') dx' dy' = 0, \quad (\text{I.5.14})$$

where [60]

$$S(x, y) = \frac{i\sqrt{2\pi^3 k}}{\sqrt{(x^2 + y^2)^3}} H_{3/2}^{(1)}(k\sqrt{(x^2 + y^2)}),$$

$H_{3/2}^{(1)}(x)$ is the Hankel function.

Derived significantly later than (I.5.12), the equation (I.5.14) is rarely quoted. There is instead a more common equivalent of (I.5.5) for the unidirectional propagation (i.e. $c_2 = 0$):

$$E(x, y, z) = -i \frac{kz}{2\pi} \int_{-\infty}^{\infty} \int_{-\infty}^{\infty} E(x', y', 0) \frac{e^{ik\sqrt{(x-x')^2 + (y-y')^2 + z^2}}}{(x-x')^2 + (y-y')^2 + z^2} \times \left(1 - \frac{1}{ik\sqrt{(x-x')^2 + (y-y')^2 + z^2}} \right) dx' dy'. \quad (\text{I.5.15})$$

Here x', y' refer to the spatial coordinates at $z = 0$. The equation (I.5.15) represents the analytical expression of Huygens–Fresnel principle [41] if $k\sqrt{x^2 + y^2 + z^2} \gg 1$.

Consequently, expression (I.5.5) and differential equations (I.5.6) and (I.5.8) obtained by the spectral approach, have very cumbersome analogous (I.5.14) and (I.5.10) equivalents as well as (I.5.15). Therefore, numerical simulation and analysis of the diffraction are conducted significantly easier employing spectral approach, considering there is a wide range of mathematical software to perform fast Fourier transform [61]. The latter is crucial, especially for wide spatial spectrum radiation.

It is important that few Helmholtz equation (I.5.2) solutions solve the initial Maxwell's equations (I.5.1) as well. Thus, (I.5.2) satisfies them only in the case of linearly polarized pulses featuring wide spatial spectrum. Then, for example, the solution along x axis can take the form of (I.5.5), being equal to zero along y and z axes. However, one characteristic of such pulses is their divergence during propagation, which conflicts with the equation (I.5.1). In this case, the solenoidal field condition can be employed to simplify the Helmholtz equation solution for the field transverse components E_x and E_y and the longitudinal component E_z :

$$\frac{\partial E_z}{\partial z} = -\frac{\partial E_x}{\partial x} - \frac{\partial E_y}{\partial y}. \quad (\text{I.5.16})$$

For the spatial spectrum, equation (I.5.3) can be written as follows [59]:

$$\frac{\partial g_z}{\partial z} = -ik_x g_x - ik_y g_y. \quad (\text{I.5.17})$$

Considering the case of unidirectional propagation and the expression (I.5.6), (I.5.17) can be rewritten as:

$$g_z = \frac{k_x}{\sqrt{k^2 - k_x^2 - k_y^2}} g_x + \frac{k_y}{\sqrt{k^2 - k_x^2 - k_y^2}} g_y. \quad (\text{I.5.18})$$

Obviously, the expression (I.5.18) is crucial when working with light fields of wide spatial spectrum. It can then be concluded that some studies of non-paraxial diffraction by means of Helmholtz (in the case of monochromatic radiation) or wave equations (if pulses are ultrashort) solve Maxwell's equations only partially [62,63]. Such solutions can be obtained as described above, but also through some other approaches. [63] suggests that the solution takes the form of a vector rotor, basing on the field scalar projections on Cartesian coordinates. The solution mentioned represents the that of the wave equation (and Helmholtz equation as well if the radiation is considered as monochromatic). Now the radiation of an infinitely narrow spatial, but ultrawide temporal spectra is addressed. The case obviously denotes transversely homogeneous plane wave dispersion. The medium of propagation is still considered as dielectric, non-magnetic, homogeneous and isotropic. Maxwell's equations can then be reduced to [26]:

$$\frac{\partial^2 \mathbf{E}}{\partial z^2} - \frac{1}{c^2} \frac{\partial^2 \mathbf{D}}{\partial z^2} = 0, \quad (\text{I.5.19})$$

where z is the propagation direction. Electric induction D is expressed as follows if there is no spatial dispersion present:

$$\mathbf{D} = \int_{-\infty}^{\infty} \varepsilon(t - t') \mathbf{E}(t') dt', \quad (\text{I.5.20})$$

where $\varepsilon(t)$ is a function of the medium inertia response.

Here, the equation (I.5.19) solution written in the form of a transverse wave satisfies the Maxwell's equations as well.

Each transverse coordinate (x and y) temporal spectrum can be represented as:

$$G(\omega, z) = \int_{-\infty}^{\infty} E(t, z) e^{-i\omega t} dt. \quad (\text{I.5.21})$$

where ω is the frequency variable. Using the expressions (I.5.20) and (I.5.21), the equation (I.5.9) can be rewritten to describe the spectrum:

$$\frac{\partial^2 G}{\partial z^2} + \frac{\omega^2 n^2(\omega)}{c^2} G = 0. \quad (\text{I.5.22})$$

Here $n(\omega)$ denote the medium refractive index in case of monochromatic radiation of frequency ω , given by $n(\omega) = \int_{-\infty}^{\infty} \tilde{n}(t) e^{-i\omega t} dt$.

The differential equation (I.5.22) solution can be written as:

$$G(\omega, z) = D_1(\omega) e^{-i\frac{\omega n(\omega)}{c} z} + D_2(\omega) e^{+i\frac{\omega n(\omega)}{c} z}, \quad (\text{I.5.23})$$

where values of D_1 and D_2 are defined according to the given boundary conditions. Like in (I.5.5), the first term in (I.5.23) characterizes the wave dispersion propagating forward along the z axis and the second one - backward.

Thus, with $D_2 = 0$ the equation (I.5.23) characterizes the case of unidirectional propagation, described by the following form of the expression (I.5.22):

$$\frac{\partial G}{\partial z} + i \frac{\omega n(\omega)}{c} G = 0. \quad (\text{I.5.24})$$

The equation (I.5.24) makes it possible to analyze the radiation dynamics for propagation in media with arbitrary dispersion even of a compound form, for example, given by Zelmeyer's formula [27]. However, regarding the main and most common case of the radiation, featuring spectrum that lies entirely in the media transparency window, the dispersion dependence can be described by the series (I.1.7).

The equation (I.5.24) field equivalent can be characterized by the following integro-differential equation:

$$\frac{\partial E}{\partial z} + \frac{1}{c} \frac{\partial}{\partial t} \int_{-\infty}^{\infty} \tilde{n}(t - t') E(t') dt' = 0, \quad (\text{I.5.25})$$

where $\tilde{n}(t - t') = \frac{1}{2\pi} \int_{-\infty}^{\infty} n(\omega) e^{i\omega(t-t')} d\omega$ describes the medium response inertia.

In view of the above, the refractive index dispersion can be written in the series form (I.1.7), the expression (I.5.25) for dielectrics will take the form (I.1.6), where

$$E(t, z) = \frac{1}{2\pi} \int_{-\infty}^{\infty} G(\omega, z) e^{i\omega t} d\omega.$$

The equation (I.1.6) is derived from (I.5.24) under the assumption of $E \rightarrow 0$ at $t \rightarrow -\infty$.

Employing the substitution (I.4.1), where $n(\omega)$ is described by the equation (I.1.7), and ω_0 denotes the frequency corresponding to the expression (I.1.7), it becomes possible to express the complex amplitude ε in the form of:

$$\frac{\partial \varepsilon}{\partial z} + \beta_1 \frac{\partial \varepsilon}{\partial t} + \frac{i}{2} \beta_2 \frac{\partial^2 \varepsilon}{\partial t^2} - \frac{1}{6} \beta_3 \frac{\partial^3 \varepsilon}{\partial t^3} - \dots = 0. \quad (\text{I.5.26})$$

Here

$$\beta_n = \left(\frac{\partial^n k}{\partial \omega^n} \right)_{\omega=\omega_0}, n = 1,2,3; k(\omega) = \frac{\omega n(\omega)}{c}.$$

The requirement for the variable ε from (I.5.26) to characterize the pulse complex envelope is ω_0 being the incident radiation central frequency. To reduce (I.5.26) for the calculation simplicity, it is not the (I.1.7) but the positive power of ω series that is to be used to approximate the dependence $k(\omega)$. However, this results in the reduction of the dispersion dependence accuracy compared to the (I.1.7), the number of terms being the same.

Both (I.1.6) and (I.5.26) can be obtained directly from (I.5.19), using the approximation of slowly varying pulse envelope ε (like in I.1 and I.4). The approximation validity for weak dispersion media case is obvious. Moreover, such requirement to the dispersion magnitude is needed only for the frequency range coinciding with the pulse spectrum. Consequently, slowly varying envelope approximation can describe the dynamics of wide spectrum pulses quite accurately for linear propagation in dielectrics featuring wide transparency window, contrary to a wide-spread presumption [1,21]. For this purpose, the pulse spectrum is to lie in the range complying with (I.3.20) and the dependences $n(\omega)$ or $k(\omega)$ to be sufficiently characterized by small number of power series terms. Thus, if the conditions are met correctly, the slowly varying envelope approximation can be employed even to accurately describe the supercontinuum generation process [10,64].

Hence, the differential spectral equation (I.5.24) has its simple field equivalents (I.1.6) and (I.5.26) (in contrast to the integral-differential equation (I.5.25)) if the medium dispersion can be well approximated by a small number of power series terms throughout the entire pulse spectrum range. However, it is difficult to meet the requirements mentioned when working with radiation featuring wide spectrum, the dynamics of which is the focus of this work.

Concluding the section, a generalization of the simplified dynamics equations of spatial (I.5.6), (I.5.18) and temporal (I.5.24) spectra, which can be quite wide in an arbitrary case, can be given:

$$\begin{cases} \frac{dg_x}{dz} + i \frac{\omega n(\omega)}{c} \sqrt{1 - \frac{c^2 k_x^2}{\omega^2 n^2(\omega)} - \frac{c^2 k_y^2}{\omega^2 n^2(\omega)}} \cdot g_x = 0 \\ \frac{dg_y}{dz} + i \frac{\omega n(\omega)}{c} \sqrt{1 - \frac{c^2 k_x^2}{\omega^2 n^2(\omega)} - \frac{c^2 k_y^2}{\omega^2 n^2(\omega)}} \cdot g_y = 0 \\ \frac{dg_z}{dz} + ik_x g_x + ik_y g_y = 0 \end{cases} \quad (\text{I.5.27})$$

Here

$$g_i(\omega, k_x, k_y) = \int_{-\infty}^{\infty} \int_{-\infty}^{\infty} \int_{-\infty}^{\infty} E(t, x, y, z) e^{i(\omega t - k_x x - k_y y)} dt dx dy$$

denote the spatio-temporal spectra of the field components E_i , where $i = x, y, z$ are Cartesian coordinates.

I.6. Nonlinear equations of the spectrum dynamics of non-paraxial waves

To demonstrate the prospects of the spatio-temporal spectra dynamics equations in case of propagation in nonlinear media, a scalar analysis of the self-action between two-dimensional waves featuring linear TE-polarization can be made to generalize the spectral approach. It is also supposed that z is the radiation propagation direction, x denotes the transverse coordinate, and y is the radiation polarization direction. The propagation medium is considered as isotropic and homogeneous and has

arbitrary dispersion dependence $n(\omega)$. The medium electric induction nonlinear part can be represented in a simple form, i.e. $D_{nl} = \varepsilon_{nl}E^3$. In this case, $\varepsilon_{nl} = 4\pi\chi$ describes the nonlinear permittivity with χ denoting the medium nonlinear susceptibility. As mentioned above, such assumption for the nonlinear response can be taken as valid, with nonresonant nonlinearity of electronic nature. Almost inertialess nonresonant nonlinearity of dielectrics in the field of ultrashort pulses is justified by their weak nonlinear refractive index coefficient dispersion throughout almost entire transparency window [43].

Considering the above assumptions, the expression for the radiation temporal spectrum dynamics in dielectric media (I.3.1)

$$G(z, x, \omega) = \int_{-\infty}^{\infty} E(z, x, t) e^{-i\omega t} dt$$

can be rewritten as [46]

$$\frac{\partial^2 G}{\partial z^2} + \frac{\partial^2 G}{\partial x^2} + \frac{\omega^2 n^2(\omega)}{c^2} G + \frac{\chi \omega^2}{\pi c^2} \int_{-\infty}^{\infty} \int_{-\infty}^{\infty} G(\omega - \alpha) G(\alpha - \beta) G(\beta) d\alpha d\beta = 0. \quad (\text{I.6.1})$$

The equation (I.6.1), in turn, can be rewritten for spatio-temporal spectrum

$$g(z, k_x, \omega) = \int_{-\infty}^{\infty} G(z, x, \omega) e^{ik_x x} dx$$

in the following form:

$$\frac{\partial^2 g}{\partial z^2} + \left(\frac{\omega^2 n^2(\omega)}{c^2} - k_x^2 \right) g + \frac{\chi \omega^2}{4\pi^3 c^2} \int_{-\infty}^{\infty} \int_{-\infty}^{\infty} \int_{-\infty}^{\infty} g(k_x - m_x - n_x, \omega - \alpha) \times g(m_x, \alpha - \beta) g(n_x, \beta) dm_x dn_x d\alpha d\beta = 0 \quad (\text{I.6.2})$$

To change from (I.6.1) to (I.6.2) the following expression is employed:

$$\frac{1}{2\pi} \int_{-\infty}^{\infty} e^{i(-k_x + l_x + m_x + n_x)x} dx = \delta(-k_x + l_x + m_x + n_x).$$

Expressions (I.6.1) and (I.6.2) characterize light propagation in both directions along the z axis and their interaction due to the medium nonlinearity.

The following expression represents the solution of (I.6.2):

$$(z, k_x, \omega) = C_1(k_x, \omega) \exp\left(-i \frac{\omega n(\omega)}{c} \sqrt{1 - \frac{k_x^2 c^2}{\omega^2 n^2(\omega)}} z\right) + C_2(k_x, \omega) \exp\left(i \frac{\omega n(\omega)}{c} \sqrt{1 - \frac{k_x^2 c^2}{\omega^2 n^2(\omega)}} z\right), \quad (\text{I.6.3})$$

with C_1 and C_2 being the parameters of integration. Similarly to the above solutions, the first term in (I.6.3) characterizes propagation in positive z -direction, whereas the second one refers to the negative one. The expression (I.6.3) demonstrates that if propagation is unidirectional ($C_2 = 0$), the non-paraxial diffraction can be described as follows, within linear mode:

$$\frac{\partial g}{\partial z} + i \frac{\omega n(\omega)}{c} \sqrt{1 - \frac{k_x^2 c^2}{\omega^2 n^2(\omega)}} g = 0. \quad (\text{I.6.4})$$

The expression (I.6.4) generally relates to linear radiation propagation modes. Its nonlinear equivalent is given by:

$$\frac{\partial g}{\partial z} + i \frac{\omega n(\omega)}{c} \sqrt{1 - \frac{k_x^2 c^2}{\omega^2 n^2(\omega)}} g + \chi N(g) = 0, \quad (\text{I.6.5})$$

where $N(g)$ denotes the undefined nonlinear parameter.

As discussed in detail in section I.5, the physical meaning of (I.6.2) to (I.6.4) change is switching to unidirectional radiation propagation analysis. Obviously, the equation (I.6.4) solution only partially solves (I.6.2). As soon as the fact the solution of (I.6.5) solves (I.6.2) as well, it becomes possible to find the value of the nonlinear parameter $N(g)$. To achieve it, the idea from [65] will help differentiate the expression (I.6.5) over z to then express $\frac{\partial g}{\partial z}$ in terms of g :

$$\begin{aligned} \frac{\partial}{\partial z} \left(\frac{\partial g}{\partial z} + i \frac{\omega n(\omega)}{c} \sqrt{1 - \frac{k_x^2 c^2}{\omega^2 n^2(\omega)}} g + \chi N(g) \right) &= \frac{\partial^2 g}{\partial z^2} + \left(\frac{\omega^2 n^2(\omega)}{c^2} - k_x^2 \right) g - \\ i \frac{\omega n(\omega)}{c} \sqrt{1 - \frac{k_x^2 c^2}{\omega^2 n^2(\omega)}} \chi N(g) + \chi \frac{\partial}{\partial z} N(g) &= 0 \end{aligned} \quad (I.6.6)$$

The following expression for $N(g)$ is obtained through comparison between (I.6.6) and (I.6.2):

$$\begin{aligned} -i \frac{\omega n(\omega)}{c} \sqrt{1 - \frac{k_x^2 c^2}{\omega^2 n^2(\omega)}} N(g) + \frac{\partial}{\partial z} N(g) &= \frac{\omega^2}{4\pi^3 c^2} \int_{-\infty}^{\infty} \int_{-\infty}^{\infty} \int_{-\infty}^{\infty} \int_{-\infty}^{\infty} g(k_x - m_x - n_x, \omega - \alpha) \times \\ g(m_x, \alpha - \beta) g(n_x, \beta) dm_x dn_x d\alpha d\beta & \end{aligned} \quad (I.6.7)$$

Then, $N(g)$ can be written as:

$$\begin{aligned} N(g) &= \int_{-\infty}^{\infty} \int_{-\infty}^{\infty} \int_{-\infty}^{\infty} \int_{-\infty}^{\infty} \Phi(k_x, \omega, m_x, n_x, \alpha, \beta) \times g(k_x - m_x - n_x, \omega - \alpha) \times g(m_x, \alpha - \\ \beta) g(n_x, \beta) dm_x dn_x d\alpha d\beta & \end{aligned} \quad (I.6.8)$$

where $\Phi(k_x, \omega, m_x, n_x, \alpha, \beta)$ denotes a yet unknown function. In order to define it, the following equations are required to be processed with high accuracy:

$$\begin{aligned} \frac{\partial}{\partial z} g(k_x - m_x - n_x, \omega - \alpha) &\approx -i \frac{(\omega - \alpha)n(\omega - \alpha)}{c} \sqrt{1 - \frac{(k_x - m_x - n_x)^2 c^2}{(\omega - \alpha)^2 n^2(\omega - \alpha)}} g, \\ \frac{\partial}{\partial z} g(m_x, \alpha - \beta) &\approx -i \frac{(\alpha - \beta)n(\alpha - \beta)}{c} \sqrt{1 - \frac{m_x^2 c^2}{(\alpha - \beta)^2 n^2(\alpha - \beta)}} g, \\ \frac{\partial}{\partial z} g(n_x, \beta) &\approx -i \frac{\beta n(\beta)}{c} \sqrt{1 - \frac{n_x^2 c^2}{\beta^2 n^2(\beta)}} g, \end{aligned} \quad (I.6.9)$$

Equations (I.6.7) and (I.6.8) together provide then:

$$\Phi = i \frac{\omega^2}{4\pi^3 c} \varphi,$$

where

$$\begin{aligned} \varphi(k_x, \omega, m_x, n_x, \alpha, \beta) &= \left(\omega n(\omega) \sqrt{1 - \frac{k_x^2 c^2}{\omega^2 n^2(\omega)}} + (\omega - \alpha)n(\omega - \alpha) \sqrt{1 - \frac{(k_x - m_x - n_x)^2 c^2}{(\omega - \alpha)^2 n^2(\omega - \alpha)}} + \right. \\ \left. (\alpha - \beta)n(\alpha - \beta) \sqrt{1 - \frac{m_x^2 c^2}{(\alpha - \beta)^2 n^2(\alpha - \beta)}} + \beta n(\beta) \sqrt{1 - \frac{n_x^2 c^2}{\beta^2 n^2(\beta)}} \right)^{-1} & \end{aligned} \quad (I.6.10)$$

Thus, the reduced nonlinear equation characterizing the spatial spectrum non-paraxial dynamics in case of unidirectional propagation can be represented as [46]:

$$\frac{\partial g}{\partial z} + i \frac{\omega n(\omega)}{c} \sqrt{1 - \frac{k_x^2 c^2}{\omega^2 n^2(\omega)}} g + i \frac{\chi \omega^2}{4\pi^3 c^2} \int_{-\infty}^{\infty} \int_{-\infty}^{\infty} \int_{-\infty}^{\infty} \int_{-\infty}^{\infty} \varphi(k_x, \omega, m_x, n_x, \alpha, \beta) \times g(k_x - m_x - n_x, \omega - \alpha) \times g(m_x, \alpha - \beta) \times g(n_x, \beta) dm_x dn_x d\alpha d\beta = 0$$
(I.6.11)

with φ obtained from the expression (I.6.10).

Applying the substitution (I.6.6) and the equations (I.6.7)–(I.6.10), it is easy to show that the equation (I.6.11) can be transformed to the form (I.6.2) with an accuracy up to the fifth order in g .

The expression obtained (I.6.11) is general enough allowing to analyze the wide (both spatial and temporal) spectrum radiation nonlinear dynamics. Using the equation (I.6.11), it becomes possible to accurately describe the phenomenon of spectral supercontinuum generation, as the expression (I.6.11) considers the refractive index linear part dispersion as arbitrary and there is almost no electrically induced nonlinear refractive index dispersion for the spectral range lying in transparency window of many dielectrics [41]. Another way to describe the radiation spatial spectrum broadening (i.e. occurring due to the self-focusing effect) is employing the equation (I.6.11) under the condition that the width is commensurate with the wavenumber. For the spatial frequency spectrum containing k_x values over the wavenumber, the second term in (I.6.11) is real. Such components correspond to the spatial spectrum, which varies along the z -direction similarly to the field change in case of total internal reflection. To correctly analyze propagation of radiation, featuring ultrawide spatial spectrum, the backwardly propagating wave generation needs to be considered.

Importantly, the pulse spectrum non-paraxial dynamics equation (I.6.11) can be easily generalized for the case of the medium featuring inertia nonlinearity of the response. For example, in [66] the spectral equation nonlinear term considers both Raman and inertialess electric nonlinearities. The spectral approach is supposed to be further developed nonlinearly generalizing the equation (I.5.27) [67]. The authors in [68,69] discuss the importance of the longitudinal field component consideration in case of the non-paraxial radiation self-focusing, however, considering only quasi-monochromatic radiation.

There is an advantage of the spectral approach over that addressing field when constructing the nonlinear dynamics equations that would be worth mentioning. It is easy to obtain iterative solutions in case of the spectral approach as the linearized equation usually has a rather simple form. It can be used as the initial iterative solution. An approximate solution of (I.6.11) can show it.

Substitution below is used

$$g(z, k_x, \omega) = U(z, k_x, \omega) \exp\left(-i \frac{\omega n(\omega)}{c} \sqrt{1 - \frac{k_x^2 c^2}{\omega^2 n^2(\omega)}} z\right),$$
(I.6.12)

which is the linearized equation (I.6.11) solution when $U = \text{const}$. Further applying Pickard's successive approximation method [70] the following expression can be obtained after the first interaction for the spectrum (I.6.12) complex amplitude [65]

$$U(z, k_x, \omega) = U_0(k_x, \omega) + \frac{\chi\omega^2}{4\pi^3} \int_{-\infty}^{\infty} \int_{-\infty}^{\infty} \int_{-\infty}^{\infty} \int_{-\infty}^{\infty} f(k_x, \omega, m_x, n_x, \alpha, \beta) \times U_0(k_x - m_x - n_x, \omega - \alpha) \times U_0(m_x, \alpha - \beta) U_0 g(n_x, \beta) dm_x dn_x d\alpha d\beta \quad (I.6.13)$$

where

$$f(k_x, \omega, m_x, n_x, \alpha, \beta) = \left\{ \exp \exp \left[-i \frac{z}{c} \left(\varphi^{-1} - 2\omega n(\omega) \sqrt{1 - \frac{k_x^2 c^2}{\omega^2 n^2(\omega)}} \right) \right] - 1 \right\} \times \varphi \left[\varphi^{-1} - 2\omega n(\omega) \sqrt{1 - \frac{k_x^2 c^2}{\omega^2 n^2(\omega)}} \right]^{-1} \quad (I.6.14)$$

where $U_0(k_x, \omega)$ stands for the spatio-temporal spectrum of the incident radiation (i.e. $z = 0$).

For the value of

$$\varphi^{-1} - 2\omega n(\omega) \sqrt{1 - \frac{k_x^2 c^2}{\omega^2 n^2(\omega)}} = 0$$

the expression below becomes valid:

$$f = -i \frac{z}{c\varphi}.$$

If $\varphi \rightarrow 0$ (as implied by the equation (I.6.11)), then $f \rightarrow 0$ as well. For $\omega \rightarrow 0$ the following expression is fulfilled:

$$\omega n(\omega) \sqrt{1 - \frac{k_x^2 c^2}{\omega^2 n^2(\omega)}} \rightarrow -ik_x c.$$

I.7. Spectral approach for femtosecond pulse reduction to the field equations of pulse dynamics

The nonlinear spectral equation (I.6.11) characterizing non-paraxial ultrawide temporal spectrum pulse dynamics includes both the particular case and the spectral and field equations quoted above [58].

Supposing radiation being monochromatic and featuring frequency ω_0 , that implies

$$g(k_x, \omega) = \pi g(k_x) \delta(\omega - \omega_0) + \pi g^*(k_x) \delta(\omega + \omega_0), \quad (I.7.1)$$

the expression (I.6.11) can be rewritten in the form of a non-paraxial monochromatic radiation self-focusing equation, neglecting harmonic generation [47]:

$$\frac{\partial g}{\partial z} + ik \sqrt{1 - \frac{k_x^2}{k^2}} g + i \frac{3k^2 \chi}{4\pi n^2(\omega_0)} \int_{-\infty}^{\infty} \int_{-\infty}^{\infty} \frac{g^*(\alpha - k_x) g(\alpha - \beta) g(\beta) d\alpha d\beta}{\sqrt{1 - \frac{k_x^2}{k^2}} \left(\sqrt{1 - \frac{(k_x - \alpha)^2}{k^2}} \right)^* + \sqrt{1 - \frac{(\alpha - \beta)^2}{k^2}} + \sqrt{1 - \frac{\beta^2}{k^2}}} = 0. \quad (I.7.2)$$

Obviously, regarding the extreme case of a plane wave propagation along the z -axis, the following expression is valid:

$$g(k_x, \omega) = 2\pi G(\omega) \delta(k_x), \quad (I.7.3)$$

which means the equation (I.6.11) takes the form of:

$$\frac{\partial G}{\partial z} + i \frac{\omega n(\omega)}{c} G + i \frac{\chi \omega^2}{\pi c} \int_{-\infty}^{\infty} \int_{-\infty}^{\infty} \frac{G(\omega-\alpha)G(\alpha-\beta)G(\beta)dad\beta}{\omega n(\omega) + (\omega-\alpha)n(\omega-\alpha) + (\alpha-\beta)n(\alpha-\beta) + \beta n(\beta)} = 0. \quad (\text{I.7.4})$$

The equation (I.7.4) describes spectral supercontinuum generation in a strong-dispersion waveguide. This equation was first obtained in [30]. The work suggests a technique to transform the expression (I.7.4) for weak dispersion as well. It takes the form of a known nonlinear field equation (I.2.1), which can be derived using slowly varying envelope approximation [32].

The equation (I.6.11) can be reduced to the following form assuming paraxial radiation and 1 weak dispersion of medium features [58]:

$$\frac{\partial g}{\partial z} + i \frac{\omega N_0}{c} g + i \frac{\omega[n(\omega)-N_0]}{c} g - i \frac{k_x^2 c}{2\omega N_0} g + i \frac{\chi \omega}{8\pi^3 c N_0} \int_{-\infty}^{\infty} \int_{-\infty}^{\infty} \int_{-\infty}^{\infty} \int_{-\infty}^{\infty} g(k_x - m_x - n_x, \omega - \alpha) \times g(m_x, \alpha - \beta) \times g(n_x, \beta) dm_x dn_x dad\beta = 0 \quad (\text{I.7.5})$$

The equation above is the spectral equivalent of the field equation:

$$\frac{\partial E}{\partial z} + \frac{N_0}{c} \frac{\partial E}{\partial t} - \alpha \frac{\partial^3 E}{\partial z^3} - \frac{c}{2N_0} \frac{\partial^2}{\partial x^2} \int_{-\infty}^t E dt' + \frac{2\pi\chi}{cN_0} E^2 \frac{\partial E}{\partial t} = 0, \quad (\text{I.7.6})$$

The expression (I.7.6) represents a two-dimensional version of the equation (I.3.22). The refractive index dispersion dependence (I.1.7) is limited by the first frequency-dependent term only when writing the equation (I.7.6).

To conclude, it was previously shown that the spectral approach is significantly more convenient than the one using fields when radiation features ultrawide temporal and spatial spectra. The fact was first proven for linear optics, by comparing the integro-differential and partial-derivative field dynamics equations with their spectral analogues, that are ordinary differential equations. It was shown then that this advantage in spectral equation construction simplicity can be employed to serve the nonlinear optics requirements as well. A way to generalize the reduced spectral equations of linear optics in case of ultrashort pulse nonlinear propagation (both temporal and spatial spectra being ultrawide) has been introduced. Regarding the extreme cases, the spectral equations take the form of already known equations, i.e. non-paraxial monochromatic radiation self-focusing or spectral supercontinuum generation in waveguides. It has also been demonstrated that their field equivalents are relatively simple only under assumptions of paraxial radiation and weak medium dispersion, which are valid for multiple practical cases. Spectral approach is still highly useful in such cases as it helps to understand the limits for field approach applicability.

The field and spectral equations discussed earlier in this section allow to analytically describe multiple effects of ultrashort pulse nonlinear optics. To proceed, it would be logical to discuss the nonlinear dynamics in optical waveguides fitting the transversely homogeneous plane wave assumption (described in section I.1).

I.8. Femtosecond pulses self-action in waveguides

The section focuses on the self-action of high-intensity femtosecond pulses featuring few oscillations. For example, the widely used Ti:sapphire laser generates pulses of 20-30 fs, which corresponds to ca. 10 full electromagnetic field oscillation cycles. Exposed to such pulses, nonlinear media appear to show new features, since their short duration allows to use higher intensity without damaging or destroying the medium. This propels the study of well-known nonlinear effects and light-matter

interaction to the next level. For example, it results in self-phase and cross-phase modulation leading to spectral supercontinuum generation, which inevitably destroys the medium if the pulses have longer duration. The previously discussed field and spectral approaches can be employed to describe the process of generating such ultrawide spectrum radiation.

First, the basics of few-cycle pulse propagation laws will be considered provided the radiation is of low-intensity.

I.8.1. Femtosecond pulses dispersion broadening

The nonlinear term can be omitted from the wave equation (I.2.1), provided the radiation is of low-intensity. It can be then written as follows:

$$\frac{\partial E}{\partial z} - a \frac{\partial^3 E}{\partial \tau^3} + b \int_{-\infty}^{\tau} E d\tau' = 0. \quad (\text{I.8.1})$$

Figures I.1–I.3 demonstrate the solution for the equation above. Broadening the dispersion influences the pulse as

$$E(0, \tau) = E_0 e^{-\frac{\ln 2}{2} \left(\frac{2\tau}{\tau_p}\right)^2} \cos(\omega_0 \tau), \quad (\text{I.8.2})$$

during its propagation. Here E_0 denotes the incident field amplitude maximum, τ_p is the pulse duration at full width half maximum, and ω_0 is the radiation central frequency [22]. Suppose that $\tau_p = 2T$ with $T = \frac{2\pi}{\omega_0}$. This implies that the pulse contains two full field oscillations at the input of the medium.

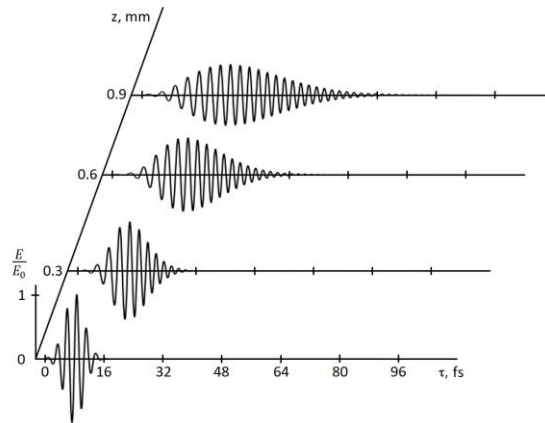


Fig. I.1. Few-cycle femtosecond pulse dispersion broadening in fused silica. The radiation spectrum lies in normal GVD range.

Figure I.1 demonstrates dispersion broadening of a pulse, the spectrum of which lies in the fiber normal group dispersion range under the assumption of $\omega_0 = 1.63\omega_{cr}$ with $\omega_{cr} = \sqrt[4]{\frac{b}{3a}}$ denoting the zero group velocity dispersion frequency (i.e. $\frac{\partial^2 k}{\partial \omega^2} = 0$ in (I.1.7)). The latter relation corresponds to the wavelength value of $\lambda_0 = \frac{2\pi c}{\omega_0} = 0.78 \mu\text{m}$ at $\lambda_{cr} = \frac{2\pi c}{\omega_{cr}} = 1.27 \mu\text{m}$ for fused silica [21]. Figure I.1 shows that the pulse featuring spectrum lying in the normal GVD range broadens during propagation

in the medium, with shorter oscillation period in its tail part relatively to the front, meaning a linear frequency modulation takes place.

Figure I.2 illustrates few-cycle femtosecond pulse field dynamics in fused silica at $\omega_0 = 0.85\omega_{cr}$ (i.e. $\lambda_0 = 1.5 \mu m$), its spectrum then lies in the medium anomalous GVD region. It shows that broadening is a backward process as referred to the case in Figure I.1, as the pulse oscillation period is longer in its tail than in its front.

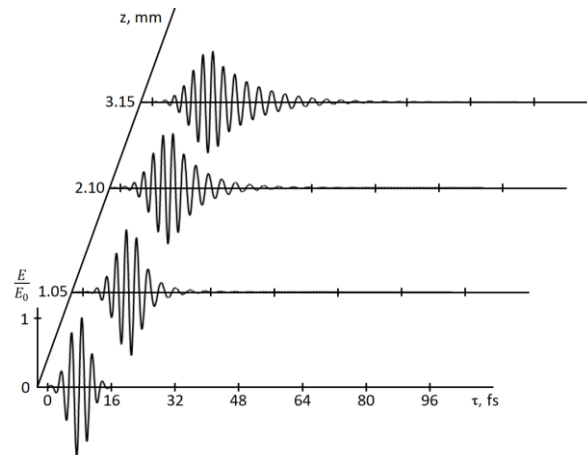


Fig. I.2. Few-cycle femtosecond pulse dispersion broadening in fused silica. The radiation spectrum lies within the anomalous GVD range.

Figure I.3 illustrates pulse dynamics in the dispersion medium, the spectrum center of which corresponds to zero GVD frequency. i.e. $\omega_0 = \omega_{cr}$. The results are obvious to differ significantly from those in Figures I.1 and I.2. Firstly, for the given parameters, the dispersion broadening proceeds much slower. Secondly, single-cycle subpulse separation takes place during the propagation. Such subpulses have a time delay from the main pulse and a phase shift relative to each other.

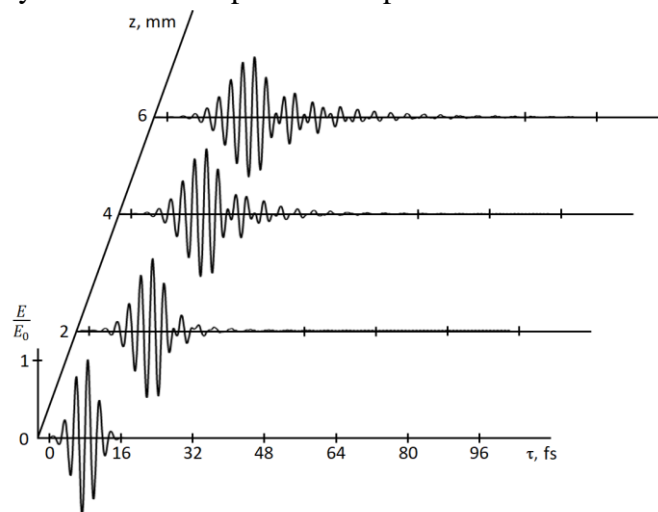


Fig. I.3 Few-cycle femtosecond pulse dispersion broadening in fused silica. The radiation spectrum lies within the zero GVD range.

In the case of high-intensity few-cycle pulses, and longer pulses as well [1,10], their propagation dynamics differs significantly depending on the GVD region of the pulse spectrum.

I.8.2. Femtosecond pulses temporal spectrum ultrabroadening

If the incident radiation spectrum is within the range of normal GVD, the third term from the expression (I.2.1) can be ignored. (I.2.1) then transforms to the modified Korteweg-de Vries equation form:

$$\frac{\partial E}{\partial z} - a \frac{\partial^3 E}{\partial \tau^3} + gE^2 \frac{\partial E}{\partial \tau} = 0. \quad (\text{I.8.3})$$

As the a and g coefficients from (I.8.3) take positive values, such equation cannot be solved in a solitary wave form [71]. This expression characterizes pulse dispersion broadening amplified due to the nonlinear refraction.

Figure I.4 represents numerical simulation results [38] for Ti:sapphire laser radiation (featuring the energy value of $W = 8.5 \text{ nJ}$ and central wavelength corresponding to the normal GVD of the medium, which is $\lambda_0 = 780 \text{ nm}$, and the pulse duration $\tau = 13 \text{ fs}$) propagating in a silica optical fiber with the core radius of $R = 1.38 \text{ mm}$. This fiber has the following dispersion parameters: $N_0 = 1.45$, $a = 4.04 \cdot 10^{-44} \text{ s}^3/\text{cm}$. The parameters allow to describe the refractive index dispersion dependence with an accuracy of down to 10^{-3} [72] using the formula (I.1.7) in the range of 550–1100 nm. The nonlinear refractive index coefficient is $n_2 = 3 \cdot 10^{-16} \text{ cm}^2/\text{W}$ for fused silica.

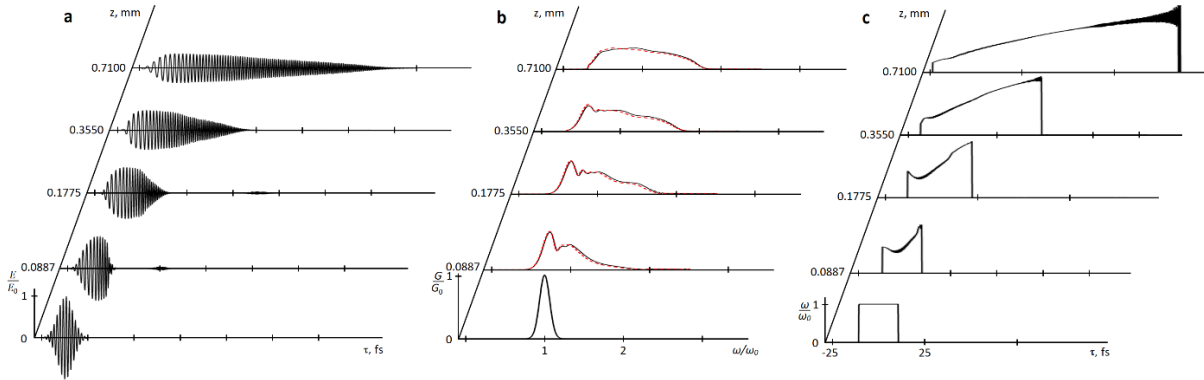


Fig. I.4 Few-cycle femtosecond pulse evolution when propagating in silica fiber in the case of normal GVD for the following input pulse parameters: $\lambda_0 = 780 \text{ nm}$, $\tau_p = 5T_0$, $I = 3.5 \cdot 10^{13} \text{ W/cm}^2$.

(a) radiation electric field dynamics; (b) instantaneous frequency ω_{inst} normalized by the input radiation central frequency value ω_0 change; (c) radiation power-density spectrum, where the dashed line refers to the electronic-vibrational nonlinearity whereas the solid line does not.

Figure I.4a shows that the nonlinear pulse broadening occurs during the propagation process. Moreover, linear phase modulation takes place, implying that the instantaneous pulse period T_{inst} grows linearly from its front to the tail. It is proved by the instantaneous frequency $\omega_{inst} = 2\pi/T_{inst}$ dynamics depicted in Fig. I.4b.

High-intensity few-cycle femtosecond radiation spectrum dynamics in the case of propagation in silica fiber is shown in Fig. I.4c. Strong asymmetric spectrum broadening is witnessed in the range of 450–1500 nm at the propagation distance $z = 0.71 \text{ mm}$. The ratio of the spectrum half-width $\Delta\omega$ to

the central frequency ω_0 , denoted as $\varepsilon = \Delta\omega/\omega_0$, increases 5 times and takes the value of 0.3. Propagating farther in space, there is not further spectral broadening, which occurs because of the pulse temporal broadening resulting in the intensity decrease and thus lessening the nonlinearity impact.

Fused silica, a widely used material for optical fiber production, is a Raman-active medium. Thus, it is not appropriate to employ either the modified Korteweg–de Vries equation (I.8.3) to describe pulse dynamics in such media, or the expression (I.2.1). To correctly address Raman nonlinearity mathematically, a nonlinear equation system (I.2.3) has to be used. Figure I.4 [73,74] shows the differences between the radiation spectra whether considering the electronic-vibrational (i.e. Raman) nonlinearity or not. The following parameters are used in this case [21,41]:

$$g = 1.8 \cdot 10^{-24} \text{ units CGSE}, g = 0.7 \cdot 10^{-24} \text{ units CGSE } (n_{2e}/n_{2ev} \approx 4), T_v \omega_v = 50, (\omega_v / \omega_0)^2 = 12 \cdot 10^{-4}$$

As shown in Fig. I.4, consideration of electronic-vibrational nonlinearity introduces minor changes to the femtosecond radiation propagating in nonlinear medium spectrum only. Besides, the contribution suppresses the spectrum broadening, the difference between the input and output spectra widths reaching 10%. The magnitude of the spectra Stokes shift caused by the electronic-vibrational nonlinearity leads to a decrease in the radiation frequency total shift to higher values.

Figure 1.4b shows that the instantaneous frequency dependence becomes quasilinear during the pulse broadening (both its temporal shape and spectrum) when it propagates in fused silica. The statement is general and follows from the modified Korteweg–de Vries equation (I.8.3) asymptotical solutions featuring positive a and g values [75]. Such simple phase modulation dependence is useful for the efficient temporal pulse compression. Employing special pulse compressors allowing to phase-match light pulse spectral components, it is possible to obtain a pulse of a duration inversely proportional to its spectrum width.

I.9. Self-focusing of femtosecond pulses in bulk media

The few-cycle femtosecond pulse transverse structure change, occurring due to self-focusing in bulk media, as well as in waveguides, is accompanied by spectral supercontinuum generation [76–80]. The phenomena (3+1)-dimensional theory is based on the equations characterizing spectral and temporal dynamics of the envelope [76–80], even in the case of ultrashort pulses, the spectra of which are subjected to ultra-broadening. However, as already discussed in section I.4, the method using envelope approach loses its advantage for few-cycle pulse description, that is, the absence of necessity to analyze each single oscillation of the pulse separately. This happens due to the fact that such pulses have the duration commensurate to a single oscillation. Moreover, the loss of the physical meaning of ultrashort pulse envelope is significantly complicates envelope dynamics equations. Most importantly, the approach implying pulse envelope concept does not allow to address effects related to considerable envelope shape modifications, e.g. shockwave breaking, whereas the field approach is free of the above drawbacks.

The few-cycle pulse self-focusing process is analyzed considering the results presented in [44] using the field equation (I.3.23) numerical solution. The input field is axially symmetric and is represented by:

$$E(z, r, t)|_{z=0} = E_0 \exp\left(-2 \frac{r^2}{\Delta r^2}\right) \exp\left(-2 \frac{t^2}{\Delta t^2}\right) \cos(\omega_0 t), \quad (\text{I.9.1})$$

featuring the central wavelength value of $\lambda_0 = 2\pi c/\omega_0 = 780 \text{ nm}$, which corresponds to the Ti:sapphire laser radiation. The pulse duration and transverse size are assumed to be $\Delta t = 7.5 \text{ fs}$ and $\Delta r = 10\lambda_0$ correspondingly. The propagation nonlinear medium is fused silica featuring the following parameters: $N_0 = 1.4508$, $a = 2.7401 \cdot 10^{-44} \text{ s}^3/\text{cm}$, $b = 3.9437 \cdot 10^{17} \text{ s}^3/\text{cm}$ and $\tilde{n}_2 = 2.9 \cdot 10^{-13} \text{ cm}^2/\text{kW}$ ($\tilde{n}_2[\text{cm}^2/\text{kW}] = (4\pi/3N_0)n_2 [\text{CGSE}]$).

Figures I.5–I.6 represent the results of few-cycle pulse propagation numerical simulation for various peak intensity values ($I[\text{kW}/\text{cm}^2] = (3N_0/8\pi)E_0^2 [\text{CGSE}]$), the propagation medium being fused silica. Figures I.5–I.6a–e depict three-dimensional axonometric visualization of the pulse field E , normalized by the maximal output value E_0 , dependence on the transverse coordinate r , normalized by the central wavelength value, and on the time t . Since the field negative values are symmetric to the positive ones, they are omitted for convenience of representation. Figures I.5–I.6f–j, in their turn, demonstrate the inplane spatial and temporal field distribution images, with red peaks corresponding to the positive maximum field values and blue ones - to the negative. Analysis of such cross-section allows to follow the pulse phase changes occurring during its propagation in the medium.

Figure I.5 demonstrates the few-cycle femtosecond pulse field dynamics, with the input field intensity of $I = 5 \cdot 10^{12} \text{ W}/\text{cm}^2$ ($G = 0.604$). This intensity value is clearly not enough to result in any significant medium nonlinearity contribution to the pulse dynamics. Consequently, the pulse is subjected to the diffraction (spatial broadening) and dispersion (temporal broadening) while propagating, which is accompanied by its wavefront curvature, typical for normal GVD.

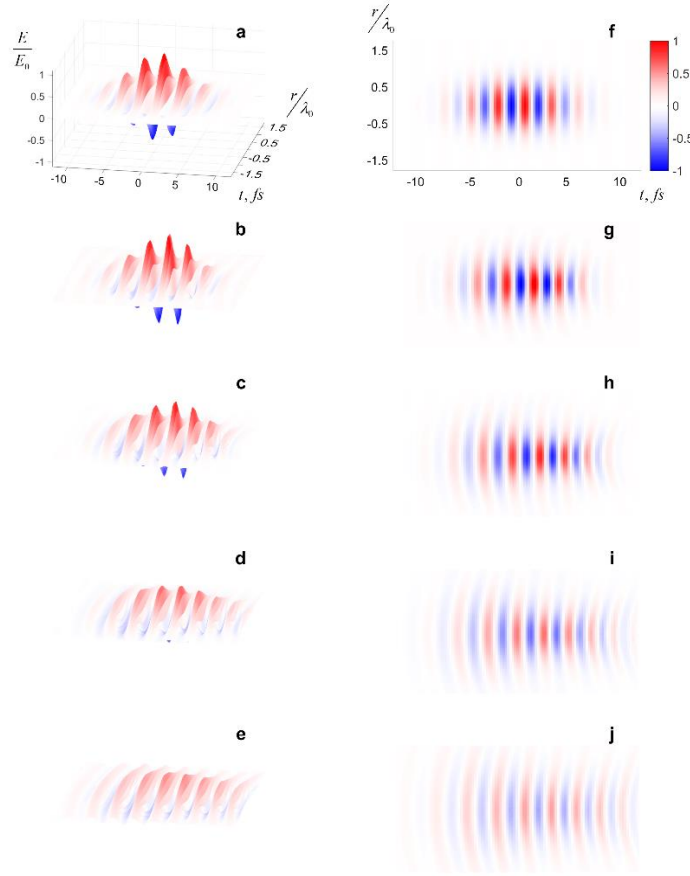


Fig. I.5. Few-cycle femtosecond pulse electric field spatio-temporal dynamics for the following input parameters: $\lambda_0 = 780 \text{ nm}$; $\Delta t = 7.5 \text{ fs}$; $\Delta r = 10\lambda_0$; $I = 5 \cdot 10^{12} \text{ W/cm}^2$ in fused silica:

$a, f - z = 0$; $b, g - z = 0.1 \text{ mm}$; $c, h = 0.2 \text{ mm}$; $d, i - z = 0.3 \text{ mm}$, $e, j - z = 0.4 \text{ mm}$.

Figure I.6 shows few-cycle femtosecond pulse electric field spatio-temporal dynamics for the maximum input intensity value $I = 1.5 \cdot 10^{13} \text{ W/cm}^2$, when propagating in fused silica. For the major part of wave packet the spatial self-focusing is seen to be dominating at the first stage of its propagation, resulting in a rise of the field amplitude on the axis where the central part is located (Fig. I.6*b*). Besides, there is a phase shift on the axis, which is significantly larger compared with the values at the periphery, i.e. by π in Fig. I.6*g*, and by more than 2π in Fig. I.6*h*.

The on-axis field amplitude increase leads to the rise in the nonlinear contribution to pulse dispersion broadening (Fig. I.6*c*, *h*). An asymmetric dumbbell-like field distribution is then formed. This field front has longer oscillation period and low-frequency components, whereas its tail features shorter oscillation period and high frequencies. A high-intensity “bridge” is likely to connect the two pulses, separated in space and featuring different spectral components. The “bridge” itself is wrapped in a light-“cloud” featuring a slightly different frequency. [81], represents a study of the ultrashort pulse self-action dynamics in terms of the generalized nonlinear Schrödinger equation for their envelopes numerical solutions, such a dumbbell-like field distribution is a butterfly-shaped structure. Regarding few-cycle pulses, the effect described is similar to the well-known effect of a longer femtosecond pulse splitting into two shorter ones [23].

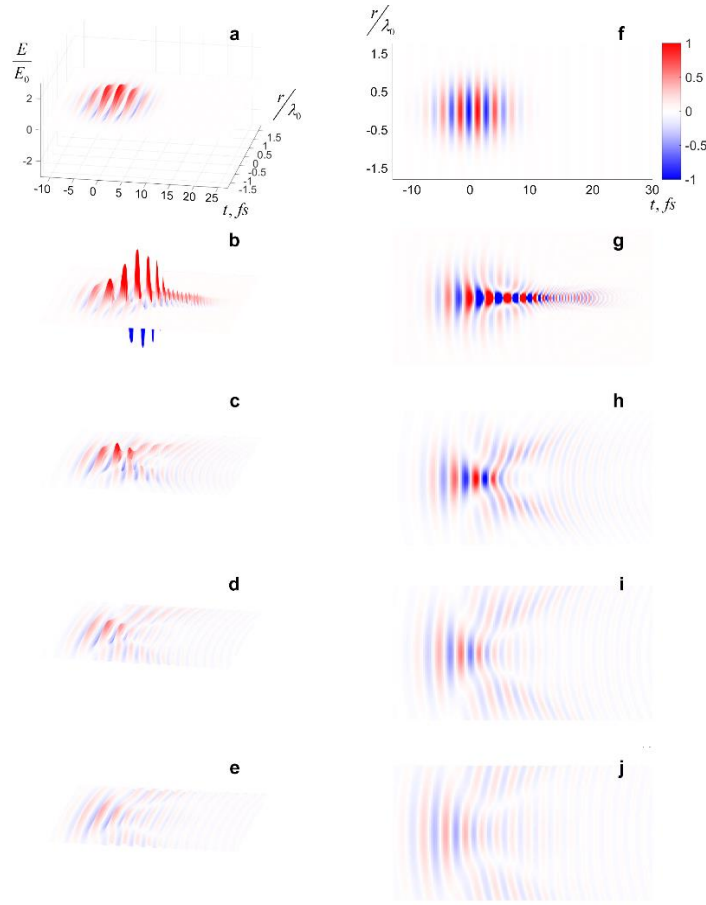


Fig. I.6. Few-cycle femtosecond pulse electric field spatio-temporal dynamics for the following input parameters: $\lambda_0 = 780 \text{ nm}$; $\Delta t = 7.5 \text{ fs}$; $\Delta r = 10\lambda_0$; $I = 1.5 \cdot 10^{13} \text{ W/cm}^2$ in fused silica:

$a, f - z = 0$; $b, g - z = 0.1 \text{ mm}$; $c, h - z = 0.2 \text{ mm}$; $d, i - z = 0.3 \text{ mm}$, $e, j - z = 0.4 \text{ mm}$.

A further electric field amplitude decrease, occurring due to the pulse nonlinear dispersion broadening, results in the intensity reduction and following diffraction-dispersion broadening of a quasi-linear dumbbell-like structure (Fig. I.6d, i).

The femtosecond pulse self-focusing critical power estimation is further considered. The ratio of the normalized constants G/D from the field equation (I.3.23) is equal to the ratio of the radiation power P_0 to self-focusing power P_{cr} up to a numeric constant [82]. In this case, the monochromatic pulse, featuring transverse Gaussian profile at its near-axial part, is transversely self-focused due to the medium nonlinearity, considering its power $P_0 > P_{cr}$ and the aberrationless approximation [26,82]. Thus, the ratio P_0/P_{cr} is a crucial parameter of the pulse transverse dynamics when it propagates in transparent nonlinear media including few-cycle femtosecond pulses [78,83]. However, the ratio P_0/P_{cr} alone is not enough to predict the behaviour of the few-cycle pulse transverse dynamics [84].

For the axially symmetric femtosecond pulse given by (I.9.1) featuring the input peak intensity value of $I = 7.5 \cdot 10^{12} \text{ W/cm}^2$, transverse width of $\Delta r_0 = 10\lambda_0$ and central wavelength $\lambda_0 = 2\pi c/\omega_0 = 780 \text{ nm}$ (corresponding to the Ti:sapphire laser radiation) propagating in bulk fused

silica, the normalized coefficients from (I.3.23) take the following values: $B = 0.422$, $D = 0.018$ and $G = 1.812$ [84].

The next step is to analyze of the self-focusing nature regarding the parameters mentioned for pulses of various duration.

Figures I.7 and I.8 illustrate the few-cycle pulse propagation numerical simulation results for various duration values, which make one and a half ($\Delta t_0 = 1.5T_0$, Fig. I.7a–e), three ($\Delta t_0 = 3T_0$, Fig. I.7f–j) and six ($\Delta t_0 = 6T_0$, Fig. I.7k–o) cycles, considering $T_0 = \lambda_0/c = 2.6 \text{ fs}$ [84]. Figure I.7 represents the few-cycle pulse electric field module $|E(r, t)|$ spatial and temporal dynamics for radiation propagating in nonlinear media at various distances z . This shows pulse spatio-temporal structure characteristic features, pulse phase front dynamics, allowing to estimate the changes occurring during propagation. Figure I.8 describes the on-axis pulse normalized temporal profile $E(r = 0, t)$ for various propagation distance z values. These graphs provide information about the pulse field dynamics on the axis of propagation. Figure I.9 shows the on-axis pulse spectrum dynamics $|G(r = 0, \omega)|$.

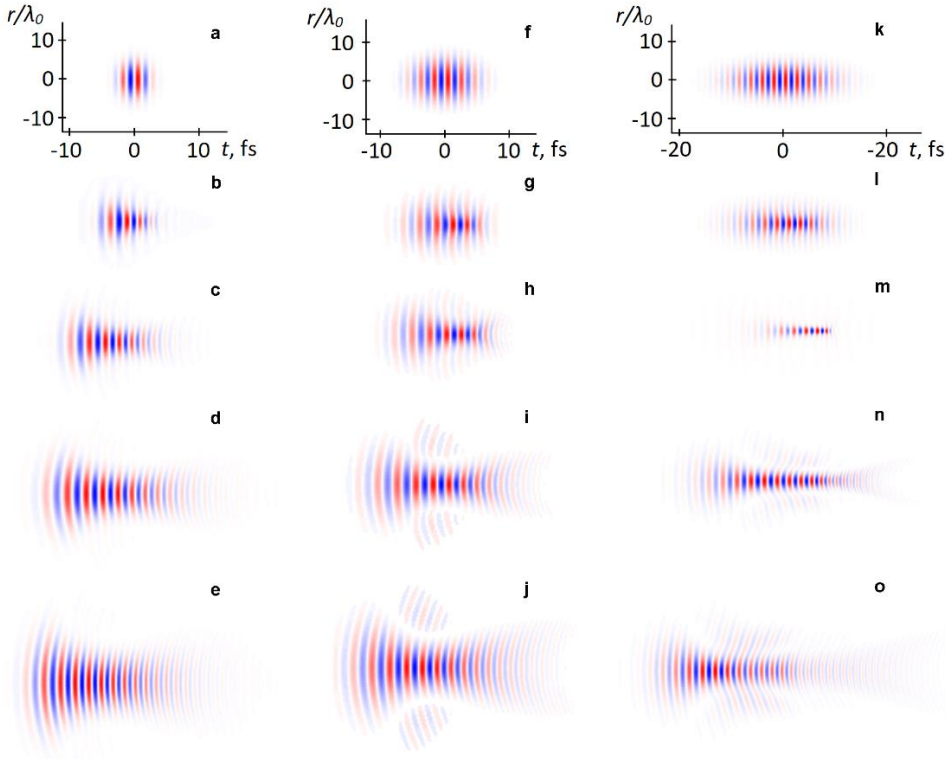


Fig. I.7a. Femtosecond pulse electric field spatio-temporal dynamics for the following input parameters: $\lambda_0 = 780 \text{ nm}$; $\Delta r_0 = 10\lambda_0$; $I = 7.5 \cdot 10^{12} \text{ W/cm}^2$ in fused silica ($B = 0.422$; $D = 0.018$; $G = 1.812$) for various duration values: a–e) $\Delta t_0 = 1.5T_0$; f–j) $\Delta t_0 = 3T_0$, k–o) $\Delta t_0 = 6T_0$ at various distances, a, f, k – $z = 0$, b, g, l – $z = 0,1 \text{ mm}$, c, h, m – $z = 0,2 \text{ mm}$, d, i, n – $z = 0,3 \text{ mm}$, e, j, o – $z = 0,4 \text{ mm}$.

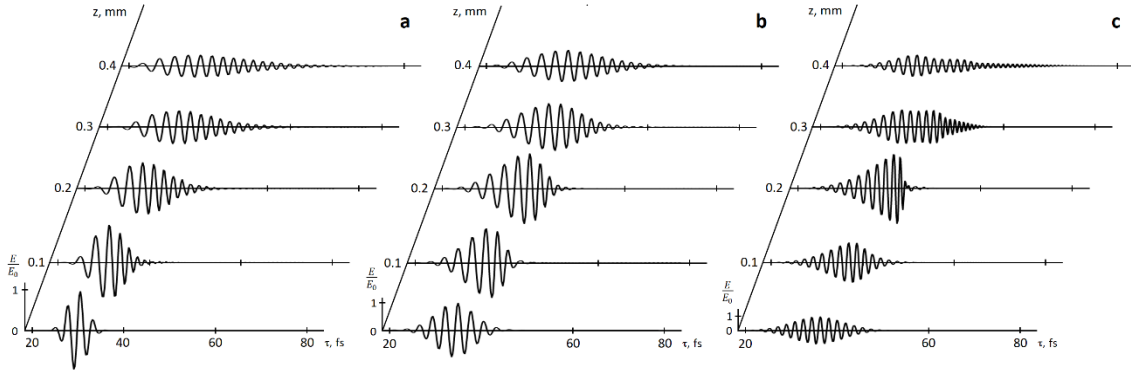


Fig. I.8. Pulse electric field paraxial dynamics ($r = 0$) in terms of its duration: $a - \Delta t_0 = 1.5T_0$; $b - \Delta t_0 = 3T_0$; $c - \Delta t_0 = 6T_0$. Propagation parameters correspond to those used in Fig. I.7.

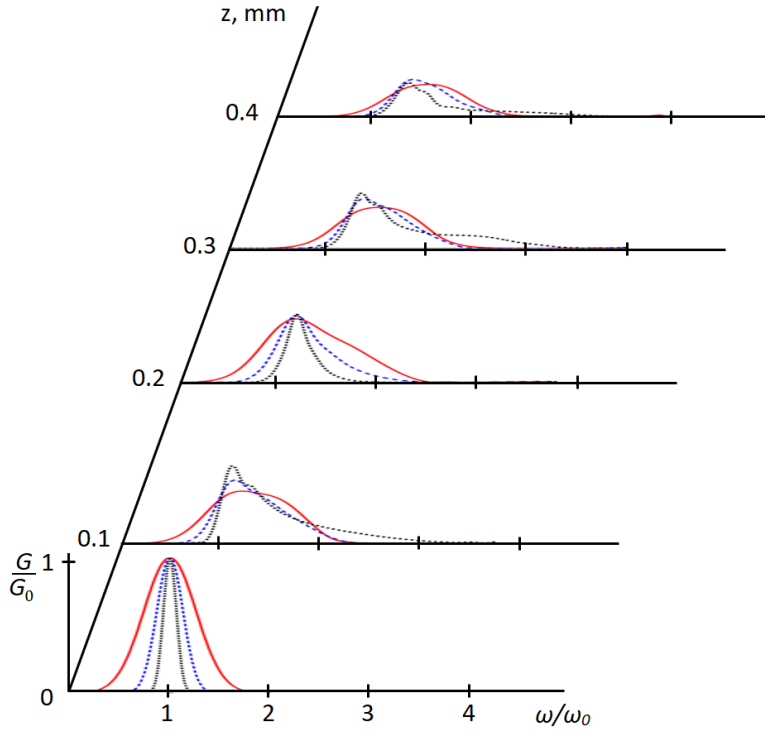


Fig. I.9. Cn-axis pulse spectrum module dynamics ($r = 0$) for radiation propagating in fused silica for the parameters corresponding to those used in Fig. I.7 and following pulse duration values: $\Delta t_0 = 1.5T_0$ (red solid curve); $\Delta t_0 = 3T_0$ (blue dashed curve); $\Delta t_0 = 6T_0$ (black dotted curve).

This self-focusing corresponds to the dumbbell-like temporal structures described above. The figures show that initial-stage field dynamics is defined by transverse compression, together with the pulse duration increase, occurring due to temporal profile nonlinear broadening and silica normal GVD in this spectral range. The pulse duration increase results in the electric field strength decrease compared to the dispersionless propagation case, and, therefore, nonlinear effect weakening. This self-action mode has a self-focusing limit, implusing the formation of a spatio-temporal structure of minimal transverse size in the “bridge” area (referred to as “nonlinear focus” in [84]). Regarding the extreme case, the amplitude increase is under a strong influence of the envelope breakdown, due to high-

frequency spectral part formation. The process description requires a consideration of the medium dispersion.

Figure I.7 shows that spatio-temporal dynamics is strongly dependent on the pulse duration. Few-cycle pulses are greatly affected by dispersion effects, which occurs due to their initial spectra being wider. As a result, the overall contribution of nonlinear effects is less for shorter pulses, the intensity value remaining unchanged. Moreover, shorter pulses exhibit less visible spatial compression (Fig. I.7) and less spectrum broadening regarding the initial ones. For longer pulses, the waist shifts closer to the pulse tail (Fig. I.7a, b, c). The pulse on-axis nonlinear phase shift increases in terms of the periphery along with the pulse duration: for the propagation distance of 0.2 mm the nonlinear phase shift has the value of $\pi/4$ for the pulse duration of $\Delta t_0 = 1.5T_0$ (Fig. I.7c), about $\pi/2$ for the pulse duration of $\Delta t_0 = 3T_0$ (Fig. I.7h) and more than π for the pulse duration of $\Delta t_0 = 6T_0$ (Fig. I.7m). The envelope breakdown and high-intensity pulse spectrum wing become apparent for the pulse of $\Delta t_0 = 6T_0$ (Figures I.8, I.9) only.

The radiation self-focusing efficiency is quantitatively defined by the pulse electric field amplitude maximum value [84]. Figure I.10 shows the field maximum amplitude dependence on the pulse propagation distance z for the same duration values as those used above (curved 1-3). To emphasize the spatial effect importance, numerical calculations have been conducted, however, neglecting the diffraction contribution (i.e. omitting the diffraction term from the equation (I.3.23)). This case corresponds to the plane-wave approximation, namely $\Delta r_0 \rightarrow \infty$, $D \rightarrow 0$ (Fig. I.10, curves I'-3'), which shows that the intensity of pulses featuring no frequency modulation at the input is monotonically decreasing due to the duration increase. Besides, similar behavior is typical for pulses of all the durations used (i.e. $1.5T_0$, $3T_0$ and $6T_0$). The field maximum amplitude decrease is more evident for shorter pulses (as expected).

Consideration of the diffraction (transverse) effects makes the propagational change in the amplitude maximum become significantly more apparent. Fig. I.10 shows that curves I-3 initially take the position above curves I'-3'. This means that the self-focusing impact is the strongest for all the three frequency values considered. Curve 1 represent the shortest duration, i.e. 1.5 field oscillations. Being almost horizontal at the input, the function is monotonically decreasing. There is no intensity increase (relative to the input value) observed, regardless of the focal region presence (Fig. I.7, b-e). This means that dispersion and diffraction are "blurring" the pulse both transversely and longitudinally, which, in the case of such a short pulse, undermines the nonlinear refraction contribution resulting in the peak intensity decrease. The radiation parameters and medium characteristics allow to conclude that duration value of $\Delta t_0 = 1.5T_0$ refers to the extreme case. For pulses featuring longer duration self-focusing leads to the field amplitude increase as early as at the initial propagation stage. For the pulse duration of $\Delta t_0 = 3T_0$ the nonlinear focus amplitude is 1.4 times higher than the input value (Fig. I.10, curve 2). For the pulse duration of $\Delta t_0 = 6T_0$ the nonlinear focus field amplitude increases exponentially becoming 2.5 times (Fig. I.10, curve 3) higher. However, the limitation is still there and the values are the same due to the envelope breakdown and high-intensity pulse tail formation (Figs. I.8 and I.9).

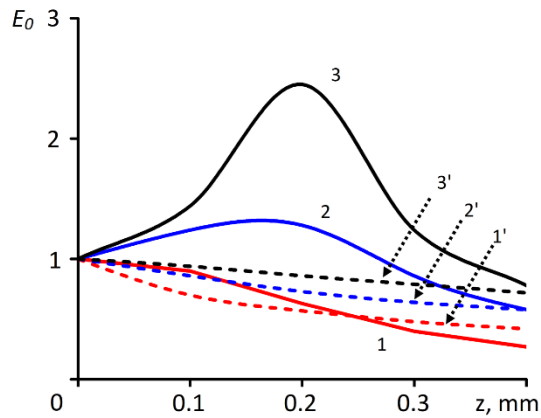


Fig. I.10. Electric field amplitude maximum value dynamics in terms of the propagation distance z in fused silica. Solid curves $1-3$ consider diffraction effects, whereas the dotted ones $1'-3'$ do not ($D = 0$). The simulation parameters used correspond to those in Fig. I.7.

Thus, the few-cycle pulse self-focusing efficiency decreases along with the pulse duration regarding the radiation propagating in transparent media featuring cubic electronic nonlinearity and normal GVD. The shorter pulses, suffering dispersion broadening, feature big transverse size in the nonlinear focus region, though small amplitude. For example, 1.5-2-cycle pulses of the peak intensity $7.5 \cdot 10^{12}$ W/cm² propagating in fused silica have minimal transverse size lower than their input value. For 5-10-cycle pulses the transverse pulse compression occurs closer to its tail, the maximum compression reaching 5-7 times.

The few-cycle pulse paraxial self-focusing process analysis demonstrates that their transverse sizes in nonlinear media can be commensurate with their central wavelength values. This leads to a conclusion that a more profound analysis of the phenomena must take into consideration non-paraxial propagation. Sections I.5 and I.6 have shown that spectral approach can be used for the above purpose.

II. Effect of laser-ionized liquid nonlinear characteristics on the optical-to-terahertz conversion efficiency

Terahertz (THz) broadband radiation is of considerable interest both for the fundamental science and for numerous applications: wireless information transmission, non-destructive materials diagnostics, biomedicine [85–87]. These applications require efficient and economical THz radiation source and motivate an active search for new methods and development of modern systems for a high-power THz wave generation.

One promising technique based on the THz generation in optical media during the plasma formation by near-IR range femtosecond pulse filamentation. In particular, this method is attractive due to a wide spectral coverage of the output THz field and its relatively simple experimental implementation. Further development of the plasma-based THz sources is associated with a search for the generation medium with a high damage threshold, weak absorption in the THz range and pronounced nonlinear effects. To date, this direction includes the research on the THz waves generation in various gases [88], metals [89] along with latest studies on the liquid media [90–92].

Considered firstly unpromising due to the relatively high THz absorption, liquid media turned out to be an optimal solution for the THz waves generation due to their high molecular density, strong nonlinearities and high damage threshold.

Among theoretical studies of spectrum superbroadening during ultrashort pulses filamentation in optical media, review [93] is of particular interest. However, most papers in this review analyze the evolution of the laser pulse complex envelope during its self-action in a nonlinear medium. This approach ceases to be applicable in the case of the intense near-infrared laser pulse propagation and subsequent generation of radiation with a spectrum so superbroadened that it also covers the THz range. In order to analyze such issues, it would be appropriate to study the pulse field dynamics itself instead of its envelope, as, for instance, in [91], where the field approach is used to describe the THz waves generation in liquid nitrogen. In addition, it was demonstrated in [94] that the THz emission in plasma formed by irradiating water with intense Ti:Sa laser subpicosecond pulses can be successfully described by field equations.

The theoretical approach used in [94] to interpret the experimental results on the THz waves generation during plasma formation in a water jet is based on a system of equations similar to (I.3.5):

$$\begin{cases} \frac{\partial E}{\partial z} - a \frac{\partial^3 E}{\partial \tau^3} + gE^2 \frac{\partial E}{\partial \tau} + \frac{2\pi}{cN_0} j = 0 \\ \frac{\partial j}{\partial \tau} + \frac{j}{\tau_c} = \beta \rho E^3 \\ \frac{\partial \rho}{\partial \tau} + \frac{\rho}{\tau_p} = \alpha E^2, \end{cases} \quad (\text{II.1})$$

where N_0 and a characterize the linear dispersion $n(\omega) = N_0 + ca\omega^2$ in liquid media, which is reasonable even for the case of spectrum superbroadening, since a high proportion of the radiation energy remains within the region of the normal group dispersion; g describes inertialess Kerr nonlinear medium response; ρ and j refer to the highly excited states population: and the current density of quasi-free electrons; τ_c and τ_p characterize the collision and relaxation time of highly excited states. The effect of diffraction is neglected here since thin (100-300 μm) liquid jets are used in the experiments which were described above.

The temporal evolution of the current density is proportional to the electric field E and the electron density ρ , the inertialess transition of which from the excited states is proportional to E^2 . This leads to cubic field dependence. The third equation of the system described above is responsible for the change in the excited states population density, which is determined by E^2 .

The latter two dynamics equations were derived in [95] on the basis of the density matrix formalism, but they can be easily explained using a well-known equation [96]:

$$\frac{\partial U_{ge}}{\partial t} + \frac{U_{ge} - U^0}{\tau_{ge}} = -\frac{2}{\hbar\omega_{eg}} \left(\frac{\partial P}{\partial t} + \frac{P}{T_{ge}} \right) E, \quad (\text{II.2})$$

which describes the population difference of the excited e and ground g electron states $U_{ge} = N_g - N_e$ dynamics for a two-level system; U^0 is equilibrium population difference, τ_{ge} is the relaxation time of electron population; T_{ge} is a characteristic oscillator intraband relaxation time; $\hbar\omega_{eg}$ determines the energy gap between the lower and upper state.

Using the non-resonant approximation with $P = \chi E$ the equation (II.2) can be written in the following form:

$$\frac{\partial N_e}{\partial t} + \frac{N_e}{\tau_{ge}} = \frac{\chi}{\hbar\omega_{eg}} \left(\frac{\partial E^2}{\partial t} + \frac{E^2}{T_{ge}} \right). \quad (\text{II.3})$$

Here the energy gap between the levels is considered large enough to take into account

equilibrium population N_e^0 . The inertial and instantaneous parts can be further studied separately as $N_e = N_{inert} + N_{inst}$:

$$\left\{ \begin{array}{l} N_{inst} = \frac{\chi}{\hbar\omega_{eg}} E^2 \\ \frac{\partial N_{inert}}{\partial t} + \frac{N_{inert}}{\tau_{ge}} = \frac{\chi}{\hbar\omega_{eg}} \frac{E^2}{T_{inert}} \end{array} \right. , \quad (II.4)$$

$$\text{where } T_{inert} = \frac{2T_{ge}\tau_{ge}}{2\tau_{ge} - T_{ge}}.$$

It is sufficient to consider only the inertialess mechanism of changing the electron density when describing the transitions from the excited states to the quasi-free ones. Thereby, the cubic field dependence of the current density is justified.

The system of equations (II.1) can be reduced to the one field equation as follows:

$$\frac{\partial E}{\partial z} - a \frac{\partial^3 E}{\partial \tau^3} + gE^2 \frac{\partial E}{\partial \tau} + g_p \int_{-\infty}^{\tau} E^3 e^{-(\tau_c^{-1}(\tau-\tau'))} d\tau' \int_{-\infty}^{\tau'} E^2 e^{-(\tau_p^{-1}(\tau-\tau''))} d\tau'' = 0. \quad (II.5)$$

Here $g_p = \frac{2\pi}{cN_0} \alpha\beta$ is an empirical coefficient, which describes the plasma nonlinearity, where $\alpha\beta$ determines the efficiency of the electrons transition to quasi-free states [94].

For the numerical simulation and further theoretical investigation, it is convenient to work with the normalized form of (II.5), introducing dimensionless parameters $\tilde{E} = E/E_0$, $\tilde{z} = za\langle\omega\rangle^3$, $\tilde{\tau} = \tau\langle\omega\rangle$, where E_0 is a pulse peak amplitude at the medium input, $\langle\omega\rangle$ is central radiation frequency corresponding to the wavelength of $\lambda_0=800$ nm:

$$\frac{\partial \tilde{E}}{\partial \tilde{z}} - \frac{\partial^3 \tilde{E}}{\partial \tilde{\tau}^3} + \tilde{g}\tilde{E}^2 \frac{\partial \tilde{E}}{\partial \tilde{\tau}} + \tilde{g}_p \int_{-\infty}^{\tilde{\tau}} \tilde{E}^3 e^{-(\tilde{\tau}_c^{-1}(\tilde{\tau}-\tilde{\tau}'))} d\tilde{\tau}' \int_{-\infty}^{\tilde{\tau}'} \tilde{E}^2 e^{-(\tilde{\tau}_p^{-1}(\tilde{\tau}-\tilde{\tau}''))} d\tilde{\tau}'' = 0, \quad (II.6)$$

where $\tilde{g} = gE_0^2/(a\langle\omega\rangle^2)$, $\tilde{g}_p = g_p E_0^4/(a\langle\omega\rangle^3)$.

In order to satisfy the experimental conditions, a chirped Gaussian pulse is used as an input field, taking upon normalization the form of:

$$\tilde{E}(\tilde{\tau}) = \exp\left(-(\tilde{\tau}/\tilde{\tau}_{pulse})^2\right) \sin(\tilde{\tau} + A\tilde{\tau}^2), \quad (II.7)$$

where τ_{pulse} is pulse duration and $\tilde{\tau}_{pulse} = \tau_{pulse}\langle\omega\rangle$; A determines frequency modulation, which is chosen so that the width of the chirped pulse spectrum fits the width of the 35 fs spectral-limited pulse.

The experimental results along with theoretical dependences of THz radiation energy on the pump pulse energy during THz generation in laser-ionized water jet are presented in Fig.II.1a Experimental setup similar to that in [96] has been used based on 800 nm femtosecond laser with a p-polarization and pulse duration of 400 fs.

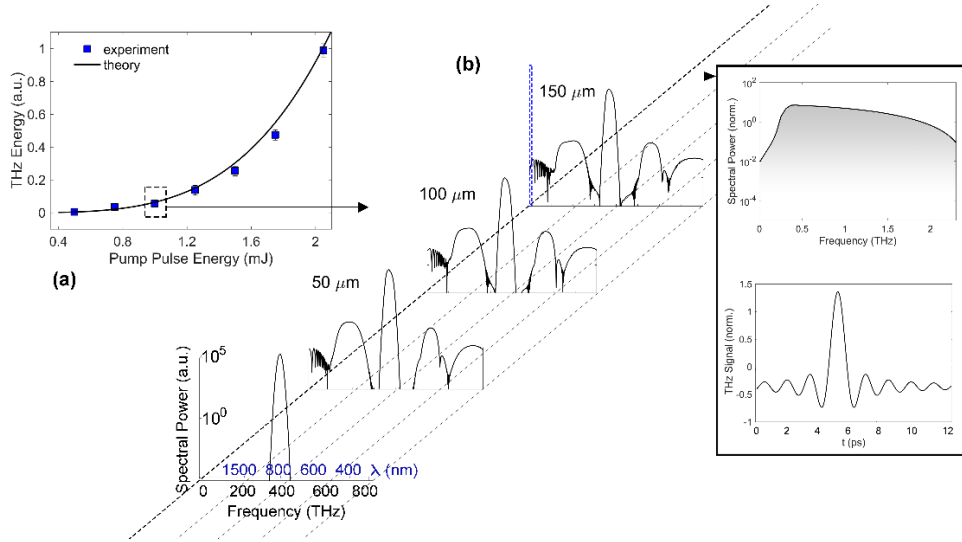


Fig. II.1 (a). Experimental and numerically simulated THz radiation energy dependence on the pump pulse energy in the case of its generation in a flat water jet. (b) Numerical simulation of the pulse spectrum dynamics during its propagation in a medium with the intensity $I = 1.5 \cdot 10^{13} \text{ W/cm}^2$ ($\sim 1 \text{ mJ}$) over the distance of $150 \mu\text{m}$. The inset shows the spectral and temporal forms of the THz signal as a numerical simulation result in the range of up to 2.5 THz.

The following medium parameters have been used: $a = 3.6 \cdot 10^{-44} \text{ s}^3/\text{cm}$, $g = 1.4 \cdot 10^{-24} \text{ cm} \cdot \text{s}/\text{W}$, $g_p = 4.5 \cdot 10^{10} \text{ cm}^3/(\text{s}^2 \cdot \text{W}^2)$, $\tau_c = 1\text{-}2 \text{ fs}$ [97] and $\tau_p = 150 \text{ fs}$ [98]. The optical-to-terahertz conversion efficiency taking the linear THz absorption into account makes 10^{-4} [94]. The numerically simulated pulse spectrum dynamics during the propagation in the medium with the above characteristics and the intensity of $1.5 \cdot 10^{13} \text{ W/cm}^2$ ($\sim 1 \text{ mJ}$) over the distance of $150 \mu\text{m}$ is presented in Fig. II.1b The inset demonstrates the spectral and temporal forms of the THz signal as a numerical simulation result in the range of up to 2.5 THz. Thereby, the described theoretical model has been confirmed to be valid for studying the THz waves generation, fitting the experimentally obtained quasi-quadratic THz energy increase with increasing pump energy.

The nature of this dependence cannot be theoretically justified in any simple fashion. However, it is possible to give an estimation. Since the Kerr third-order nonlinear effect induces cubic temporal field dependence, and the plasma nonlinearity is proportional to E^5 , multiplying the field equation (II.5) by E , it can be shown that $\frac{\partial E^2}{\partial \tau} \sim (E^2)^2, (E^2)^3$. Summarizing all these assumptions, this estimate demonstrates almost quadratic and cubic dependence of the THz radiation energy on the pump intensity, being in good agreement with the experiment.

Moreover, it is now possible to estimate the relative contribution of the third-order nonlinearity and induced plasma using the normalized coefficients in (II.6), which determine the effect of each physical process on the strong field dynamics during the pulse propagation. Fig. II.2. shows the comparison of the THz signal generated in the cases of only Kerr or plasma nonlinearity contribution, as well as their mutual effect. It can be seen that the contribution of plasma nonlinearity is stronger. Furthermore, taking into account both plasma and Kerr nonlinearities, THz signal decreases due to the redistribution of energy between the third and fifth-order nonlinearity

mechanisms.

It is then of considerable interest to study the influence of the ratio \tilde{g}_p/\tilde{g} on the THz generation efficiency. Fig. II.3. represents the THz radiation energy dependence on the induced plasma effect contribution with various fixed values of the third-order nonlinearity contribution. A characteristic curve, which can be separated into two regimes of THz waves generation, is observed for each fixed value of \tilde{g} .

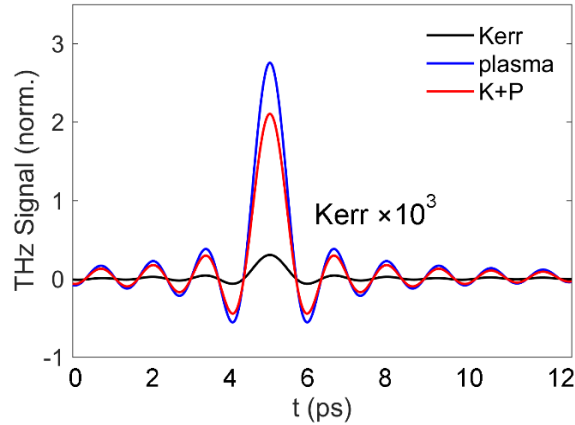


Fig.II.2. Generated THz pulse temporal form, considering the effect of only Kerr (black) or plasma nonlinearity (blue) during its propagation, as well as their mutual contribution (red).

The first mode corresponds to a weak ionization of the medium, in which there is an increase in optical-to-THz conversion efficiency with the dominance of third-order effects and a following decrease, which can be explained through the destructive mutual Kerr and plasma formation effect. The second mode (strong ionization) corresponds to a sharp THz radiation energy growth starting after a characteristic minimum, which, presumably, corresponds to the medium ionization threshold. In this case, the contribution of plasma nonlinearity over the Kerr one prevails.

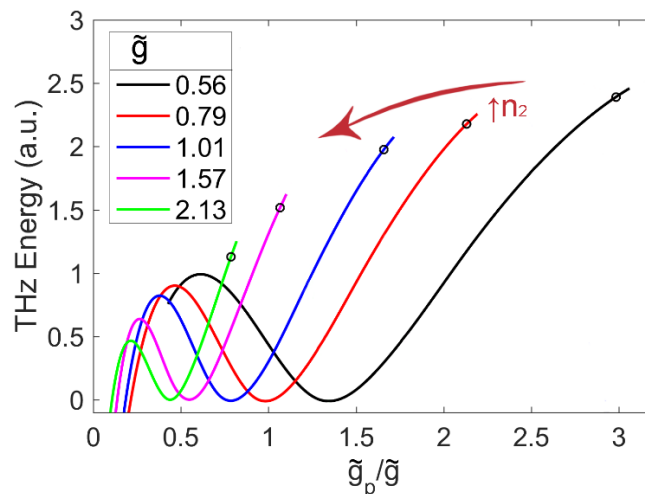


Fig.II.3. THz radiation energy dependences with the growth of the ratio \tilde{g}_p/\tilde{g} for a range of fixed normalized third-order nonlinearity coefficient \tilde{g} .

Furthermore, it has been revealed that with an increase in the third-order nonlinearity effect, the described minimum (a transition between the modes) is shifted towards smaller ratio values. The ratio studies can be expressed through the equation $\tilde{g}_p/\tilde{g} = (g_p/g)E_0^2/\langle\omega\rangle$, from which it can be seen that it is proportional to the pump energy. Thereby, a decrease in this ratio for media with a strong Kerr nonlinearity corresponds to the case in which less pump energy is required to overcome the transition between the modes. The arrow and dots in Fig. II.3 demonstrate the THz radiation energy growth with an increase in the normalized Kerr nonlinearity coefficient for a fixed plasma effect. This result can be explained by a redistribution of the pump energy to the third-order nonlinearity mechanism.

III. Nonlinear refractive index in the THz frequency range in semiconductor crystals and liquids

There are various phenomena that contribute to the nonlinear optical response in the media studied [41,99–101]. Some of these phenomena are based on the nonlinear response of each atom or molecule, while others are associated with a change in the concentration of these particles, for example, due to thermal expansion of the substance in the presence of high-intensity radiation. The first case is called “low-inertia” nonlinearity, and the second one - “high-inertia” nonlinearity. In the case of ultrashort optical pulses, including intense picosecond pulses of the THz frequency range, the dominant nonlinearity mechanism, as a rule, is the low-inertia one. For pulses in the visible and near-IR spectral ranges, the dominant low-inertial nonlinearity mechanism is electronic. It was previously shown that for pulses in the far infrared region, which in the generalized case also includes the THz range, the dominant nonlinearity mechanism is associated with anharmonic lattice vibrations [99,102].

III.1. Theoretical approach for assessing vibrational low-inertial nonlinearity of crystals within the THz frequency range

Following the theoretical approach proposed in [99] for calculating the coefficient of the nonlinear refractive index in the THz frequency range of the crystal, the structural unit of which in this case is the classical anharmonic oscillator with quadratic and cubic nonlinearities, we give a brief conclusion of this formula described in [99]. To analyze the vibrational nonlinearity of a crystalline material, we consider the dynamics of ions in the lattice caused by the action of an external electromagnetic field. The equation of the classical oscillator is defined as:

$$\ddot{x} + 2\gamma\dot{x} + \omega_0^2x + ax^2 + bx^3 = \alpha E, \quad (\text{III.1})$$

where x is the displacement of the lattice ion from its equilibrium position, γ is the damping coefficient, ω_0 is the natural frequency of the ion, a and b are nonlinear coefficients characterizing the anharmonicity of the oscillator, and E is the intensity of the applied electric field. The parameter α is defined as the ratio of the ion charge q to the reduced mass of the vibrational mode m . In a more detailed consideration, the parameter q describes the magnitude of the electrical coupling of the

vibrational mode with the electric field vector and depends on whether the chemical bond is ionic or vibrational. Equation (III.1) is solved using perturbation theory with the following substitution:

$$x = \lambda x^{(1)} + \lambda^2 x^{(2)} + \lambda^3 x^{(3)} + \dots, \quad (\text{III.2})$$

where λ is the decomposition parameter with conditions $0 \leq \lambda \leq 1$. It is assumed that the electric field interacting with ions is monochromatic with a frequency ω . This approach considers nonlinear optical effects that occur without changing the frequency spectrum. Oscillations of the ions of the crystal lattice occur only at the fundamental frequency. Given these approximations, we obtain:

$$x_\omega = \frac{\alpha E_\omega}{\omega_0^2 - \omega^2 - 2\gamma i \omega} + \frac{1}{(\omega_0^2 - \omega^2 - 2\gamma i \omega)^4} \times \times \left[2a^2 \alpha^3 \frac{3\omega_0^2 - 8\omega^2 - 8\gamma i \omega}{\omega_0^2(\omega_0^2 - 4\omega^2 - 4\gamma i \omega)} + 3b\alpha^3 \right] |E_\omega|^2 E_\omega. \quad (\text{III.3})$$

Here, the nonlinear susceptibility associated with the Kerr effect is considered. The total polarization in the medium, which includes both the electronic P_{el} and the vibrational P_v contribution to the susceptibility, is determined by the following expression:

$$P = P_{el} + P_v = Nqx = P_\omega e^{-i\omega t} + \text{c. c.} \quad (\text{III.4})$$

The amplitude of the polarization component oscillating at the frequency ω includes both linear and nonlinear parts:

$$P_\omega = \chi^{(1)} E_\omega + 3\chi^{(3)} |E_\omega|^2 E_\omega = \chi_{\text{eff}} E_\omega, \quad (\text{III.5})$$

$$\text{where } \chi_{\text{eff}} = \chi_{el}^{(1)} + \chi_v^{(1)} + 3\chi_{el}^{(3)} |E_\omega|^2 + 3\chi_v^{(3)} |E_\omega|^2.$$

The complex refractive index (hereinafter “ \sim ” shows the complex value, then when considering the real part it will be omitted; “ $-$ ” determines that the value is considered in the CGSE system; the index “ v ” denotes the vibrational nature of the effect, “ el ” the electronic one) of the medium can be represented through the effective susceptibility as:

$$\tilde{n} = 1 + 4\pi\chi_{\text{eff}} = \tilde{n}_0 + \tilde{n}_2 \langle E^2 \rangle = \tilde{n}_0 + 2\tilde{n}_2 |E_\omega|^2, \quad (\text{III.6})$$

$$\text{where } \tilde{n}_0 = \sqrt{1 + 4\pi\chi^{(1)}}, \tilde{n}_2 = \tilde{n}_{2,el} + \tilde{n}_{2,v} = \frac{3\pi\chi^{(3)}}{\tilde{n}_0}.$$

Taking into account (III.3) - (III.5), we can express $\chi^{(1)}$ and $\chi^{(3)}$, and then substitute them into the expression for the coefficient of nonlinear refractive index in the CGSE system \tilde{n}_2 :

$$\tilde{n}_2 = \frac{\pi q N}{\tilde{n}_0} \frac{\alpha^3}{(\omega_0^2 - \omega^2 - 2\gamma i \omega)^4} \times \left[2a^2 \frac{3\omega_0^2 - 8\omega^2 - 8\gamma i \omega}{\omega_0^2(\omega_0^2 - 4\omega^2 - 4\gamma i \omega)^4} + 3b \right]. \quad (\text{III.7})$$

This derivation of n_2 is obtained using the approximation of a single vibrational resonance. This approximation is also suitable for the situation when one resonance dominates the others.

Dividing \tilde{n}_0 and \tilde{n}_2 by their real and imaginary parts, from expressions (III.6) and (III.7) one can find linear and nonlinear refractive indices and absorption coefficients of the medium. Expression (III.7) can be used to consider four different cases of the relationship between the frequency of the incident radiation ω and ω_0 : the low-frequency limit $\omega \ll \omega_0$, the two-photon resonance $\omega \approx \omega_0/2$, the almost resonant case $\omega \approx \omega_0$, and for frequencies much higher than the resonance frequencies $\omega \gg \omega_0$.

To consider the nonlinearities of electro-optical crystals, as well as crystals applicable in the THz frequency range (0.1-3 THz), we elaborate on the case of the low-frequency limit $\omega \ll \omega_0$:

$$\bar{n}_{2,v}^{\omega \ll \omega_0} = \text{Re}[\bar{n}_{2,v}^{\omega \ll \omega_0}] \approx \frac{\pi q N \alpha^3}{n_0 \omega_0^8} \left(\frac{6a^2}{\omega_0^2} + 3b \right). \quad (\text{III.8})$$

It is important to note that expressions (III.7) and (III.8) in this form are not suitable for estimating the coefficient of the nonlinear refractive index, since the parameters and coefficients present in them do not have a direct and obvious connection with the real properties of the media that can be measured or found in reference book. Therefore, we further consider how the authors of this theoretical approach associate the parameters a and b with the real properties of the medium.

The relationship between the vibrational contribution to the nonlinear refractive index and thermal expansion [100] is given in [99], provided that the electronic contribution to both the linear and nonlinear refractive indices is prevailed in magnitude by the vibrational contribution. Potential energy, based on the expression (III.1), is determined as follows:

$$U(x) = \frac{m\omega_0^2}{2}x^2 + \frac{ma}{3}x^3 + \frac{mb}{4}x^4 \quad (\text{III.9})$$

The coefficient a is related to the coefficient of thermal expansion α_T , taking into account the average displacement of the ion from its equilibrium position, which determines the total linear expansion of the solid:

$$f(x) = Ae^{-\frac{U(x)}{k_B T}} = Ae^{-\frac{m\omega_0^2 x^2}{2 k_B T} + \frac{ma x^3}{3 k_B T} + \frac{mb x^4}{4 k_B T}},$$

$$\bar{x} = \frac{\int x f(x) dx}{\int f(x) dx} = \frac{ak_B T}{m\omega_0^4}, \quad (\text{III.10})$$

$$L(T) = L_0(1 + \alpha_T T), \alpha_T = \frac{\bar{x}}{a_l T},$$

$$a = -\frac{\alpha_T m \omega_0^4 a_l}{k_B},$$

where a_l is the lattice constant, k_B is the Boltzmann constant, α_T is the temperature expansion coefficient, and parameter m can be defined as the reduced mass of the vibrational mode.

It is important to emphasize that the nature of the nonlinearity of the refractive index in this case is not due to the thermal expansion of the substance caused by a change in its density. The root cause of the low inertia nonlinearity of the refractive index and subsequent inertial thermal expansion of the substance is the anharmonicity of the vibrations of the lattice ions.

Returning to the expression (III.8) and dividing it by two terms defining a different nature the following form is obtained:

$$\bar{n}_{2,v}^{\omega \ll \omega_0} \approx \frac{\pi q N}{n_0} \left(\frac{6a^2 \alpha^3}{\omega_0^{10}} + \frac{3b \alpha^3}{\omega_0^8} \right),$$

$$\bar{n}_{2,v}^{\omega \ll \omega_0} = \bar{n}_{2,v}^{(1)} + \bar{n}_{2,v}^{(2)}, \quad (\text{III.11})$$

therefore,

$$\bar{n}_{2,v}^{(1)} = \frac{\pi q N}{n_0} \frac{6a^2 \alpha^3}{\omega_0^{10}}, \quad (\text{III.12})$$

$$\bar{n}_{2,v}^{(2)} = \frac{\pi q N}{n_0} \frac{3b\alpha^3}{\omega_0^8}. \quad (\text{III.13})$$

The parameter α in expression (III.1) was determined as q/m . However, later it was introduced in a different way, for example, through linear susceptibility with respect to resonance parameters (III.7), (III.8). Given the expressions for parameter a , expression (III.12) takes the form:

$$\bar{n}_{2,v}^{(1)} = \frac{3a_1^2 m^2 \omega_0^4 \alpha_T^2}{32n_0 \pi^2 q^2 N^2 k_B^2} \left[(\bar{n}_{2,v}^{\omega \ll \omega_0})^2 - 1 \right]^3. \quad (\text{III.14})$$

Expression (III.13), which describes the second term in the contribution to the nonlinear refractive index, is associated with a change in the frequency of oscillations in the field of intense radiation (dynamic Stark effect) [101]. In the case of nonresonant isotropic media at low THz frequencies and the assumption that only one excited state makes a significant contribution to the vibrational nonlinearity, the third-order susceptibility will be described by the following expression:

$$\chi_{v,ST}^{(3)\omega \ll \omega_0} = -\frac{2N|\mu|^4}{3\hbar^3 \omega_0^3}, \quad (\text{III.15})$$

where μ is the dipole moment of the transition, which must be determined through the "measured" parameters of the medium. In [99], it was proposed to express this parameter in terms of a linear refractive index considering the vibrational contribution:

$$\begin{aligned} \chi_v^{(1)\omega \ll \omega_0} &= -\frac{2N|\mu|^2}{3\hbar\omega_0}, \\ (n_{0,v}^{\omega \ll \omega_0})^2 - 1 &= 4\pi\chi_v^{(1)\omega \ll \omega_0} = \frac{8\pi N|\mu|^2}{3\hbar\omega_0}. \end{aligned} \quad (\text{III.16})$$

Then the final expression for the coefficient of the nonlinear refractive index of the medium in the THz frequency range, considering the vibrational nonlinearity, will take the form [99]:

CGSE:

$$\bar{n}_{2,v} = \frac{3a_l^2 m^2 \omega_0^4 \alpha_T^2}{32n_0 \pi^2 q^2 N^2 k_B^2} [n_{0,v}^2 - 1]^3 - \frac{9}{32\pi N n_0 \hbar \omega_0} [n_{0,v}^2 - 1]^2, \quad (\text{III.17})$$

SI:

$$n_{2,v} = 4,2 \times 10^{-7} \frac{\bar{n}_{2,v}}{n_0} \text{ cm}^2/\text{W}$$

(for simplicity, we omit the spelling “ $\omega \ll \omega_0$ ” in the indices).

III.2. Calculation of the coefficient of nonlinear refractive index considering the vibrational nonlinearity of electro-optical crystals in the THz frequency range

Earlier, using this theoretical approach, the coefficient n_2 in the terahertz frequency range for crystalline quartz (SiO_2) were estimated [99]. Crystalline quartz has high transparency in the visible and IR spectral ranges, as well as in the THz frequency range (starting from 100 μm), therefore, it is actively used as a material for components (transparency windows, lenses) in terahertz technology [103]. It is anisotropic and has birefringence in the THz spectral region [104].

SiO_2 crystal parameters necessary for calculating the coefficient of the nonlinear refractive index by the formula (III.17) are given in the table below [99]:

Cry stal	ω_0 , cm^{-1}	$\frac{\omega}{2\pi}$, THz	n_0	n_{el}	a_l $\times 10^{-8}$ cm	m $\times 10^{-23}$	α_T $\times 10^{-6}$ $^\circ\text{C}^{-1}$	S	$N \times 1$ 0^{22}	$n_{0,v}$	$n_{2,IR}$, cm^2/W	n_2 , cm^2/W
SiO ₂	1242	37.2	2.1	1.4	5.24	1.69	7.6	2.65	2.65	1.8 6	3×10^{-1} 6	5.9×10^{-12}

where:

- ω_0 – fundamental vibration frequency.
- n_0 – linear refractive index for the frequency range 0,5 – 1,5 THz.
- n_{el} – refractive index in the range with a nonresonant electron contribution (800 nm).
- a_l – lattice constant.
- m – reduced mass of the vibrational mode which can be calculated for A_xB_y crystal as

$$m = \frac{m_A \times m_B}{m_A + m_B}$$
- α_T – thermal expansion coefficient.
- q – effective charge of a chemical bond, in this case is considered as an electron charge
- S – relative density
- N – numerical density of vibrations in the crystal A_xB_y lattice per 1 cm^3 $N = \frac{S}{x \cdot m_A + y \cdot m_B}$
- $n_{0,v}$ – vibrational contribution to the low-frequency refractive index $n_{0,v} = \sqrt{1 + n_0^2 - n_{el}^2}$
- $n_{2,IR}$ – nonlinear refractive index coefficient in the IR frequency range
- n_2 – calculated nonlinear refractive index coefficient in the THz frequency range

It is seen that for SiO_2 crystal the nonlinear refractive index coefficient in the THz frequency range exceeds this value in the IR range by 4 orders.

If we analyze the parameters of media that affect the value of n_2 , then an increase in this coefficient can be inherent in media with a higher coefficient of thermal expansion, a larger lattice constant, a larger natural frequency of vibration and a reduced value of the numerical density of vibrations, which is ensured by an increase in the total mass of atoms and a decrease in the relative density of the medium.

It is also important that the vibrational contribution to the low-frequency refractive index be larger, and this depends on the difference in the values of the linear refractive index in the THz frequency range and the linear refractive index in the range with non-resonant electronic contribution ($n_0 > n_{el}$).

The calculated coefficient n_2 changes its sign to negative, provided that the contribution made by changing the oscillation frequency in the intense radiation field (dynamic Stark effect) for a given medium is higher than the contribution associated with the inertial thermal expansion of the substance.

III.3. Application and modification of the theoretical approach to assess the vibrational nonlinearity of liquid water in the THz frequency range

Until recently, the use of various liquids, and especially water, in the THz frequency range was considered difficult due to their large absorption. The possibility of generating a broadband THz radiation from a volume of water, a water jet, and a film was experimentally demonstrated in [105,106]. These results have opened a new field of study.

The previous section showed the parameters that affect the increase of the Kerr nonlinearity of the vibrational nature of the medium in the THz frequency range. Liquids are characterized by a large coefficient of thermal expansion than solids, as well as fundamental vibrations of molecules at high frequencies.

The estimation of the nonlinear refractive index of liquid water of great interest. To do this, we consider the possibility of applying the previously proposed theoretical approach for calculating the coefficient n_2 (III.17) [99] and modify it.

Water, in comparison with other liquids that have recently been used in the THz range (alcohols, esters and other organic compounds) [107], is a simple and convenient model for modifying the theoretical approach for assessing vibrational nonlinearity in the THz frequency range. This is due to the certainty in the description of molecular vibrations in such a triatomic molecule and quite obvious resonances in the high-frequency THz region. Despite the strong absorption of water in the THz range, the use of a thin layer circumvents the limitation of its use in the THz frequency range.

Equation (III.17) is applicable in a situation when the central THz frequency of the incident radiation ω is much less than the fundamental frequency of the medium ω_0 . For water, $\omega_0 \sim 100$ THz [108], which corresponds to the peak of water absorption at a wavelength of $\lambda_0 = 3 \mu\text{m}$ (see Figure III.1). Accordingly, this condition is satisfied.

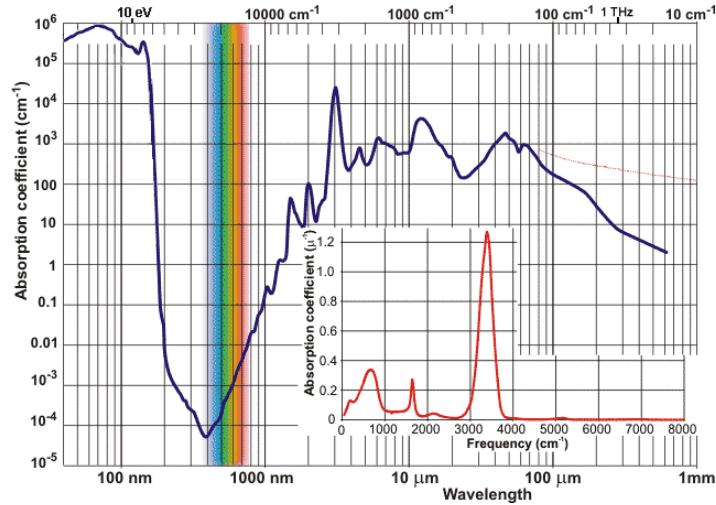


Fig. III.1. Absorption of liquid water in the IR spectral range [109] (for reference $3338 \text{ cm}^{-1} \approx 100 \text{ THz}$).

It is also important that the medium has a single vibrational resonance, or one clearly dominant. When considering liquid water, there is a dominant resonance at a frequency of $\sim 100 \text{ THz}$.

Next, the total polarization of liquid water associated with the summation ($\langle \dots \rangle$ is considered averaging over the volume) of the contribution from each molecule:

$$P = \frac{1}{2} N \langle p_{\omega} e^{i\omega t} + p_{2\omega} e^{i2\omega t} + p_{3\omega} e^{i3\omega t} + \text{c. c.} \rangle, \quad (\text{III.18})$$

$$p_{2\omega} e^{i2\omega t} \approx 0$$

Both quadratic and cubic nonlinearity of molecular vibrations determine the cubic nonlinearity of an isotropic medium. However, due to the random orientation of the molecules in the volume of water (see Figure III.2a), with averaging, the quadratic contribution of the nonlinearity of molecular vibrations becomes equal to zero.

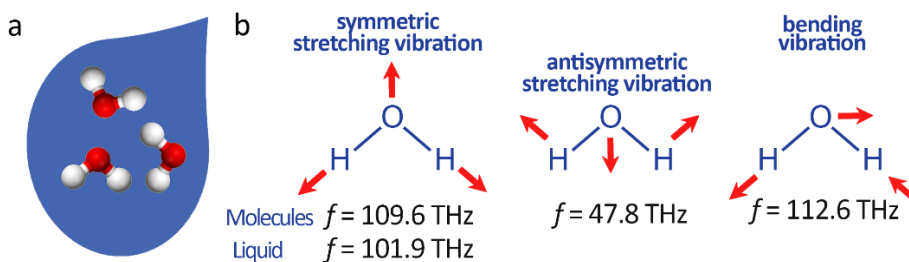


Fig. III.2. (a) The random orientation of molecules in the water; (b) three vibrational modes of a water molecule with corresponding vibration frequencies in the terahertz frequency range.

Next, the vibrational contribution to the nonlinear refractive index is considered (III.14). In the case of liquid water, instead of the lattice constant a_l of the crystal, which limits the length of the displacement of the ion from the equilibrium position, this parameter will be interpreted as the unit cell size a_c , by which the vibration under consideration is limited. In the case of liquid water, a_c is the diameter of the molecule. In addition, when calculating n_2 for crystals, the ratio between the change

in the lattice constant due to thermal expansion is used. For liquids, we consider the change in the size of the molecules due to the stretching of various bonds in the molecule from thermal expansion.

This model assumes that the nature of the nonlinearity of the refractive index of water is not due to the thermal expansion of the substance (as well as a change in its density). The process of liquid expansion is inertial. The root cause of the low inertia nonlinearity of the measured refractive index and subsequent inertial thermal expansion of the substance is the anharmonicity of molecular vibrations.

As for the contribution caused by the change in the oscillation frequency in the intense radiation field (III.13), (III.16), in the case of liquid water, only one excited state is also taken into account, which makes a significant contribution to the vibrational nonlinearity.

Thus, the theoretical approach (III.17) [99] is also applicable to liquid water with a slight modification of the parameters described above. The resulting expression for water nonlinear refractive index coefficient in the THz frequency range in SI system takes the form:

$$n_{2,v} = 4,2 \times 10^{-7} \frac{1}{n_0} \frac{3a_c^2 m^2 \omega_0^4 \alpha_T^2}{32n_0 \pi^2 q^2 N^2 k_B^2} [n_{0,v}^2 - 1]^3 - \frac{9}{32\pi N n_0 \hbar \omega_0} [n_{0,v}^2 - 1]^2. \quad (\text{III. 19})$$

The parameters of liquid water for n_2 estimation are given in the table below.

Parameter	Value
ω_0 fundamental vibration frequency	100 THz [108]
n_0 linear refractive index for the frequency range 0,3-1ТГц	2.3 [110]
n_{el} refractive index (800 nm)	1.33 [108]
a_c unit cell dimension (molecule size)	0.28×10^{-7} cm [111]
α_T thermal expansion coefficient	0.2×10^{-3} /°C [112]
S specific gravity	1
m reduced mass of the vibrational mode	$\frac{m_H \times m_O}{m_H + m_O} = 1.6 \times 10^{-24}$ g
q reduced mass of the vibrational mode	electron charge
N numerical density of vibrations per 1 cm ³	$\frac{S}{1 \times m_H + 2 \times m_O} = 3.3 \times 10^{22}$
$n_{2,IR}$ nonlinear refractive index coefficient in the IR frequency range, cm ² /W, for reference	4.1×10^{-16} [113]
n_2 nonlinear refractive index coefficient in the THz frequency range, cm ² /W	5.1×10^{-10}

Using these values, the calculated value of n_2 for water in the low-frequency range is $n_2 = 5 \times 10^{10}$ cm²/W, which is 6 orders of magnitude higher than the similar coefficient in the near infrared range $n_{2,IR} = 4.1 \times 10^{-16}$ cm²/W [113].

III.4. Z-scan technique for measuring third-order nonlinearities

The z-scan technique is one of the most widespread methods for assessing the nonlinear properties of thin media. It was first proposed in [114] and is based on the measuring the change in phase induced on a laser beam upon propagation through a nonlinear material, which is simply related to the change in index of refraction. Below we present more detailed description of the technique.

Using a single highly focused Gaussian pulse, as shown in Figure III.3, it is possible to measure the transmission of a nonlinear medium through a finite aperture in the far field as a function of the position of the sample z measured relative to the focal plane. In the following example, it will be qualitatively clarified how such a curve (z-scan) is associated with nonlinear refraction of the sample. Suppose, for example, a material with a negative nonlinear refractive index and a thickness less than the diffraction length of the focused beam (thin medium). This can be considered as a thin lens with a variable focal length. Starting scanning at a distance far from the focus (negative z), the radiation intensity is low and slight nonlinear refraction is observed; therefore, the transmittance (D_2/D_1 in Figure III.3) remains relatively constant. When the sample approaches the focus, the radiation intensity increases, which leads to the Kerr lens formation within the sample. A negative induced lens in front of the focus will tend to collimate the beam, which leads to a narrowing of the beam at the aperture, which leads to an increase in the measured transmittance. As the scanning along z continues and the sample passes through the focal plane and is to the right of it (positive z), self-defocusing increases the beam divergence, which leads to broadening of the beam at the aperture and, consequently, to a decrease in the transmittance. This suggests that there is zero when the sample crosses the focal plane. Z-scan is completed as the sample moves away from the focus (positive z), so that the transmittance becomes linear again.

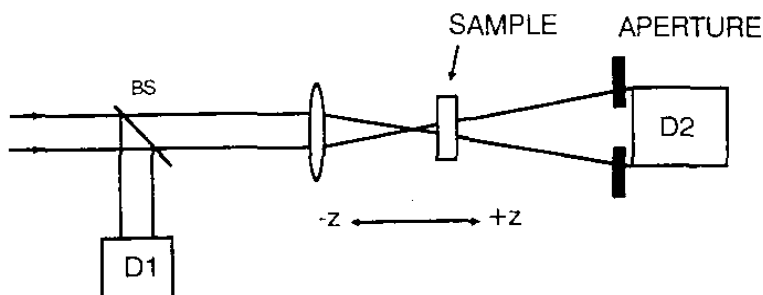


Fig. III.3. Example of an experimental setup where the ratio D_2/D_1 is represented as a function of the position of the sample z [114].

The prefocal transmittance maximum (peak), followed by the postfocal minimum transmittance limit (valley), is thus a z-scan signal of negative nonlinear refraction. Positive nonlinear refraction, following the same analogy, gives rise to the opposite configuration of the valley-peak. An extremely useful feature of the Z-scan method is that the sign of the nonlinear refractive index immediately becomes apparent from the data, and, the value can be easily estimated using simple analysis for a thin medium.

In the Fig. III.3, it should be borne in mind that only nonlinear refraction was considered, assuming

that absorption nonlinearities (such as multiphoton absorption or saturable absorption) are absent. Qualitatively, multiphoton absorption suppresses the peak and enhances the valley, while saturable absorption causes the opposite effect. Sensitivity to nonlinear refraction is completely determined by the aperture, and removal of the aperture completely eliminates the effect. However, in this case, the Z scan will still be sensitive to nonlinear absorption. From such experiments with an “open” aperture, nonlinear absorption coefficients can be extracted.

III.5. Theory of Z-scan technique

In the general case, nonlinearities of any order can be considered; however, for simplicity, we consider only cubic nonlinearity, where the refractive index n is expressed in terms of the nonlinear indices n_2 (CGSE) or γ (m^2/W):

$$n = n_0 + \frac{n_2}{2} |E|^2 = n_0 + \gamma I \quad (\text{III.20})$$

where n_0 is the linear refractive index, E is the peak value of the electric field (CGSE), and I is the intensity of the laser beam (SI) in the sample (n_2 and γ are related by the formula $n_2(\text{CGSE}) = (cn_0/40\pi) \gamma$ (m^2/W), where c (m/s) is the speed of light in vacuum). Assuming that a Gaussian beam TEM_{00} with a beam waist w_0 moves in the $+z$ direction, we can write E as:

$$E(z, r, t) = E_0(t) \frac{w_0}{w(z)} \exp\left(-\frac{r^2}{w^2(z)} - \frac{ikr^2}{2R(z)}\right) e^{-i\varphi(z,t)} \quad (\text{III.21})$$

where $w^2(z) = w_0^2(1 + z^2/z_0^2)$ is the beam radius, $R(z) = z(1 + z_0^2/z^2)$ is the radius of curvature of the wavefront at the point z , $z_0 = kw_0^2/2$ is the beam diffraction length, $k = 2\pi/\lambda$ is the wave vector and λ is the laser wavelength, all values are in free space. $E_0(t)$ indicates the electric field of radiation in focus and contains the envelope of the temporal profile of the laser pulse. The term $e^{-i\varphi(z,t)}$ contains all radially homogeneous phase changes. Since we are dealing only with the calculation of the radial phase changes $\Delta\varphi(r)$, the slowly varying envelope approximation is applied, and all other phase changes that are uniform in r are ignored.

If the sample thickness is small enough, i.e. changes in the beam diameter due to diffraction or nonlinear refraction can be neglected, then the medium is considered “thin”, and in this case the self-focusing process is called “external self-action” [115]. For linear diffraction, this means that $L \ll z_0$, and for nonlinear refraction, $L \ll z_0/\Delta\varphi(0)$. In most experiments using the Z-scan technique, the second criterion is automatically satisfied, since $\Delta\varphi$ is small. In addition, the first criterion for linear diffraction is too strict and it is enough to replace it with $L < z_0$. This assumption greatly simplifies the problem, and the amplitude \sqrt{I} and the phase φ of the electric field as a function of z are now determined by a pair of simple equations:

$$\frac{d\Delta\varphi}{dz'} = \Delta n(I)k \quad (\text{III.22})$$

$$\frac{dI}{dz'} = -\alpha(I)I \quad (\text{III.23})$$

where z' is the propagation distance in the sample and $\alpha(I)$ includes linear and nonlinear absorption. It should be noted that z' should not be confused with the position of sample z . In the case of cubic nonlinearity and negligible nonlinear absorption, (III.22) and (III.23) give a phase shift $\Delta\varphi$ on the output surface of the sample, which simply follows the radial change in the incident intensity at a given position of the sample z . In this case,

$$\Delta\varphi(z, r, t) = \Delta\varphi_0(z, t) \exp\left(-\frac{2r^2}{w^2(z)}\right) \quad (\text{III.24})$$

where

$$\Delta\varphi_0(z, t) = \frac{\Delta\Phi_0(t)}{1+z^2/z_0^2} \quad (\text{III.25})$$

$\Delta\Phi_0(t)$ is the phase shift on the axis in focus and is defined as

$$\Delta\Phi_0(t) = k\Delta n_0(t)L_{eff} \quad (\text{III.26})$$

where $L_{eff} = (1 - e^{-\alpha L})/\alpha$, L is the length of the sample, and α is the linear absorption coefficient. Here $\Delta n_0 = \gamma I_0(t)$, and $I_0(t)$ is the intensity on the axis in focus (i.e., $z = 0$). Fresnel reflection losses are ignored, so, for example, $I_0(t)$ is the intensity inside the sample.

The complex electric field emerging from sample E_e now contains nonlinear phase distortion

$$E_e(r, z, t) = E(z, r, t) e^{-\alpha L/2} e^{i\Delta\varphi(z, r, t)} \quad (\text{III.27})$$

By virtue of the Huygens principle, it is possible to obtain the field distribution in the far field on the aperture plane through the Hankel transform of the zero order from E_e [116]. However, it is also possible to use a more convenient approach to Gaussian input beams, which is called the ‘‘Gaussian Decomposition’’ method described in [115], which expanding the complex electric field on the exit plane of the sample into the sum of Gaussian beams through Taylor series expansion of nonlinear phase term $e^{i\Delta\varphi(z, r, t)}$ in (III.27). I.e,

$$e^{i\Delta\varphi(z, r, t)} = \sum_{m=0}^{\infty} \frac{[i\Delta\varphi_0(z, t)]^m}{m!} e^{-2mr^2/w^2(z)} \quad (\text{III.28})$$

Each Gaussian beam can be propagated to the aperture plane, where they will be summed to reconstruct the beam. When considering the initial curvature of the focused beam, the resulting field distribution at the aperture is as follows:

$$E_a(r, t) = E(z, r = 0, t) e^{-\alpha L/2} \sum_{m=0}^{\infty} \frac{[i\Delta\varphi_0(z, t)]^m}{m!} \frac{w_{m0}}{w_m} \exp\left(-\frac{r^2}{w_m^2} - \frac{ikr^2}{2R_m} + i\theta_m\right) \quad (\text{III.29})$$

Defining d as the propagation distance in free space from the sample to the aperture plane, and $g = 1 + d/R(z)$, the remaining parameters in (III.29) can be expressed as

$$w_{m0}^2 = \frac{w^2(z)}{2m + 1}$$

$$d_m = \frac{kw_{m0}^2}{2}$$

$$w_m^2 = w_{m0}^2 \left[g^2 + \frac{d^2}{d_m^2} \right]$$

$$R_m = d \left[1 - \frac{g}{g^2 + d^2/d_m^2} \right]^{-1}$$

$$\theta_m = \arctan \left[\frac{d/d_m}{g} \right]$$

Expression (III.29) is a general case with respect to [116], where a collimated beam ($R = \infty$) was considered, for which $g = 1$. It was found that the ‘‘Gaussian Decomposition’’ method is very useful for small phase distortions detected using the z-scan technique, since only a few terms of the sum in (III.29) are needed. The method also extends easily to higher-order nonlinearities.

The power transmitted through the aperture is obtained by spatial integration of $E_a(r, t)$ up to the radius of the aperture r_a and can be expressed as:

$$P_T(\Delta\Phi_0(t)) = c\varepsilon_0 n_0 \pi \int_0^{r_a} |E_a(r, t)|^2 r dr \quad (\text{III.30})$$

where ε_0 is the dielectric constant. Given the temporal change in the pulse, the normalized z-scan transmittance $T(z)$ can be calculated as

$$T(z) = \frac{\int_{-\infty}^{\infty} P_T(\Delta\Phi_0(t)) dt}{S \int_{-\infty}^{\infty} P_i(t) dt} \quad (\text{III.31})$$

where $P_i(t) = \pi w_0^2 I_0(t)/2$ is the instantaneous input power (inside the sample) and $S = 1 - \exp(-2r_a^2/w_a^2)$ is the linear transmission of the aperture, and w_a is the beam radius at the aperture in linear regime.

First, consider instantaneous nonlinearity and a square pulse in time domain to illustrate the general features of z-scan technique. This is equivalent to the assumption that the radiation is continuous, and the nonlinearity has reached a steady state. The normalized transmittance $T(z)$ in the far field is shown in Fig. III.4 for $\Delta\Phi_0 = \pm 0.25$ and a small aperture ($S = 0.01$). It demonstrates the expected features, namely, the valley and peak (v-p) for positive nonlinearity and the peak and valley (p-v) for negative one.

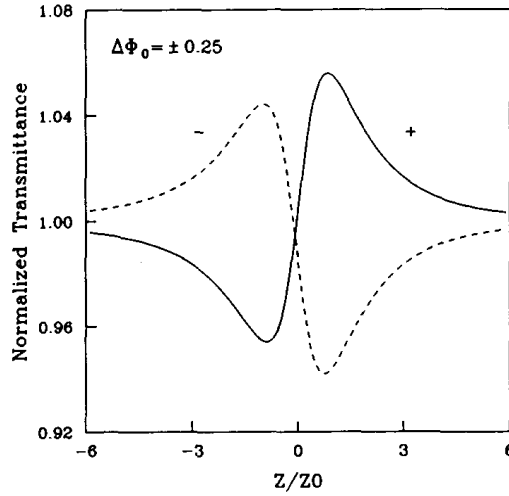


Fig. III.4. Calculated Z-scan transmission curves for cubic nonlinearity with two polarities and small aperture ($S = 0.01$) [114].

For a given $\Delta\Phi_0$, the magnitude and shape of $T(z)$ are independent of wavelength or geometry if the far field condition for the aperture plane is satisfied ($d \gg z_0$). Aperture size S , however, is an important parameter since a large aperture reduces the differential $T(z)$. This decrease is more noticeable at the peak where the beam narrows and can lead to a peak transmittance that cannot exceed $(1 - S)$. With a very large aperture or no aperture ($S = 1$), the effect disappears and $T(z) = 1$ for all z and $\Delta\Phi_0$. For small $|\Delta\Phi_0|$ peak and valley occur at the same distance relative to the focus, and for cubic nonlinearity this distance turns out to be $\cong 0,86z_0$. For large phase distortions ($|\Delta\Phi_0| > 1$), the numerical estimate (III.29) - (III.31) shows that this symmetry is no longer fulfilled, and the peak and valley move toward $\pm z$ for the corresponding sign of nonlinearity ($\pm\Delta\Phi_0$), so that the separation remains almost constant:

$$\Delta Z_{p-v} \cong 1,7z_0 \quad (\text{III.32})$$

The measured value of ΔT_{p-v} can be defined as the difference between the normalized transmission peak and valley: $T_p - T_v$. The change in this value depending on $|\Delta\Phi_0|$ calculated for different aperture sizes is shown in Figure III.5.

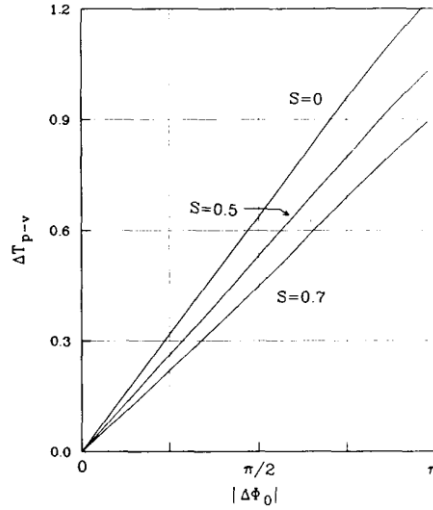


Fig. III.5. Calculated ΔT_{p-v} values as a function of the phase shift in focus ($\Delta\Phi_0$). Sensitivity as indicated by the slope of the curves, decreases slowly with increase in the size of the aperture ($S > 0$) [114].

These curves demonstrate some useful features. First, for a given order of nonlinearity, they can be considered universal. In other words, they are independent of the laser wavelength, geometry (as long as the far field condition is satisfied), and the sign of nonlinearity. Secondly, for all aperture sizes, the change in ΔT_{p-v} turns out to be almost linearly dependent on $|\Delta\Phi_0|$. For small phase distortion and small aperture ($S \cong 0$):

$$\Delta T_{p-v} \cong 0.406|\Delta\Phi_0| \quad (\text{III.33})$$

Numerical calculations show that this ratio has an accuracy of up to 0.5% for $|\Delta\Phi_0| \leq \pi$. As shown in Figure III.5, for large apertures the linear coefficient 0.406 decreases, so that at $S = 0.5$ it becomes $\cong 0.34$, and at $S = 0.7$, it decreases to $\cong 0.29$. Based on the numerical fit, the following relationships can be used to include such changes with an accuracy of $\pm 2\%$:

$$T_{p-v} \cong 0.406(1 - S)^{0.25}|\Delta\Phi_0|, \text{ for } |\Delta\Phi_0| \leq \pi \quad (\text{III.34})$$

The consequences of (III.33) and (III.34) are very promising in the sense that they can be used to easily estimate the nonlinear refractive index (n_2) with good accuracy based on z-scan experimental results. The most intriguing thing about these expressions is that they show the very sensitive nature of the z-scan method. For example, if the experimental apparatus and data acquisition systems are capable of resolving transmittance changes $T_{p-v} \cong 1\%$, this makes it possible to measure phase changes corresponding to wavefront distortions of less than $\lambda/250$. However, to achieve this sensitivity, a relatively good optical quality of the test sample is required.

Now the stationary results can easily be expanded to include transition effects caused by pulsed radiation, using the time-averaged changes in the refractive index $\langle \Delta n_0(t) \rangle$, where

$$\langle \Delta n_0(t) \rangle = \frac{\int_{-\infty}^{\infty} \Delta n_0(t) I_0(t) dt}{\int_{-\infty}^{\infty} I_0(t) dt} \quad (\text{III.35})$$

The time-averaged $\langle \Delta \Phi_0(t) \rangle$ is related to $\langle \Delta n_0(t) \rangle$ through (III.26). With nonlinearity having an instantaneous response time and fall time relative to the pulse duration for a temporary Gaussian pulse:

$$\langle \Delta n_0(t) \rangle = \Delta n_0 / \sqrt{2} \quad (\text{III.36})$$

where Δn_0 now represents the change in the maximum of the refractive index on the axis in focus. For a cumulative nonlinearity having a fall time much longer than the pulse duration (for example, thermal), the instantaneous change of the refractive index is given by the following integral:

$$\Delta n_0(t) = A \int_{-\infty}^t I_0(t') dt' \quad (\text{III.37})$$

where A is a constant depending on the nature of the nonlinearity. If we substitute (III.37) into (III.35), we obtain the averaging coefficient of the energy density 1/2. I.e,

$$\langle \Delta n_0(t) \rangle = \frac{1}{2} AF \quad (\text{III.38})$$

where F is the energy density in focus inside the sample. Interestingly, the coefficient 1/2 is independent of the temporal form of the pulse.

These equations were obtained based on cubic nonlinearity (i.e., the $\chi^{(3)}$ effects). A similar analysis can be performed for higher order nonlinearities. Regardless of the order of nonlinearity, the same qualitative characteristics should be expected from a z-scan analysis. Nonlinearities encountered in semiconductors, where the refractive index changes due to charge carriers generated by two-photon absorption (ie, the sequential effect $\chi^{(3)}$: $\chi^{(1)}$) manifest themselves as a fifth-order nonlinearity [117].

III.6. Experimental verification of the water nonlinear refractive index estimation in the THz frequency range by z-scan technique

Usually, the z-scan technique is strictly applicable only to quasimonochromatic radiation. However, it is also widely used in the case of femtosecond pulsed radiation, which has a wide spectrum [118]. Even though the method involves the use of nonparaxial linearly polarized radiation, the differences between the paraxial and nonparaxial modes for pulses of a small number of oscillations are insignificant, as was shown in [119]. It was also shown in [120] that the z-scan technique is also applicable to pulsed THz radiation, but to minimize the error in determining n_2 it is necessary to use a thin sample with a thickness equal to or less than the longitudinal spatial size of the pulse. In the experiment below thin flat water jet was used. A water jet, unlike a film and other thin fixed surfaces, provides a constant change of liquid in the region of interaction with radiation, which eliminates the contribution of thermal cumulative effects (when selecting the correct liquid flow rate) to the nonlinearity under study.

Figure III.6 shows the experimental setup for measuring the nonlinear refractive index of a flat liquid jet using THz pulses. The generation of THz radiation in this system is based on the optical rectification of femtosecond pulses in a lithium niobate crystal [121]. The TERA-AX (Avesta Project) generator is pumped using a laser femtosecond system (pulse duration 30 fs, pulse energy 2.2 mJ, repetition rate 1 kHz, central wavelength 800 nm).

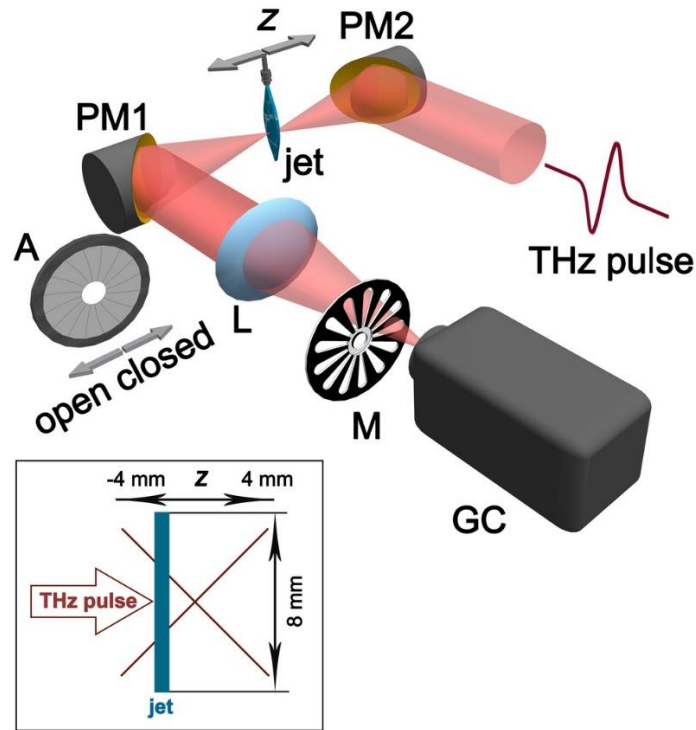


Fig. III.6. Experimental setup for measuring the nonlinear refractive index (n_2) of a flat water jet in the THz spectral range. Insert - the geometric position of the jet when moving along the z axis relative to the THz pulse.

The energy of a THz pulse is 400 nJ, the pulse duration is 1.5 ps (see Figure III.7a) and the spectrum width is 0.1-2.5 THz (see Figure III.7b). The THz electric field was measured using a conventional electro-optical detection system. The intensity of the THz radiation is controlled by decreasing the intensity of the femtosecond pump beam. A change in the pump intensity during the generation of THz radiation leads to a change in the divergence of the terahertz beam and also affects the position of the maxima of the spectrum [122]. The experiment uses a parabolic mirror with a focal length of 25 mm to collimate the THz radiation generated by the LiNbO₃ crystal. Then, when adjusting the experimental setup, THz beam with a diameter of 25.4 mm obtained at the TERA-AX output is adjusted to be collimated at all femtosecond pump energies, and its optical axis passes through the center of the parabolic mirror PZ1. Pulse THz radiation is focused and collimated by two parabolic mirrors (PZ1 and PZ2) with a focal length of 12.5 mm. The spatial size of the THz radiation at the generator output is 25.4 mm. Caustic diameter 1 mm (full width at half maximum). To obtain a higher intensity in the caustic, a short-focus parabolic mirror with a large numerical aperture is used.

Such a geometry makes it possible to achieve a peak intensity in the caustic of a THz beam of $0.5 \times 10^8 \text{ W/cm}^2$.

A flat water jet (jet) is moved along the caustic region from -4 mm to 4 mm using a linear motorized translator; the displacement limitation is determined by the jet width and the focus geometry of the THz radiation (see insert Figure III.6). The polarization of THz radiation is vertical.

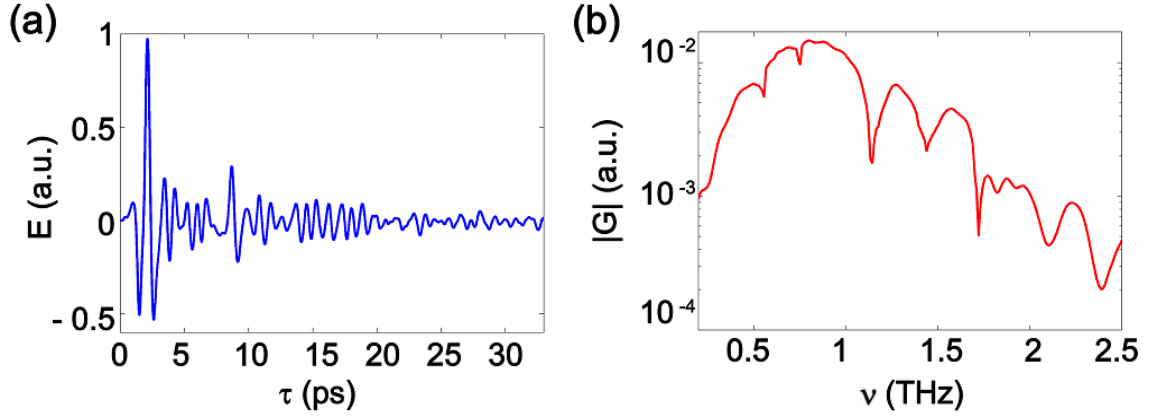


Fig. III.7. (a) Temporal form and (b) spectrum of a THz pulse generated by the TERA – AX system.

The experiment used distilled water, which does not contain any impurities, and is a clean medium. The jet is oriented along the normal to the incident radiation and has a thickness of 0.1 mm, which corresponds to condition [120] for the ratio of the sample thickness (L) to the spatial pulse size (x):

$$\frac{L}{x} = \frac{100 \times 10^{-6} \text{ m}}{1 \times 10^{-12} \text{ s} \cdot 3 \times 10^8 \text{ m/s}} = \frac{1}{3} < 1. \quad (\text{III.39})$$

The jet is created using a nozzle, which is a hollow cylinder with a compressed tube and two blades overlapping the edges [123,124]. This design forms a flat surface of water with a laminar flow. The optical axis of the THz pulse passes through the center of the jet region with a constant thickness. Thanks to the use of a pump, it is possible to select the flow rate, so each THz pulse interact with new volume of water (10^3 mm/s in this experiment). The hydraulic accumulator in the water supply system can significantly reduce the ripple associated with the operation of the water pump. THz radiation is collimated by a parabolic mirror PZ2 and is focused by a lens (L) on a Golay cell (G). For closed aperture geometry, the aperture (A) moves into the beam (closed position). Detection synchronization is performed using a mechanical modulator (M) located between the lens and the Golay cell. When the jet moves along the z axis through the focal region of THz radiation, the average power of the latter is measured in open and closed aperture regimes.

Figure III.5 shows z -scan curves for the water jet measured with an open (Figure III.8a) and a closed aperture (Figure III.8b) for different THz radiation energies. Each curve is averaged over 50 measurements. Figure III.8a shows about 2% saturable absorption, caused by an increase in the THz radiation energy by 2 orders of magnitude. This confirms the nonlinear absorption of the medium. To

determine n_2 , we will use experimental data with a closed aperture. According to [114], for a more correct calculation of n_2 from the closed aperture data, it is necessary to subtract the effect of nonlinear absorption, for which the curve for closed aperture should be divided by open aperture one.

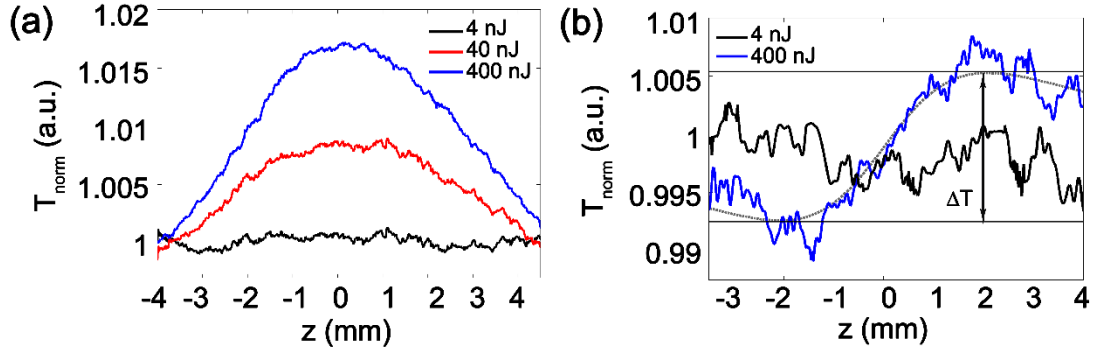


Fig. III.8. Z-scan curves for a 0.1 mm thick water jet with (a) open and (b) closed aperture for different THz radiation energies of 4 nJ, 40 nJ and 400 nJ.

As can be seen from Figure III.8b, the movement of the jet along the z axis leads to a change in the measured THz radiation intensity, which is a unique feature of the z -scan curves. This is caused by a change in the divergence of radiation at different positions of the water jet in the caustic, where the nonlinear Kerr lens is induced by the THz radiation field. In this case, it is advisable to use standard equations that are applicable for monochromatic radiation [114,125,126] in order to estimate n_2 of water in accordance with the measurement results:

$$n_2 = \frac{\Delta T}{0.406 I_{in}} \times \frac{\sqrt{2} \lambda}{2\pi L_{\alpha} (1 - S)^{0.25}} \quad (\text{III.40})$$

where $\Delta T = 0.013$ (Figure III.9) is the peak-to-valley ratio of the transmission curve, S is the linear transmission of the aperture, L is the sample thickness, $L_{\alpha} = \alpha^{-1}[1 - \exp(-\alpha L)]$ is the effective interaction length, α is the absorption coefficient ($\alpha = 100 \text{ cm}^{-1}$ for water), λ is the wavelength, and I_{in} is the input radiation intensity. The linear transmittance of the aperture is 2%, which allows to maximize the sensitivity of the measurement method but reduces the signal-to-noise ratio. The radiation wavelength $\lambda = 0.4 \text{ mm}$ ($\nu = 0.75 \text{ THz}$) corresponds to the maximum in the spectrum of the generation of THz radiation (see Figure III.7b). The result of the estimation of the coefficient of the nonlinear refractive index for water from experimentally obtained data according to formula (III.40) was $n_2 = 7 \times 10^{-10} \text{ cm}^2/\text{W}$.

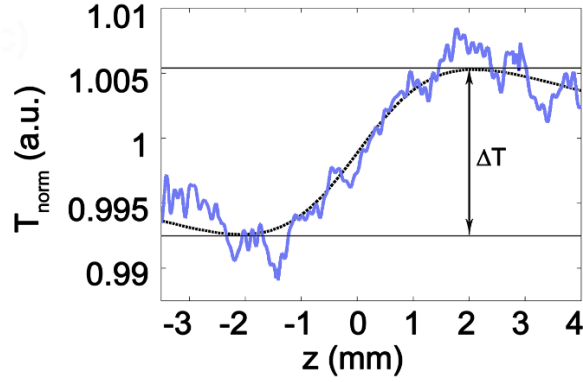


Fig. III.9. Z-scan peak-to-valley ratio estimation.

To illustrate the correct use of equation (III.40) for calculating the coefficient of nonlinear refractive index in the case of broadband THz radiation, we compare the experimental data for closed aperture with the analytical z-scan curve for monochromatic radiation (Figure III.10) according to equation (III.29 - III.31).

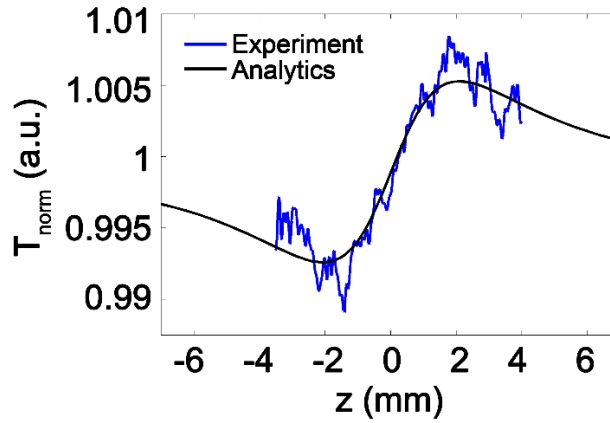


Fig. III.10. Comparison of experimental z-scan curve for a 0.1 mm thick water jet for pulsed broadband THz radiation in the case of a closed aperture with an analytical curve for monochromatic radiation with a wavelength of 0.4 mm.

As can be seen, the experimental z-scan curve for broadband THz radiation is in good agreement with the analytical z-scan curve for monochromatic radiation. This confirms the reliability of the obtained value n_2 of liquid water in the experiment.

The value of $n_2 = 7 \times 10^{-10} \text{ cm}^2/\text{W}$ obtained during the experiment for liquid water coincides in order with the calculated $n_2 = 5 \times 10^{-10} \text{ cm}^2/\text{W}$, which was obtained using the modified theoretical approach, which takes into account the anharmonicity of molecular vibrations. Therefore, the coefficient of the nonlinear refractive index of water in the THz frequency range (0.2 -2.5 THz) exceeds the value in the infrared region of the spectrum $n_{2,IR} = 4.1 \times 10^{-16} \text{ cm}^2/\text{W}$ by 6 orders of magnitude. Thus, from the point of view of the application and further development of research, these results open up new prospects for the study of various materials in the THz frequency range.

References

1. Akhmanov S.A., Vysloukh V.A., Chirkin A.S. Optics of Femtosecond Laser Pulses, American Inst // Phys., New York. Moscow, Izdatel'stvo Nauka, 1992. P. 312.
2. Spielmann C. et al. Ultrabroadband Femtosecond Lasers // IEEE J. Quantum Electron. Institute of Electrical and Electronics Engineers (IEEE), 1994. Vol. 30, № 4. P. 1100–1114.
3. Paul P.M. et al. Observation of a train of attosecond pulses from high harmonic generation // Science (80-.). American Association for the Advancement of Science (AAAS), 2001. Vol. 292, № 5522. P. 1689–1692.
4. von der Linde D., Schüler H. Breakdown threshold and plasma formation in femtosecond laser–solid interaction // J. Opt. Soc. Am. B. The Optical Society, 1996. Vol. 13, № 1. P. 216.
5. The Supercontinuum Laser Source // The Supercontinuum Laser Source / ed. Alfano R.R. Springer New York, 1989.
6. Karasawa N. et al. Generation of intense ultrabroadband optical pulses by induced phase modulation in an argon-filled single-mode hollow waveguide // Opt. Lett. The Optical Society, 2000. Vol. 25, № 3. P. 183.
7. Karasawa N. et al. Comparison between theory and experiment of nonlinear propagation for a few-cycle and ultrabroadband optical pulses in a fused-silica fiber // IEEE J. Quantum Electron. Institute of Electrical and Electronics Engineers (IEEE), 2001. Vol. 37, № 3. P. 398–404.
8. Ranka J.K., Windeler R.S., Stentz A.J. Visible continuum generation in air–silica microstructure optical fibers with anomalous dispersion at 800 nm // Opt. Lett. The Optical Society, 2000. Vol. 25, № 1. P. 25.
9. Li H. et al. Supercontinuum generation in tapered fibers // 2009 Asia Communications and Photonics Conference and Exhibition, ACP 2009. The Optical Society, 2009. Vol. 25, № 19. P. 1415.
10. Zheltikov A.M. Holey fibers // Uspekhi Fiz. Nauk. Uspekhi Fizicheskikh Nauk (UFN) Journal, 2000. Vol. 170, № 11. P. 1214–1215.
11. Nishioka H. et al. Ultrabroadband flat continuum generation in multichannel propagation of terrawatt Ti:sapphire laser pulses // Opt. Lett. The Optical Society, 1995. Vol. 20, № 24. P. 2505.
12. Chin S.L. et al. Filamentation and supercontinuum generation during the propagation of powerful ultrashort laser pulses in optical media (white light laser) // J. Nonlinear Opt. Phys. Mater. World Scientific Pub Co Pte Lt, 1999. Vol. 8, № 1. P. 121–146.
13. Brodeur A., Chin S.L. Ultrafast white-light continuum generation and self-focusing in transparent condensed media // J. Opt. Soc. Am. B. The Optical Society, 1999. Vol. 16, № 4. P. 637.
14. Baltuška A. et al. Optical pulse compression to 5 fs at a 1-MHz repetition rate // Opt. Lett. The Optical Society, 1997. Vol. 22, № 2. P. 102.
15. Nisoli M. et al. Compression of high-energy laser pulses below 5 fs // Opt. Lett. The Optical

Society, 1997. Vol. 22, № 8. P. 522.

16. Brabec T., Krausz F. Intense few-cycle laser fields: Frontiers of nonlinear optics // *Rev. Mod. Phys.* American Physical Society (APS), 2000. Vol. 72, № 2. P. 545–591.
17. Auston D.H. et al. Cherenkov radiation from femtosecond optical pulses in electro-optic media // *Phys. Rev. Lett.* American Physical Society (APS), 1984. Vol. 53, № 16. P. 1555–1558.
18. Jaroszynski D.A. et al. Superradiance in a short-pulse free-electron-laser oscillator // *Phys. Rev. Lett.* American Physical Society (APS), 1997. Vol. 78, № 9. P. 1699–1702.
19. Kim A.V., Ryabikin M.Y., Sergeev A.M. From femtosecond to attosecond pulses // *Uspekhi Fiz. Nauk. Uspekhi Fizicheskikh Nauk (UFN) Journal*, 1999. Vol. 169, № 1. P. 58.
20. Scrinzi A., Geissler M., Brabec T. Attosecond cross correlation technique // *Phys. Rev. Lett.* American Physical Society (APS), 2001. Vol. 86, № 3. P. 412–415.
21. Agrawal G.P. *Nonlinear Fiber Optics // Nonlinear Science at the Dawn of the 21st Century.* Springer Berlin Heidelberg, 2007. P. 195–211.
22. Brabec T., Krausz F. Nonlinear optical pulse propagation in the single-cycle regime // *Phys. Rev. Lett.* American Physical Society (APS), 1997. Vol. 78, № 17. P. 3282–3285.
23. Ranka J.K., Gaeta A.L. Breakdown of the slowly varying envelope approximation in the self-focusing of ultrashort pulses // *Technical Digest - European Quantum Electronics Conference. The Optical Society*, 1998. Vol. 23, № 7. P. 244.
24. Boyer G. High-power femtosecond-pulse reshaping near the zero-dispersion wavelength of an optical fiber // *Opt. Lett.* The Optical Society, 1999. Vol. 24, № 14. P. 945.
25. Milosevic N., Tempea G., Brabec T. Optical pulse compression: bulk media versus hollow waveguides // *Opt. Lett.* The Optical Society, 2000. Vol. 25, № 9. P. 672.
26. Vinogradov M.B., Rudenko O.V., Sukhorukov A.P. *Wave theory.* Moscow, Nauka, 1990.
27. Copson E.T., Born M., Wolf E. *Principles of Optics // Math. Gaz.* Moscow, Nauka, 1961. Vol. 45, № 353. P. 274.
28. Kozlov S.A. Problems of nonlinear optical pulses of extremely short duration // *Bull. young Sci. Fiz. ser.* 2000. Vol. 1. P. 7–16.
29. Bespalov V.G., Kozlov S.A., Shpolyanski Y.A. Method for analyzing the propagation dynamics of femtosecond pulses with a continuum spectrum in transparent optical media // *J. Opt. Technol.* The Optical Society, 2000. Vol. 67, № 4. P. 303.
30. Bespalov V.G., Kozlov S.A., Shpolyanskiy Y.A. Simplified field wave equations for the nonlinear propagation of extremely short light pulses // *Phys. Rev. A - At. Mol. Opt. Phys.* American Physical Society (APS), 2002. Vol. 66, № 1. P. 138111–1381110.
31. Shpolyanskiy Y.A., Kozlov S.A., Bespalov V.G. Features of spectrum supercontinuum generation by intensive femtosecond laser pulses in transparent optical media propagation // *Novel Lasers and Devices-Basic Aspects.* 2014. P. LMB1.

32. Kozlov S.A., Sazonov S. V. Nonlinear propagation of optical pulses of a few oscillations duration in dielectric media // *J. Exp. Theor. Phys.* Pleiades Publishing Ltd, 1997. Vol. 84, № 2. P. 221–228.
33. Azarenkov A.N., Altshuler G.B., Kozlov S.A. Self-action of supremely short light pulses in fibers // *Nonlinear Optics II*. 1991. Vol. 1409. P. 166.
34. Kozlov S.A. Polarization self pulses of several fluctuations of the light field in dielectric media // *Opt. i Spektrosk.* 1998. Vol. 84, № 6. P. 979–981.
35. Ukrainsky A.O., Kozlov S.A. Polarization effects in the interaction of extremely short light pulses with nonlinear media // *Journal of Optics B: Quantum and Semiclassical Optics*. IOP Publishing, 2001. Vol. 3, № 2. P. S180.
36. Maimistov A.I. Some models of propagation of extremely short electromagnetic pulses in a nonlinear medium // *Kvantovaya Elektron.* IOP Publishing, 2000. Vol. 30, № 4. P. 303–304.
37. Mishkin E.A. Propagation of ultrashort light pulses in a laser medium // *Physica*. 1974. Vol. 73, № 3. P. 459–473.
38. Bepalov V.G. et al. Spectral superbroadening of high-power femtosecond laser pulses and their time compression down to one period of the light field // *J. Opt. Technol. (A Transl. Opt. Zhurnal)*. Optical Society of America, Inc., 1998. Vol. 65, № 10. P. 823–825.
39. Belenov E.M., Prokopovich I.P. Dynamics of high-power ultrashort laser pulses in resonant media // *J. Russ. Laser Res.* Springer Science and Business Media LLC, 1994. Vol. 15, № 4. P. 283–327.
40. Belenov É. et al. Transformation of the field of an intense ultrashort pulse in a Raman-active medium // *Sov. J. Exp. Theor. Phys. Lett.* AMERICAN INSTITUTE OF PHYSICS, 1994. Vol. 60. P. 770.
41. Azarenkov A.N. et al. Fast nonlinearity of the refractive index of solid-state dielectric active media // *Quantum Electron.* IOP Publishing, 1993. Vol. 23, № 8. P. 633–655.
42. Stumpf S.A., Korolev A.A., Kozlov S.A. On the nature and persistence linear polarized dielectrics in the light pulses containing a small number of vibrations of the optical field // *Izv. Ross. Akad. Nauk. Fiz. Seriya*. 2006. Vol. 70, № 1. P. 118–125.
43. NN R. *Opticheskaya bistabil'nost' i gisteresis v raspredelennykh nelineinykh sistemakh (Optical Bistability and Hysteresis in Distributed Nonlinear Systems)*. Moscow: Nauka, 1997.
44. Berkovsky A.N., Kozlov S.A., Shpolyanskiy Y.A. Self-focusing of few-cycle light pulses in dielectric media // *Phys. Rev. A - At. Mol. Opt. Phys.* American Physical Society (APS), 2005. Vol. 72, № 4.
45. Berkovskii A.N., Kozlov S.A., Shpolyanskii Y.A. Self-focusing of pulses with a small number of vibrations of the light field // *J. Opt. Technol.* The Optical Society, 2002. Vol. 69, № 3. P. 163.
46. Kozlov S.A., Petrosenko P.A. Self-division of a pulse consisting of several light-field oscillations in a nonlinear medium with dispersion // *JETP Lett.* Pleiades Publishing Ltd, 2002.

Vol. 76, № 4. P. 206–210.

47. Kozlov S.A., Petrosenko P.A. The dynamics of space-time spectrum of few-cycle light pulses along with the nonparaxial self focusing in dielectric media // *ICONO 2007: Nonlinear Space-Time Dynamics* / ed. Kivshar Y., Rosanov N. SPIE, 2007. Vol. 6725. P. 67251O.
48. Ames J.N. et al. Excess noise generation during spectral broadening in a microstructured fiber // *Appl. Phys. B Lasers Opt.* Springer Science and Business Media LLC, 2003. Vol. 77, № 2–3. P. 279–284.
49. Tzortzakis S. et al. Self-guided propagation of ultrashort ir laser pulses in fused silica // *Phys. Rev. Lett. American Physical Society (APS)*, 2001. Vol. 87, № 21. P. 213902-1-213902–213904.
50. Kandidov V.P., Kosareva O.G., Koltun A.A. Nonlinear optical transformation of a high-power laser pulse in air // *Kvantovaya Elektron.* IOP Publishing, 2003. Vol. 33, № 1. P. 69–75.
51. Chen Y. et al. Evolution and termination of a femtosecond laser filament in air // *Opt. Lett. The Optical Society*, 2007. Vol. 32, № 24. P. 3477.
52. Kosareva O.G. et al. Optimization of a femtosecond pulse self-compression region along a filament in air // *Appl. Phys. B Lasers Opt.* Springer Science and Business Media LLC, 2008. Vol. 91, № 1. P. 35–43.
53. Sudrie L. et al. Femtosecond Laser-Induced Damage and Filamentary Propagation in Fused Silica // *Phys. Rev. Lett. American Physical Society (APS)*, 2002. Vol. 89, № 18.
54. Belenov E.M., Nazarkin A.V. Nonstationary diffraction effectsyou clot propagation of the electromagnetic field in a vacuum // *Zhurnal Eksp. i Teor. Fiz.* 1991. Vol. 53, № 4. P. 188–191.
55. Ukrainsky A.O., Kozlov S.A. Polarization effects in the interaction of extremely short light pulses with nonlinear media // *Journal of Optics B: Quantum and Semiclassical Optics.* IOP Publishing, 2001. Vol. 3, № 2. P. S180–S184.
56. Shpolyanskiy Y.A. et al. Analytic study of continuum spectrum pulse dynamics in optical waveguides // *Appl. Phys. B Lasers Opt.* Springer Science and Business Media LLC, 2003. Vol. 77, № 2–3. P. 349–355.
57. Litvinenko O. Fundamentals of radio optics. Kiev, Tekhnika, 1974.
58. Kozlov S.A. Spectral equations in femtosecond nonlinear optics, in: *Problemy Kogerentnoy i Nelineynoy Optiki* // St. Petersburg. State Univ. Inf. Technol. 2002. P. 143–160.
59. Fishman L., McCoy J.J. Derivation and application of extended parabolic wave theories. II. Path integral representations // *J. Math. Phys.* AIP Publishing, 1984. Vol. 25, № 2. P. 297–308.
60. Charushin A.N., Kozlov S.A., Simovski C.R. Nonlinear diffraction of strong-focusing light beams // *Optical Pulse and Beam Propagation* / ed. Band Y.B. SPIE, 1999. Vol. 3609. P. 238–244.
61. Shvartsburg A.B. Transient waveforms and nonperiodic waves in dispersive media (exactly solvable models) // *Uspekhi Fizicheskikh Nauk. Uspekhi Fizicheskikh Nauk (UFN) Journal*,

1998. Vol. 168, № 1. P. 103.
62. Aleshkevich V., Kartashov Y., Vysloukh V. Diffraction and focusing of extremely short optical pulses: generalization of the Sommerfeld integral // *Appl. Opt.* The Optical Society, 1999. Vol. 38, № 9. P. 1677.
 63. Kiselev A.P., Perel M. V. Highly localized solutions of the wave equation // *J. Math. Phys.* AIP Publishing, 2000. Vol. 41, № 4. P. 1934–1955.
 64. Zheltikov A.M. *Ultrashort Pulses and Methods of Nonlinear Optics* // Moscow, Fiz. 2006.
 65. Vasil'ev V.N. et al. Self-Broadening of Space-Time Spectra of Few-Cycle Pulses in Dielectric Media // *Opt. Spectrosc.* (English Transl. *Opt. i Spektrosk.* Pleiades Publishing Ltd, 2004. Vol. 96, № 2. P. 182–186.
 66. Shpolyanskiy Y.A. et al. Theory of spectral supercontinuum generation in microstructure fibers // *Optical Devices for Fiber Communication III* / ed. Digonnet M.J.F. SPIE, 2002. Vol. 4638. P. 107–114.
 67. Ivanov D.V., Petrosenko P.A., Kozlov S.A. Non-paraxial evolution of the space-time spectra of light wave of a small number fluctuations in nonlinear dielectric medium // In. *Proceedings Conf. Young Scientists and Specialists "Optics-2007."* 2007. P. 55.
 68. Vlasov S.I., Talanov V.I. *Self-focusing of waves.* Nizhny Novgorod, Institute of Applied Physics, 1997.
 69. Vysotina N. V et al. Polarization locking and nonparaxial spatial solitons in media with electronic Kerr nonlinearity // *Opt. Spectrosc.* (English Transl. *Opt. i Spektrosk.* Pleiades Publishing Ltd, 2005. Vol. 98, № 6. P. 895–903.
 70. Korn G., Korn T. *Mathematical Handbook (Schaums).pdf.* Moscow, Nauka, 1977.
 71. Kosevich A.M. et al. *An introduction to nonlinear physical mechanics* // KiIND. 1989.
 72. Bakhtin M., Shpolyansky Y. Limits of applicability of the honey- slowly varying envelope in ultrafast optics Limits of applicability of the honey- slowly varying envelope in ultrafast optics // *Mod. Technol. St. Petersburg. State Univ. Inf. Technol.* 2000. P. 12–29.
 73. Shpolyansky Y.A. Scenarios for the development of femtosecond spectral supercontinuum, Problems of coherent and nonlinear optics // *St. Petersburg. State Univ. Inf. Technol.* 2000. P. 136–153.
 74. Shpolyansky Y.A. Superbroadening spectrum intense femtosecond laser pulses in a medium with electronic and vibronic nonlinearities // *Bull. young Sci. Fiz. Seriya.* 2000. Vol. 1. P. 17–27.
 75. Deift P., Zhou X. A steepest descent method for oscillatory Riemann-Hilbert problems // *Bulletin of the American Mathematical Society.* American Mathematical Society (AMS), 1992. Vol. 26, № 1. P. 119–123.
 76. Kandidov V.P. et al. Self-transformation of a powerful femtosecond laser pulse into a white-light laser pulse in bulk optical media (or supercontinuum generation) // *Appl. Phys. B Lasers*

- Opt. Springer Science and Business Media LLC, 2003. Vol. 77, № 2–3. P. 149–165.
77. Fang X.J., Kobayashi T. Evolution of a super-broadened spectrum in a filament generated by an ultrashort intense laser pulse in fused silica // *Appl. Phys. B Lasers Opt.* Springer Science and Business Media LLC, 2003. Vol. 77, № 2–3. P. 167–170.
 78. Aközbek N. et al. Extending the supercontinuum spectrum down to 200 nm with few-cycle pulses // *New Journal of Physics.* IOP Publishing, 2006. Vol. 8, № 9. P. 177.
 79. Kolesik M. et al. Theory and simulation of supercontinuum generation in transparent bulk media // *Appl. Phys. B Lasers Opt.* Springer Science and Business Media LLC, 2003. Vol. 77, № 2–3. P. 185–195.
 80. Gaeta A.L. Catastrophic collapse of ultrashort pulses // *Phys. Rev. Lett.* American Physical Society (APS), 2000. Vol. 84, № 16. P. 3582–3585.
 81. Balakin A.A., Mironov V.A. Dynamics of self ultrashort electromagnetic pulse // *Pisma v Zhurnal Eksp. i Teor. Fiz.* 1967. Vol. 75, № 12. P. 741–745.
 82. Levenson M. The principles of nonlinear optics // *IEEE J. Quantum Electron.*, Moscow, Mir, 2004. Vol. 21, № 4. P. 400–400.
 83. Hosseini S.A. et al. Competition of multiple filaments during the propagation of intense femtosecond laser pulses // *AIP Conference Proceedings.* American Institute of Physics, 2005. Vol. 748. P. 198–214.
 84. Berkovskiĭ A.N., Kozlov S.A., Shpolyanskiĭ Y.A. Reducing the self-focusing efficiency of a femtosecond pulse in a transparent medium with dispersion when the number of light vibrations in it is decreased // *J. Opt. Technol.* The Optical Society, 2008. Vol. 75, № 10. P. 631.
 85. Grachev Y. V et al. Wireless data transmission method using pulsed THz sliced spectral supercontinuum // *IEEE Photonics Technol. Lett.* Institute of Electrical and Electronics Engineers (IEEE), 2018. Vol. 30, № 1. P. 103–106.
 86. Ferguson B., Zhang X.C. Materials for terahertz science and technology // *Nature Materials.* Springer Science and Business Media LLC, 2002. Vol. 1, № 1. P. 26–33.
 87. Smolyanskaya O.A. et al. Glycerol dehydration of native and diabetic animal tissues studied by THz-TDS and NMR methods // *Biomed. Opt. Express.* The Optical Society, 2018. Vol. 9, № 3. P. 1198.
 88. Rodriguez G., Dakovski G.L. Scaling behavior of ultrafast two-color terahertz generation in plasma gas targets: energy and pressure dependence // *Opt. Express.* The Optical Society, 2010. Vol. 18, № 14. P. 15130.
 89. Oladyshkin I. V, Fadeev D.A., Mironov V.A. Optical excitation of surface plasmons and terahertz emission from metals // *Phys. Rev. B.* American Physical Society (APS), 2019. Vol. 100, № 8.
 90. Ponomareva E. et al. Comparison of various liquids as sources of terahertz radiation from one-color laser filament // *Infrared, Millimeter-Wave, and Terahertz Technologies VI* / ed. Zhang X.-C., Tani M., Zhang C. SPIE, 2019. P. 7.

91. Balakin A. V et al. Terahertz wave generation from liquid nitrogen // Optics InfoBase Conference Papers. The Optical Society, 2019. Vol. Part F154-, № 6. P. 678.
92. Jin Q. et al. Preference of subpicosecond laser pulses for terahertz wave generation from liquids // Adv. Photonics. SPIE-Intl Soc Optical Eng, 2020. Vol. 2, № 01. P. 1.
93. Dubietis A. et al. Femtosekundinio superkontinuomo generavimas plačios apertūros kondensuotose terpėse // Lithuanian Journal of Physics. Lithuanian Academy of Sciences, 2017. Vol. 57, № 3. P. 113–157.
94. Tcypkin A.N. et al. Flat liquid jet as a highly efficient source of terahertz radiation // Opt. Express. The Optical Society, 2019. Vol. 27, № 11. P. 15485.
95. Stumpf S.A., Korolev A.A., Kozlov S.A. Few-cycle strong light field dynamics in dielectric media / ed. Andreev A.A. SPIE, 2007. P. 661408-661408–661412.
96. Eberly L., Allen J.H. Optical Resonance and Two Level Atoms // Physik in unserer Zeit. Wiley, 1976. Vol. 7, № 1. 31–32 p.
97. Kennedy P.K. et al. A First-Order Model for Computation of Laser-Induced Breakdown Thresholds in Ocular and Aqueous Media: Part II—Comparison to Experiment // IEEE J. Quantum Electron. Institute of Electrical and Electronics Engineers (IEEE), 1995. Vol. 31, № 12. P. 2250–2257.
98. Lindner J., Unterreiner A.N., Vöhringer P. Femtosecond relaxation dynamics of solvated electrons in liquid ammonia // ChemPhysChem. Wiley, 2006. Vol. 7, № 2. P. 363–369.
99. Dolgaleva K. et al. Prediction of an extremely large nonlinear refractive index for crystals at terahertz frequencies // Phys. Rev. A - At. Mol. Opt. Phys. American Physical Society (APS), 2015. Vol. 92, № 2.
100. Milam D. Review and assessment of measured values of the nonlinear refractive-index coefficient of fused silica // Appl. Opt. The Optical Society, 1998. Vol. 37, № 3. P. 546.
101. Boyd R.W. Nonlinear Optics // Nonlinear Optics. Academic press, 2008.
102. Tcypkin A.N. et al. High Kerr nonlinearity of water in THz spectral range // Opt. Express. The Optical Society, 2019. Vol. 27, № 8. P. 10419.
103. Rogalin V.E., Kaplunov I.A., Kropotov G.I. Optical Materials for the THz Range // Opt. Spectrosc. Pleiades Publishing Ltd, 2018. Vol. 125, № 6. P. 1053–1064.
104. Sajadi M., Wolf M., Kampfrath T. Terahertz-field-induced optical birefringence in common window and substrate materials // Opt. Express. The Optical Society, 2015. Vol. 23, № 22. P. 28985.
105. Yiwen E. et al. Terahertz wave generation from liquid water films via laser-induced breakdown // Appl. Phys. Lett. AIP Publishing, 2018. Vol. 113, № 18. P. 181103.
106. Jin Q. et al. Observation of broadband terahertz wave generation from liquid water // Appl. Phys. Lett. AIP Publishing, 2017. Vol. 111, № 7. P. 71103.
107. Ponomareva E.A. et al. Impact of laser-ionized liquid nonlinear characteristics on the efficiency

- of terahertz wave generation // *Opt. Lett.* The Optical Society, 2019. Vol. 44, № 22. P. 5485.
108. Hale G.M., Querry M.R. Optical Constants of Water in the 200-nm to 200- μ m Wavelength Region // *Appl. Opt.* The Optical Society, 1973. Vol. 12, № 3. P. 555.
 109. Chaplin M.F. Structure and Properties of Water in its Various States // *Encyclopedia of Water.* Wiley, 2019. P. 1–19.
 110. Thrane L. et al. THz reflection spectroscopy of liquid water // *Chem. Phys. Lett.* 1995. Vol. 240, № 4. P. 330–333.
 111. Schatzberg P. On the molecular diameter of water from solubility and diffusion measurements // *Journal of Physical Chemistry.* American Chemical Society (ACS), 1967. Vol. 71, № 13. P. 4569–4570.
 112. Kell G.S. Precise Representation of Volume Properties of Water at One Atmosphere // *J. Chem. Eng. Data.* American Chemical Society (ACS), 1967. Vol. 12, № 1. P. 66–69.
 113. Ho P.P., Alfano R.R. Optical Kerr effect in liquids // *Phys. Rev. A.* American Physical Society (APS), 1979. Vol. 20, № 5. P. 2170–2187.
 114. Sheik-Bahae M. et al. Sensitive Measurement of Optical Nonlinearities Using a Single Beam // *IEEE J. Quantum Electron.* Institute of Electrical and Electronics Engineers (IEEE), 1990. Vol. 26, № 4. P. 760–769.
 115. Weaire D. et al. Effect of low-power nonlinear refraction on laser-beam propagation in InSb // *Opt. Lett.* The Optical Society, 1979. Vol. 4, № 10. P. 331.
 116. Gaskill J.D., Wiley J. *Linear Systems, Fourier Transforms, and Optics* (Wiley Series in Pure and Applied Optics). 1978.
 117. Van Stryland E.W. et al. Two Photon Absorption, Nonlinear Refraction, And Optical Limiting In Semiconductors // *Opt. Eng.* NBS, 1985. Vol. 24, № 4. P. 404–423.
 118. Zheng X. et al. Characterization of nonlinear properties of black phosphorus nanoplatelets with femtosecond pulsed Z-scan measurements // *Opt. Lett.* The Optical Society, 2015. Vol. 40, № 15. P. 3480.
 119. Kislin D.A. et al. Self-Action of Nonparaxial Few-Cycle Optical Waves in Dielectric Media // *JETP Lett.* Pleiades Publishing Ltd, 2018. Vol. 107, № 12. P. 753–760.
 120. Melnik M. et al. Methodical inaccuracy of the Z-scan method for few-cycle terahertz pulses // *Sci. Rep.* Springer Science and Business Media LLC, 2019. Vol. 9, № 1.
 121. Yang K.H., Richards P.L., Shen Y.R. Generation of Far-infrared radiation by picosecond light pulses in LiNbO₃ // *Appl. Phys. Lett.* AIP Publishing, 1971. Vol. 19, № 9. P. 320–323.
 122. Lombosi C. et al. Nonlinear distortion of intense THz beams // *New J. Phys.* IOP Publishing, 2015. Vol. 17, № 8. P. 83041.
 123. Watanabe A. et al. A new nozzle producing ultrathin liquid sheets for femtosecond pulse dye lasers // *Opt. Commun.* Elsevier BV, 1989. Vol. 71, № 5. P. 301–304.

124. Kondoh M., Tsubouchi M. Liquid-sheet jets for terahertz spectroscopy // Opt. Express. The Optical Society, 2014. Vol. 22, № 12. P. 14135.
125. Yin M. et al. Determination of nonlinear absorption and refraction by single Z-scan method // Appl. Phys. B Lasers Opt. Springer Science and Business Media LLC, 2000. Vol. 70, № 4. P. 587–591.
126. Cheung Y.M., Gayen S.K. Optical nonlinearities of tea studied by Z-scan and four-wave mixing techniques // J. Opt. Soc. Am. B. The Optical Society, 1994. Vol. 11, № 4. P. 636.



Миссия университета – открывать возможности для гармоничного развития конкурентоспособной личности и вдохновлять на решение глобальных задач.

Мельник Максим Владимирович
Воронцова Ирина Олеговна
Пономарева Евгения Андреевна
Жукова Мария Олеговна
Цыпкин Антон Николаевич
Козлов Сергей Аркадьевич

Mathematical methods in femtosecond optics

Учебно-методическое пособие

В авторской редакции

Редакционно-издательский отдел Университета ИТМО

Зав. РИО

Н.Ф. Гусарова

Подписано к печати

Заказ №

Тираж

Отпечатано на ризографе

Редакционно-издательский отдел
Университета ИТМО
197101, Санкт-Петербург, Кронверский пр., 49